

## Dissertation

# Multi-Mission Satellite Ground Station for Education and Research

ausgeführt zum Zwecke der Erlangung des akademischen Grades eines  
Doktors der technischen Wissenschaften unter Leitung von

Univ.Prof. Dr. Arpad L. Scholtz  
Institute of Telecommunications, E389

eingereicht an der  
Technischen Universität Wien  
Fakultät für Elektrotechnik und Informationstechnik

von

**Michael Fischer**  
Matrikelnummer 9725775  
Karmeliterhofgasse 2/3/60  
1150 Wien

Wien, im Juni 2012

# Abstract

In this work, the TU Wien Ground Station – a satellite ground station built at the Vienna University of Technology – is presented. The ground station supports a variety of satellite missions and currently operates two research satellites from the field of astronomy: CoRoT and MOST. It has a focus on small satellites in low Earth orbits (LEOs) as often seen in education.

Small satellites in LEOs give low-cost access to space for research and education at universities. A key element in every satellite mission is the communication between the satellite and Earth, for example for spacecraft control and scientific data download. Such small satellites and ground stations are an excellent tool in education, because they offer complex and interdisciplinary, yet divisible challenges for students with different skills. The TU Wien Ground Station has been designed to also serve the education of students, for example in student labs. Therefore, it has been built at the university, right in the center of Vienna. This urban environment however is not the ideal location for a ground station, for example because of strong radio interferers.

This work first describes a few satellites which the ground station is required to operate with. It collects communication parameters of these and other prospective satellites. Then it analyzes the requirements imposed by the urban environment of the location of the ground station and the use of the ground station in education and in ground station networks.

In the second part, the thesis describes the design and realization of the ground station in detail under the above requirements and presents the characterization of its components. The ground station allows fully autonomous operation and is remotely controllable. Because of clear and open interfaces, the ground station can adapt to different ground station networks and can be easily expanded in the future to support different satellite missions. Finally, the thesis reports performance measurements which prove the successful operation of the ground station. Some of the measurements are repeated automatically on a regular basis to assure the quality of the ground station.

# Kurzfassung

In dieser Arbeit wird die TU Wien Ground Station vorgestellt: eine Satelliten-Bodenstation gebaut an der Technischen Universität Wien. Die Bodenstation unterstützt mehrere unterschiedliche Satellitenmissionen und arbeitet derzeit mit zwei Forschungssatelliten aus dem Bereich der Astronomie zusammen: CoRoT und MOST. Die Erdefunkstelle ist auf kleine Satelliten mit niedriger Flugbahn (Low Earth Orbit, LEO) ausgerichtet.

Kleine Satelliten mit niedriger Flugbahn erlauben Universitäten einen kostengünstigen Zugang zu Weltraumtechnik in Forschung und Lehre. Ein wichtiges Element jeder Satellitenmission ist die Kommunikation zwischen Satellit und Erde, zum Beispiel für die Steuerung des Raumfahrzeugs oder für den Empfang der wissenschaftlichen Daten. Solche kleinen Satelliten und Bodenstationen sind ein ausgezeichnetes Mittel in der akademischen Lehre, weil sie komplexe und interdisziplinäre, jedoch teilbare Aufgaben für Studenten mit unterschiedlichem Wissen bieten. Die TU Wien Ground Station wurde auch zur Verwendung in Studierendenlabors entwickelt. Daher ist sie direkt an der Universität gebaut worden, im Zentrum von Wien. Dieses städtische Umfeld ist jedoch kein idealer Standort für eine Bodenstation, insbesondere wegen der starken elektromagnetischen Einflüsse.

Diese Arbeit beschreibt zunächst einige Satelliten mit denen die Bodenstation zusammenarbeiten soll. Sie fasst Kommunikationsparameter dieser und anderer für sie interessanter Satelliten zusammen. Dann analysiert sie die Anforderungen an die Bodenstation durch das städtische Umfeld des Standortes und ihre geplante Verwendung in der Ausbildung von Studenten und in Bodenstationsnetzwerken.

Im zweiten Teil beschreibt die Arbeit das Design und die Realisierung der Bodenstation unter diesen Anforderungen im Detail und präsentiert die Charakterisierung ihrer Subsysteme. Die Bodenstation ermöglicht vollkommen autonomen Betrieb und ist fernsteuerbar. Aufgrund der klaren und offenen Schnittstellen kann die Bodenstation an verschiedene Bodenstationsnetzwerke oder weitere Satellitenmissionen angepasst werden. Abschließend präsentiert die Arbeit Messungen zur Qualität der Bodenstation welche ihren erfolgreichen Betrieb belegen. Ein Teil dieser Messungen wird zur Qualitätskontrolle in regelmäßigen Abständen automatisch wiederholt.

# Contents

<b>1</b>	<b>Introduction</b>	<b>1</b>
<b>2</b>	<b>Satellites for the TU Wien Ground Station</b>	<b>3</b>
2.1	CoRoT Satellite . . . . .	4
2.2	MOST Satellite . . . . .	5
2.3	BRITE Constellation . . . . .	7
2.4	CubeSats and Satellites in Education . . . . .	8
2.5	Amateur Radio Satellites . . . . .	10
2.6	Requirements for the Ground Station . . . . .	11
<b>3</b>	<b>LEO Ground Stations in Urban Environments</b>	<b>12</b>
3.1	Low Earth Orbits . . . . .	12
3.2	Urban Environment . . . . .	15
3.2.1	Man-Made Radio Noise and Interferers . . . . .	16
3.2.2	Radio Horizon . . . . .	20
3.3	Ground Stations in Education . . . . .	20
3.4	Ground Station Networks and GENSO . . . . .	20
3.5	Vienna Ground Station for MOST . . . . .	21
<b>4</b>	<b>TU Wien Ground Station Concept</b>	<b>22</b>
4.1	Segments of the Ground Station . . . . .	22
4.1.1	RF Front Ends . . . . .	24
4.1.2	Signal Processing Segment . . . . .	25
4.1.3	Mission Specific Segment . . . . .	26
4.1.4	Control and Supervisory Block . . . . .	26
4.2	Ground Station Interfaces and Multi-Mission Support . . . . .	26
4.2.1	HTTP Interface . . . . .	28
4.2.2	Matlab Interface . . . . .	28
4.2.3	Remote Access to the Ground Station . . . . .	29
4.3	Virtualization and Ground Station Networks . . . . .	29
4.4	The TU Wien Ground Station in Education . . . . .	30
4.5	Pipelines for Different Missions . . . . .	31
4.5.1	CoRoT Pipeline . . . . .	31
4.5.2	MOST Pipeline . . . . .	32

4.5.3	Future Pipeline for BRITE . . . . .	32
4.5.4	Proposed Interaction with GENSO . . . . .	32
<b>5</b>	<b>Realization of the TU Wien Ground Station</b>	<b>34</b>
5.1	S-Band Antenna System . . . . .	34
5.2	S-Band Downlink . . . . .	36
5.2.1	Link Budget . . . . .	37
5.2.2	S-Band Feed . . . . .	42
5.2.3	Duplex Filters . . . . .	42
5.2.4	S-Band LNAs . . . . .	45
5.2.5	S-Band Feed Assembly/LNB . . . . .	45
5.2.6	Bandpass Filters . . . . .	50
5.2.7	Buffer Amplifiers and Alternate Receiver Output . . . . .	50
5.2.8	Dual Downconverter . . . . .	50
5.2.9	Polarization Selection . . . . .	53
5.2.10	Satellite Modem . . . . .	53
5.3	S-Band Uplink . . . . .	56
5.3.1	Link Budget . . . . .	56
5.3.2	Modulator . . . . .	59
5.3.3	Upconverter . . . . .	59
5.3.4	Power Amplifier . . . . .	59
5.3.5	MOST Output Signal . . . . .	62
5.4	UHF/VHF Antenna System . . . . .	64
5.5	UHF/VHF Front Ends . . . . .	65
5.5.1	UHF Link Budgets . . . . .	66
5.5.2	UHF Polarization Selector . . . . .	68
5.5.3	UHF LNAs . . . . .	68
5.5.4	UHF Power Amplifier . . . . .	70
5.5.5	UHF/VHF Radio . . . . .	70
5.5.6	Differences in the VHF Front End . . . . .	71
5.6	Mission Specific Segment . . . . .	74
5.6.1	CoRoT TNC and Data Storage . . . . .	74
5.6.2	MOST TNC and Computer . . . . .	75
5.6.3	BRITE TNC and Computer . . . . .	75
5.7	TU Wien Ground Station Control Software . . . . .	76
5.7.1	Inter-Block Messaging . . . . .	78
5.7.2	Hardware Control . . . . .	80
5.7.3	Built-In Webserver . . . . .	81
5.7.4	User Interfaces . . . . .	83
5.8	Pass and Task Schedulers . . . . .	87
5.8.1	Pass Scheduler . . . . .	87
5.8.2	Task Scheduler . . . . .	87

5.8.3	Tasks During a Satellite Pass . . . . .	88
5.9	Antenna Rotator and Satellite Tracking . . . . .	90
5.9.1	Antenna Rotator and Rotator Controller . . . . .	90
5.9.2	SGP4 Satellite Tracker . . . . .	93
<b>6</b>	<b>Performance Measurements</b>	<b>95</b>
6.1	Rotator Tracking Accuracy . . . . .	95
6.2	CoRoT Radio Horizon . . . . .	95
6.3	CoRoT Satellite Antenna Pattern . . . . .	98
6.4	MOST Up- and Downlink . . . . .	100
6.5	Automatic Noise Figure Assessment . . . . .	102
6.6	Environmental Monitoring . . . . .	103
<b>7</b>	<b>Summary and Conclusions</b>	<b>107</b>
<b>A</b>	<b>Topocentric-Horizon Coordinate System</b>	<b>111</b>
<b>B</b>	<b>Propagation Effects and Losses</b>	<b>112</b>
<b>C</b>	<b>Polarization Selection for Satellites</b>	<b>115</b>
<b>D</b>	<b>Satellite Link Budgets</b>	<b>117</b>
D.1	Link Budget for CoRoT . . . . .	117
D.2	Link Budget for MOST . . . . .	118
D.3	Link Budget for BRITE Constellation . . . . .	118
	<b>Acknowledgments</b>	<b>121</b>
	<b>List of Abbreviations</b>	<b>122</b>
	<b>List of Symbols</b>	<b>125</b>
	<b>Bibliography</b>	<b>128</b>

# Chapter 1

## Introduction

For some 50 years, satellites are somehow present in our day-to-day life and supply us with television, navigation and communication possibilities or enable accurate weather forecasts. Beside these more common applications, there are lots of others including diverse fields of research. Satellites come in all shapes and masses and can be found in different orbits [1, 2].

Space is a very challenging environment. This makes the development of a satellite a very demanding and complex task. From the engineers it asks for widespread and interdisciplinary knowledge. This in turn makes satellites an excellent exercise for higher education. Since the advent of small satellites more than 10 years ago, these low-cost satellites are more and more accessible to students at universities. At different levels in their curriculum and from different fields, students can work on a satellite and so deepen their knowledge by problem based learning [3–5].

Despite their variety, all satellites have in common that they do not make sense when people on Earth cannot communicate or somehow interact with them. Some means of control from Earth is necessary, which is usually accomplished with at least one ground station per satellite mission. This makes ground stations an integral part of a satellite and in turn makes ground stations another excellent tool for education of students. Depending on the satellite and its orbit, several ground stations per satellite are reasonable or necessary. This requires communication among the ground stations. As an example, our institute built a ground station in 2003 dedicated to the MOST mission which is connected with two ground stations in Canada [6–9].

In 2008, it was decided to build a ground station at our university for use in education and research – the TU Wien Ground Station. The choice of the location allows easy access for students and the use of the ground station in education. The requirements include the support of multiple different satellite missions and easy

future expandability. For convenient use of the ground station, it must operate fully autonomously and be remotely controllable.

When a ground station is dedicated to a single satellite in a low Earth orbit (LEO), it is idle for most of the day between passes of the satellite over the station. In the meantime, it could communicate with other satellites. If the satellites that a ground station wants to communicate with are very different in their communication parameters – which is often the case with small satellites in the context of universities – it is a challenging task for the ground station to support all of them. Great care has been taken for the TU Wien Ground Station to make it flexible in order to support multiple satellite missions. The idea of sharing ground stations between satellite missions also leads to ground station networks. [9–11].

This thesis presents the TU Wien Ground Station and documents some six months of successful operation with the CoRoT and MOST satellite missions which is further continuing.

Chapter 2 introduces a few satellites for research from the field of astronomy which are of interest to the TU Wien Ground Station. It evaluates the communication parameters of these satellites which are relevant to the ground station and deduces design requirements for the ground station.

Then, Chapter 3 treats ground stations for LEO satellites. It further focuses on an urban environment and gives measurement results on possible interferers in the city of Vienna. Chapter 3 also treats some aspects of ground stations when used in education, in ground station networks or for multiple missions.

After this introduction, the next chapters concentrate on the TU Wien Ground Station. Chapter 4 gives the concept of the ground station and explains its use in education and ground station networks.

Chapter 5 presents the design details of the ground station and its actual realization. It describes the hardware and software in detail and gives the characterizations of several of the components used.

Chapter 6 illustrates the successful operation of the TU Wien Ground Station with performance measurements and shows means of automatic long term quality assurance of the ground station.

Finally, Chapter 7 gives a summary and the conclusions of the thesis.



# Chapter 2

## Satellites for the TU Wien Ground Station

Since the launch of the first satellite Sputnik 1 on the 4<sup>th</sup> of October 1957, we find lots of different satellites in space. Among others we find

- television broadcast satellites,
- radionavigation satellites,
- telecommunication satellites,
- Earth exploration/observation satellites
- weather observation satellites,
- military satellites,
- astronomical satellites,
- educational or technology demonstration satellites and
- other scientific or experimental satellites.

This thesis concentrates on educational and research satellites.

Satellites can be characterized for example by their mass, altitude or purpose. Small satellites are often classified using their mass:

- Minisatellites are below 500 kg,
- Microsatellites are below 100 kg,
- Nanosatellites are below 10 kg and
- Picosatellites are below 1 kg.

All types of satellites can be categorized by their type of orbit and altitude. Although there exist no strict boundaries,

- low Earth orbit (LEO) satellites have a typical altitude of 160 km to 2 500 km (see Section 3.1),
- medium Earth orbit (MEO) satellites have a typical altitude of 6 000 km to 20 000 km and

- geostationary Earth orbit (GEO) satellites have an altitude of 35 786 km which results in a speed equal to the rotational speed of the Earth.

The next sections give details on three LEO satellites, which are of interest to the TU Wien Ground Station – CoRoT, MOST and BRITE Constellation. In Sections 2.4 and 2.5, I gather common parameters of further satellites with educational background which are also of interest to the ground station. Finally, Section 2.6 sums up some design requirements for the ground station because of these satellites.

## 2.1 CoRoT Satellite

CoRoT (convection, rotation and planetary transits) is a mission of astronomy led by the Centre National d'Études Spatiales (CNES) dedicated to stellar seismology and the search for extra-solar planets. The CoRoT spacecraft is equipped with a 27 cm diameter afocal telescope and four charge-coupled devices (CCDs) sensitive to tiny variations of the light intensity of stars. With this telescope, it performs ultra-high-precision photometry from space. A typical observation run lasts 25 to 150 days [12–14].

The CoRoT satellite is composed of a PROTEUS platform (Plate-forme Reconfigurable pour l'Observation, les Télécommunications et les Usages scientifiques) and the payload (i.e. the scientific part of the satellite) consisting of the telescope and its accompanying electronics. The payload mass is 300 kg and it has a power consumption of 150 W. The total mass is 626 kg and the total power consumption is 450 W. Its maximum dimension is 4.1 m. The PROTEUS platform is designed for LEOs with up to 1500 km altitude. The platform offers star trackers, inertial wheels, magnetorquers and gyrometers to stabilize its pointing direction. Together with measurements from one of the CCDs a pointing accuracy of 0.3 arcseconds is achieved. CoRoT was launched into a polar orbit with a mean altitude of 897 km in December 2006 from Baikonur Cosmodrome in Kazakhstan [13, 15].

The CoRoT satellite has an on-board data memory of 256 Mbyte. It records data during the observation which is later downloaded to Earth. CoRoT uses the Consultative Committee for Space Data Systems (CCSDS) standards for communications with Earth. The payload data is packed into virtual channels together with the housekeeping data (i.e. status information on the satellite like temperature and power consumptions of modules) and then transmitted to Earth in the S-band around 2280 MHz with some 800 kbit/s and quadrature phase shift keying (QPSK) modulation (see Section 5.6.1) [15, 16].

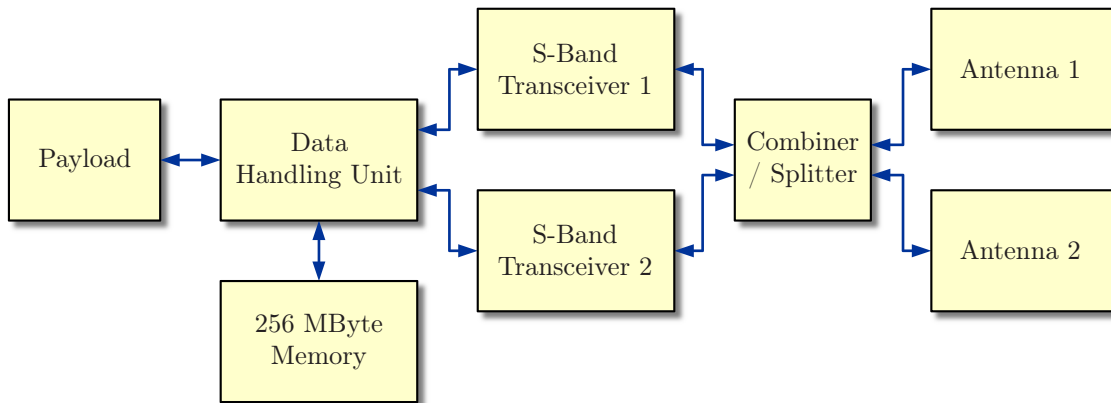


Figure 2.1: Block diagram of the communication blocks of the CoRoT satellite [15].

Figure 2.1 shows a block diagram with these communications blocks of CoRoT. The data handling unit takes care of all the data processing and virtual channel combining. Next, there are two S-band transceivers for redundancy reasons and two antennas. The transceivers share the two antennas with a combiner/splitter. Together, the two antennas provide an almost spherical radiation characteristic (see Section 6.3) [15, 16].

CoRoT's ground control segment consists of the mission control center and the control center in Toulouse and several ground stations spread over the world. The main CNES ground stations are in Kiruna (Sweden), Aussaguel (France), Hartebeesthoek (South Africa) and Kourou (French Guiana). Furthermore, there are secondary ground stations, part of the CoRoT operational ground station network, in Alcantara (Brazil) and now also in Vienna [12].

## 2.2 MOST Satellite

The MOST (microvariability and oscillations of stars) astronomy mission led by the Canadian Space Agency (CSA) is Canada's first space science microsatellite. The satellite is equipped with a 15 cm aperture optical Rumak-Maksutov telescope which feeds two frame-transfer CCDs. It has been designed to detect low-degree acoustic oscillations with micromagnitude precision in solar-type stars and metal-poor subdwarfs [18, 19].

The satellite has a size of 65 cm × 65 cm × 30 cm and a mass of 60 kg. Its nickel-cadmium battery system allows for a maximum power consumption of 35 W. For accurate measurements, the satellite is stabilized in three axes by reaction wheels, magnetotorquers, a star tracker, magnetometers, sun sensors and rate sensors. With

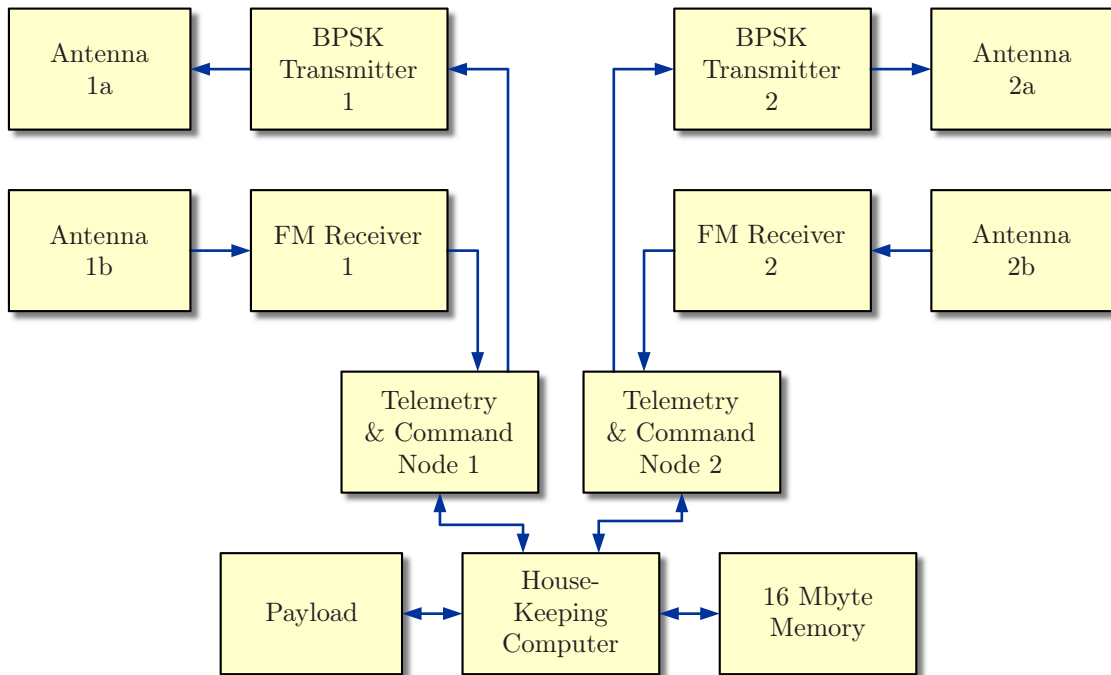


Figure 2.2: Block diagram of the communication blocks of the MOST satellite [17].

these components a pointing accuracy of better than 25 arcseconds is achieved. MOST was launched into a polar, sun-synchronous, dawn-dusk orbit with a mean altitude of 826 km in June 2003 from the Plesetsk Cosmodrome in northern Russia. This LEO orbit allows MOST to observe the same region of the sky (i.e. one field of stars) for up to 60 days. Typical observation runs have a length of some 25 days. The light curves from such an observation are used to extract the pulsation periods of the observed stars, which are in the order of  $\mu\text{Hz}$  [17, 18, 20–22].

Figure 2.2 shows a block diagram of the communication elements of MOST. The instrument photographs stars and forwards these data to the housekeeping computer – a NEC V53 central processing unit (CPU). The housekeeping computer temporarily stores the data in a 1.5 Mbyte memory. When communicating with Earth, the computer utilizes one out of the two telemetry & command nodes. Each of these nodes is connected to an S-band binary phase shift keying (BPSK) transmitter and an S-band frequency modulation (FM) receiver. Each of the transmitters and receivers is connected to a quadrifilar antenna. A transmit/receive pair of antennas is mounted on one side, the other pair on the other side of the satellite. This results in an almost spherical coverage. There are two uplink (i.e. from Earth to the satellite) frequencies and two downlink (i.e. from the satellite to Earth) frequencies. Each transmitter/receiver pair utilizes its own pair of up-/downlink frequencies.

The uplink uses two frequencies around 2055 MHz with Gaussian minimum shift keying (GMSK) modulation and 9.6 kbit/s, the downlink uses frequencies around 2232 MHz with 38.4 kbit/s. The appropriate frequency pair is selected at the ground station by trial-and-error based on the resulting received signal power on ground. Scramblers and convolutional encoders are used for the uplink and are implemented on separate boards. The ground segment of MOST consists of three ground stations located in Toronto, Vancouver and Vienna [8, 17, 20].

## 2.3 BRITE Constellation

BRITE (bright target explorer) Constellation is a group of six nanosatellites from Austria, Poland and Canada carrying 3 cm aperture optical telescopes. The purpose of the mission is to photometrically measure low-level oscillations and temperature variations in stars. The satellites are equipped with CCD cameras and optical filters – each of the satellites is measuring in a different spectrum range [24–27].

Each of the BRITE satellites is 20 cm × 20 cm × 20 cm big and has a mass of 6.5 kg. Similar to MOST, BRITE utilizes a star tracker, Sun sensors, magnetometers, reaction wheels and magnetotorquers for three-axis attitude control better than 1.5 arcminutes [23, 25].

Currently, the two Austrian and one Polish satellite are ready for launch. The launch of the two Austrian satellites – which are also Austria’s first satellites – is scheduled for end of 2012 or beginning of 2013 and will be carried out by the Indian Space Research Organization (ISRO) from Sriharikota, near Cheney in India. The orbit will be a sun-synchronous, polar, dawn-dusk orbit with 800 km altitude. The first Polish BRITE satellite – which is Poland’s first scientific satellite – is scheduled in a similar timeframe with a Russian launcher. The remaining satellites from Canada and Poland should be ready for launch in 2013 [25, 28].

Figure 2.3 gives a block diagram of the communication blocks of the BRITE satellites. The uplink uses the ultra high frequencies (UHF) near 437 MHz in an amateur radio frequency band together with GMSK and a bit rate of 4 kbit/s. Four antennas around the spacecraft result in good spherical coverage. The downlink utilizes S-band frequencies near 2.23 GHz, BPSK and a configurable bit rate of 32 kbit/s to 256 kbit/s. Two circularly polarized (CP) patch antennas are used for the downlink – again placed on opposite sides for good coverage. For up- and downlink, a receiver and a transmitter are connected to the main on-board computer. The main on-board computer performs the (de)packetizing and communicates with

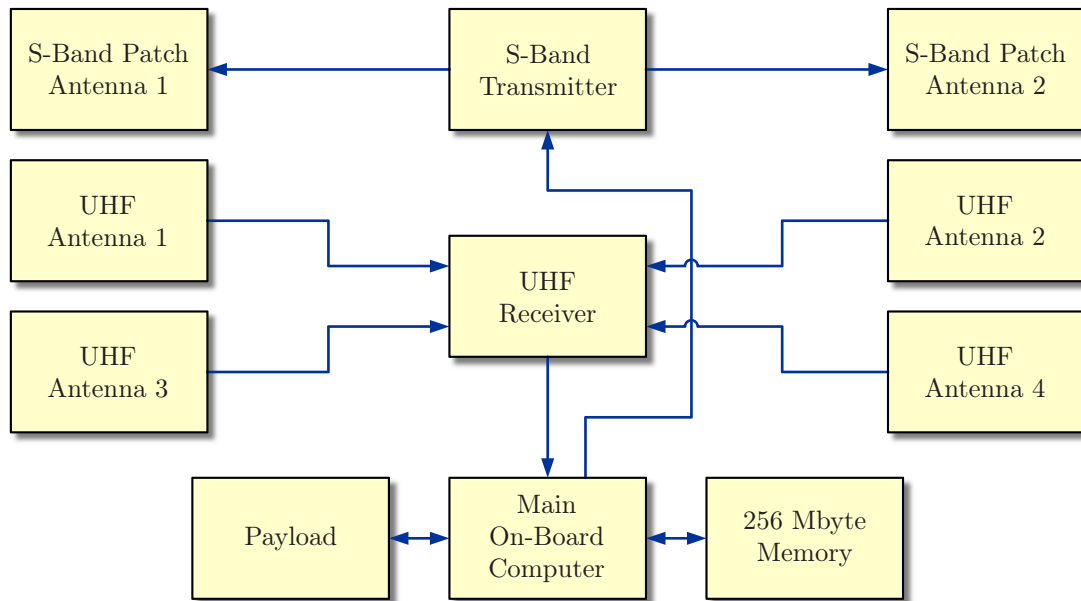


Figure 2.3: Block diagram of the communication blocks of the BRITE satellites [23, 24].

the receiver and the transmitter. The computer is connected to 256 Mbyte of external flash memory where the payload data is stored before transmission to ground [6, 23, 24].

BRITE Constellation builds upon experience of the University of Toronto, Institute for Aerospace Studies - Space Flight Laboratory (UTIAS-SFL) with the MOST, the CanX-2 (Canadian Advanced Nanospace eXperiment) and the CanX-6 (NTS, nanosatellite tracking ships) missions. The BRITE satellites are built using SFL's generic nanosatellite bus (GNB). This bus enables bigger and heavier satellites than the CubeSat standard (see Section 2.4) and so allows for more complex payloads. Similar to CubeSats, the GNB uses a specific deployer tube which is shared between missions [29–31].

## 2.4 CubeSats and Satellites in Education

A CubeSat is a picosatellite with a size of  $10\text{ cm} \times 10\text{ cm} \times 10\text{ cm}$  and a mass below 1.33 kg which adheres to the CubeSat standard. This standard was first introduced by Jordi Puig-Suari from California Polytechnic State University (CalPoly) and Robert Twiggs from Stanford University in 1999 [32–35]. Since the first launch of five CubeSats in 2003, more than 30 have been successfully launched and many

more are under development or waiting for launch [35–39]. Further examples of CubeSats can be found in [30, 40, 41].

A key component for CubeSats is the CubeSat Design Specification together with the standard poly picosatellite orbital deployer (P-POD). The standard size and physical requirements shared by a large number of spacecrafts allow the reuse of components in new satellites and led to the general availability of generic modules for CubeSats. This significantly reduces the development effort and since many of such modules are already space qualified, the risk of a mission failure is lowered, which results in reduced overall costs. Beside the traditional CubeSat size with 10 cm height (called 1U), there are also bigger versions with 20 cm and 30 cm height respectively (called 2U and 3U) [32, 34].

The standard P-POD encapsulates three CubeSats during launch and protects the CubeSats on the one hand and the launcher from a malfunction of a CubeSat on the other hand [32]. Because one P-POD accommodates several CubeSats, launches are often coordinated between CubeSats by launch brokers like CalPoly or UTIAS-SFL [39]. The P-PODs are seldom the primary payload of the launching rocket – again extensive coordination is necessary. Sometimes CubeSats are even deployed from another satellite. SSETI Express (Student Space Exploration and Technology Initiative Express) for example launched three CubeSats in 2005 [38].

Regarding communications, there is no common standard among CubeSats. The data rates are typically between 1200 Baud and 9600 Baud. Often, the uplink operates in the very high frequency (VHF) band near 145 MHz and the downlink in the UHF band near 437 MHz. However, there are lots of other frequencies and combinations thereof. The protocol mostly used is AX.25 or a derivative [38, 42]. For future use, a standard CubeSat frequency of 437.35 MHz in the amateur radio UHF band has been selected [36]. This selection allows to share resources and gives a meaning to ground station networks like GENSO (see Section 3.4).

CubeSats and nanosatellites in a LEO offer a cheaper alternative and feature faster development cycles than traditional space missions and therefore give access to space science for education and research at universities [3, 4]. For students, satellite missions represent a challenging exercise which is ideal for problem based learning. Satellites require lots of interdisciplinary skills, teamwork and project management. The satellite’s design, building and testing can be broken down into subprojects which can then be solved by different teams with different states of knowledge or with different locations [5]. As an example, the CubeSat Program with its extensive developer community has become truly international, reaches across dozens of nations and affects thousands of students worldwide. With a few exceptions, all CubeSats have been built in the context of universities [36].

CubeSats and other small satellites are often supported by different educational programs of various space agencies. Examples are NASA's ELaNa missions (Educational Launch of Nanosatellites) [43] or ESA's Vega launcher carrying CubeSats on its maiden flight in the first quarter of 2012 [44]. An interesting launch opportunity is in 2015, when the QB50 mission will launch 50 2U and 3U CubeSats into an orbit with 230 km altitude to explore the lower thermosphere [45].

## 2.5 Amateur Radio Satellites

Four years after the launch of the world's first satellite Sputnik 1 in October 1957, the first amateur satellite was launched in December 1961. It was named OSCAR I (orbiting satellite carrying amateur radio I). Since then, satellites carrying amateur radio services have a long tradition. The community of The Radio Amateur Satellite Corporation (AMSAT) builds and/or supports these missions. About 70 amateur radio satellites have been launched and assigned an OSCAR number since 1961 [46].

Amateur satellite radio services are radiocommunication services using Earth satellites for the purpose of self-training, intercommunication and technical investigations by authorized amateurs solely with a personal aim and without pecuniary interest (source: provisions of No.1.56 and No.1.57 of [47]). Lots of CubeSats or other educational satellites have similar orientation and are operated by students with an amateur radio license. Such missions therefore often choose to utilize amateur radio frequencies [46].

Table 2.1 lists the four frequency bands for amateur radio satellite services between 100 MHz and 10 GHz [46]. For CubeSats, a specially interesting frequency

Name	Wavelength	Start MHz	Stop MHz
VHF	2 m	144	146
UHF	70 cm	435	438
L-band	23 cm	1260	1270
S-band	13 cm	2400	2450
C-band uplink	6 cm	5650	5670
C-band downlink	6 cm	5830	5850

Table 2.1: Band names, approximate wavelengths and border frequencies for amateur radio satellite services between 100 MHz and 10 GHz [46].



is 437.35 MHz [36]. For the TU Wien Ground Station, I decided to support the three amateur radio frequency bands around 145 MHz, around 437 MHz and around 2.4 GHz, respectively.

## 2.6 Requirements for the Ground Station

The satellites highlighted in the previous sections set several requirements on the ground station for enabling communication with them. For CoRoT, MOST and BRITE, Table 2.2 gives

- the required  $G/T_s$  of the ground station for the downlink from the satellites and
- the required  $EIRP$  of the ground station for the uplink to the satellites.

The  $G/T_s$  is called the “figure of merit” of a receiving system. It is the ratio between the gain  $G$  of its receive (Rx) antenna system and its system noise temperature  $T_s$ . Details are given in Section 5.2.1 and measurements on the ground station’s  $G/T_s$  can be found in Section 6.5.

The equivalent isotropically radiated power  $EIRP$  is the product of the gain  $G_{tx}$  of the transmit (Tx) antenna and the transmit power  $P_{tx}$ ,  $EIRP = G_{tx} P_{tx}$ .

The figures arise from the radio frequency (RF) power levels of the satellites and are calculated in Appendix D. The necessary  $G/T_s$  and  $EIRP$  set two requirements for the communication with the respective satellite, and because I want to communicate with CoRoT, MOST and the BRITE satellites, they are respected in Chapter 5. Other parameters are e.g. the modulation scheme or the data rate.

Satellite	Direction	Frequency	Parameter	Value
CoRoT	down	S-band	$G/T_s \geq$	8.2 dB/K
MOST	down	S-band	$G/T_s \geq$	9.9 dB/K
MOST	up	S-band	$EIRP \geq$	69.4 dBm
BRITE	down	S-band	$G/T_s \geq$	7.9 dB/K
BRITE	up	UHF	$EIRP \geq$	63.0 dBm

Table 2.2: Satellites which are of interest for the TU Wien Ground Station and their requirements.

# Chapter 3

## LEO Ground Stations in Urban Environments

A key element for every space mission is the communication with Earth. Without communication, most satellites would not be able to perform their mission. In case of scientific satellites, they would not be able to transmit their measurement results down to Earth without a ground station. All for the TU Wien Ground Station relevant satellites are in LEOs. The characteristics of LEOs from the ground station's view point are detailed in Section 3.1. Section 3.2 deals with the urban environment and its impact on ground stations and Section 3.3 deals with the use of ground stations in education. A LEO satellite normally requires more than one ground station, whereas each of these ground stations are idle for most of the day. By means of ground station networks, resources can be shared and used more efficiently – which is discussed in Section 3.4. As explained in Section 3.5, the TU Wien Ground Station builds upon experience with a ground station built in 2002 in Vienna for MOST.

### 3.1 Low Earth Orbits

As shown in Chapter 2, lots of scientific satellites and most of the educational satellites are in a LEO. LEOs are commonly defined as orbits with an altitude from 160 km to 2500 km. They are significantly lower than a GEO with 35786 km altitude [1]. CoRoT, MOST and BRITE Constellation use a LEO orbit. The orbital period  $t_o$  of a satellite in a perfectly circular orbit – i.e. when ignoring influences like the oblateness of the Earth – is [2, 48]

$$t_o = 2 \pi \sqrt{\frac{r^3}{GM}} = 2 \pi \sqrt{\frac{r^3}{\mu}}. \quad (3.1)$$

$r = r_E + h$  is the radius of the orbit – the sum of the radius of the Earth  $r_E$  and the satellite’s altitude  $h$  (see Figure 3.1).  $\mu$  is the standard gravitational parameter – a short form for the product of the gravitational constant  $G$  and the mass of the Earth  $M$ . This gives periods of 88 minutes to 139 minutes for LEO satellites and more specific some 101 minutes for CoRoT, MOST and BRITE Constellation.

LEOs are ideally suited for scientific and educational missions, because they are cheaper to reach than a GEO, because of the lower energy needed for the launch. In addition, they are well suited for example for astronomical measurements, because there is no disturbance from the Earth’s atmosphere.

In contrast – because the period of LEO satellites is smaller than the rotational period of the Earth – LEO satellites are not fixed in the sky from the ground station’s view point. Therefore, ground stations for LEO satellites do not have full day access to the satellites and require antenna systems with tracking capabilities.

In the best case – as depicted in Figure 3.1 a) – when the satellite passes straight over the ground station (i.e. in a plane through the Earth’s center and the ground station), it comes up at one horizon, reaches the zenith with an elevation of  $\vartheta = 90^\circ$  and sets at the other horizon. The arc length  $2\theta$ , during which communication is possible, is proportional to the pass duration  $t_p$  with

$$2\theta = \dot{\theta} t_p = \frac{2\pi}{t_o} t_p, \quad (3.2)$$

where  $\dot{\theta}$  is the angular speed of the satellite. This leads to

$$t_p = \frac{2\theta}{2\pi} t_o = 2\theta \sqrt{\frac{r^3}{\mu}}. \quad (3.3)$$

The angle  $\theta$  measured from the horizon to the zenith is given by

$$\cos \theta = \frac{r_E}{r} \quad \rightarrow \quad \theta = \arccos \frac{r_E}{r}. \quad (3.4)$$

The resulting  $t_o$  for these best-case passes with  $\vartheta_{\max} = 90^\circ$  and varying altitudes  $h$  is given in Figure 3.2 on the top.

Normally, a satellite pass does not have a maximum elevation of  $90^\circ$ . Then, the orbital plane of the satellite is tilted relative to plane through the ground station by some angle  $\alpha$  – as depicted in the side view given in Figure 3.1 b). The angle  $\alpha$  is

$$\alpha = 90^\circ - \vartheta_{\max} - \arcsin \frac{r_E \cos \vartheta_{\max}}{r} \quad (3.5)$$

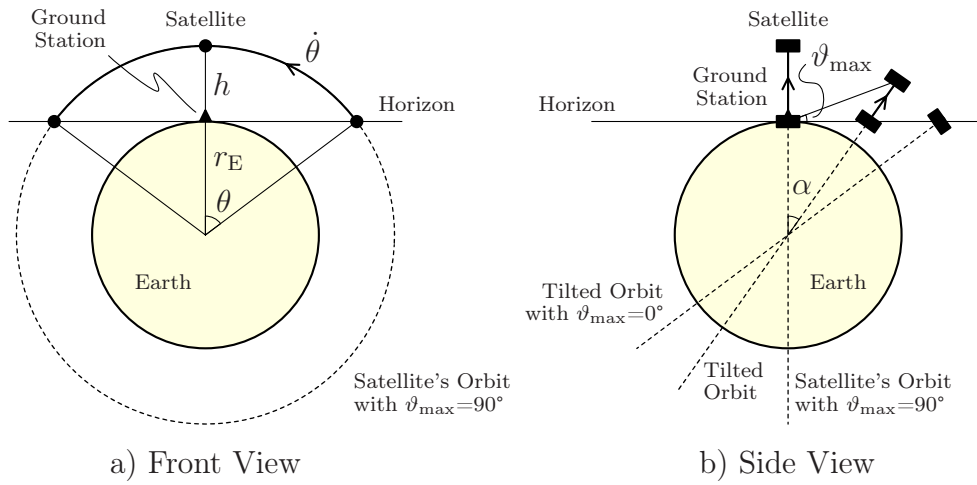


Figure 3.1: Illustrating the calculation of the pass time for a circular LEO satellite from the front and the side. The ground station is assumed fixed on top of the Earth regardless of the Earth's current position and orientation.

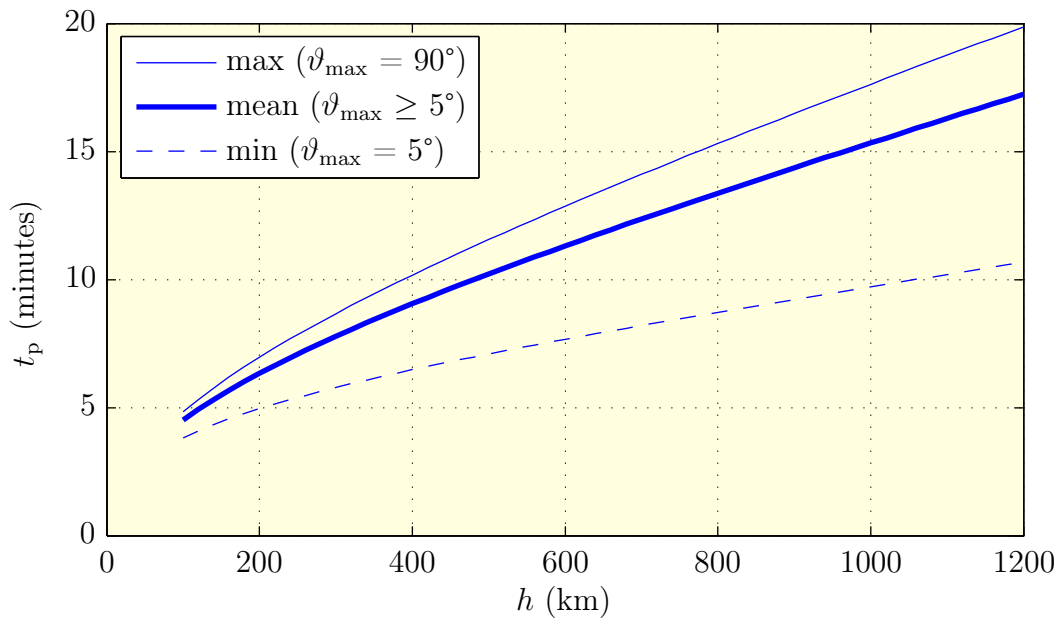


Figure 3.2: Pass duration  $t_p$  in minutes for circular LEOs with varying altitude  $h$ .

and goes from the best case of  $\alpha = 0^\circ$  discussed before to the worst case with  $\alpha = \theta$ . The arc length for this tilted case can be calculated as [49]

$$\theta_\alpha = \arcsin \frac{\sqrt{\cos^2 \alpha - r_E^2 / r^2}}{\cos \alpha}. \quad (3.6)$$

Typically, one would not consider the satellite passes with a very low  $\vartheta_{\max}$ , because there the distance from satellite to ground station is at its maximum. As an example, the communication duration  $t_p$  for  $\vartheta_{\max} = 5^\circ$  is given in Figure 3.2 at the bottom.

When the orbital period  $t_o$  is not in resonance with the rotation time of the Earth,  $\alpha$  can be considered equally distributed between  $0^\circ$  and  $\theta$  for the calculation of the mean communication time  $\bar{t}_p$ . The mean pass duration is

$$\bar{t}_p = \frac{1}{\alpha_{\max}} \int_0^{\alpha_{\max}} 2 \theta_\alpha \sqrt{r^3 / \mu} d\alpha \quad (3.7)$$

with an  $\alpha_{\max}$  calculated from an assumed minimum  $\vartheta_{\max}$ . Such a numerically calculated mean is given in Figure 3.2 in the middle. The mean communication duration is some 10 minutes to 15 minutes per pass for altitudes between 600 km and 1000 km.

All four satellites – CoRoT, MOST and the two Austrian BRITE satellites – have a sun-synchronous orbit. This means, that the orientation of the orbit remains fixed relative to the Sun. MOST and the two Austrian BRITE satellites have a special dawn-dusk orbit. In this case, the satellites fly at the terminator – the line on the Earth between day and night. Consequently, communication with the satellites is possible wherever there is dawn or dusk on Earth. This type of orbit can be achieved by carefully selecting the altitude and the inclination of the orbital plane before launch. Furthermore, the dawn-dusk orbit has the advantage of a rather constant thermal load on the satellite and results in a good stray light situation for astronomical measurements [50, 51].

## 3.2 Urban Environment

The ideal place for a satellite ground station is in a quite, rural environment on an elevated location without much climatic influences like wind, rain or snow [2, 52]. Such a place is seldom available. In contrast, it was decided to place the TU Wien Ground Station right in the center of Vienna in the 4<sup>th</sup> district. While this location has lots of drawbacks regarding environmental influences, it has the huge benefit of accessibility to students of the university.

### 3.2.1 Man-Made Radio Noise and Interferers

Every city – compared to a rural environment – has the drawback for a ground station of strong man-made radio interferers. These include mobile communication systems, wireless local area network (WLAN), broadcasting stations, as well as millions of other electronic devices emitting intentionally or unintentionally radio signals. If not appropriately dealt with, these interferers severely degrade the performance of a satellite downlink [8, 53].

As detailed later in Chapter 4, the TU Wien Ground Station has two S-band RF front ends between 2.0 GHz and 2.1 GHz for the uplink and between 2.2 GHz and 2.45 GHz for the downlink. These two bands, together with other radio services in this frequency area, are illustrated in Figure 3.3. These other services include satellite services, mobile communication systems like the global system for mobile communications (GSM), the universal mobile telecommunications system (UMTS) or long term evolution (LTE) and other services. Furthermore, the up- and downlink frequencies of CoRoT, MOST and BRITE are shown in the figure. The frequency bands designated to space operations and amateur radio (both in green) led to the selection of the frequency bands for the two S-band RF front ends of the ground

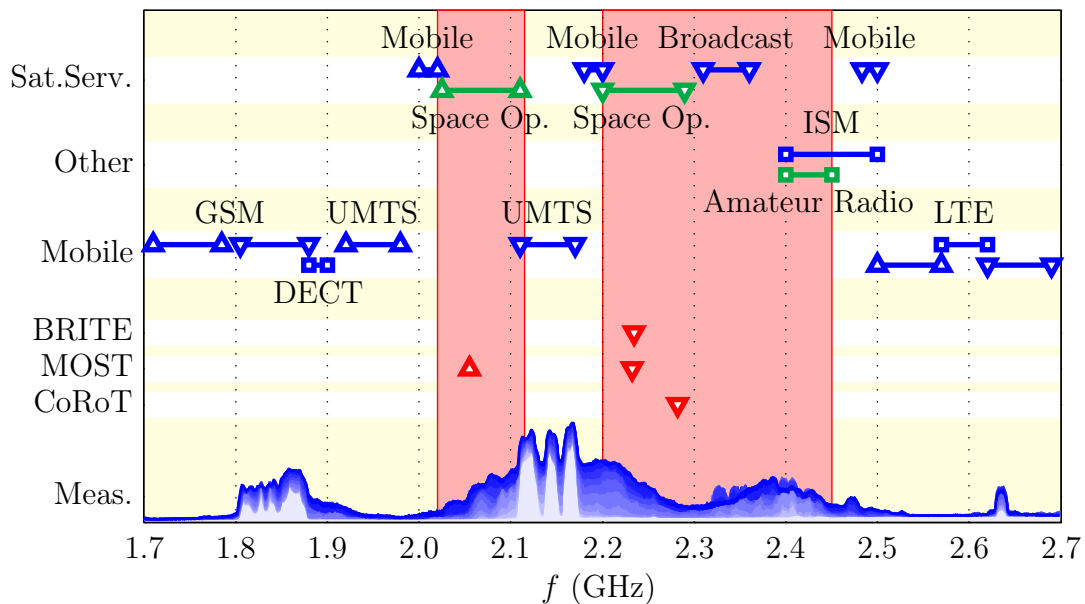


Figure 3.3: A detailed frequency domain view of the two S-band RF front ends of the ground station and typical services utilizing the same frequency range.

station (see Section 4.1.1). The red areas indicate the pass bands of the filters used in the front ends (see Sections 5.2.3 and 5.2.6).

On the bottom of the figure, a plot shows a qualitative spectrum from a measurement at the roof of the institute covering a power range of some 60 dB. It shows the maximum received power level as a function of frequency. Furthermore, the different shades of blue indicate the elevation of the measurement, where dark blue corresponds to the horizon with  $\vartheta = 0^\circ$  and light blue is  $\vartheta = 10^\circ$ .

Some of the interferers are visible to the ground station similar to noise, others are so strong, that they saturate the low noise amplifiers (LNAs) of the downlink – this effect is called blocking. The strongest signals received are the downlinks of the mobile communication base stations of GSM 1800, UMTS and LTE [54, 55].

In 2002, a ground station for MOST was built by our institute in the 18<sup>th</sup> district of Vienna (see Section 3.5). Figure 3.4 gives the mobile communication base stations around this location. Colors are used to differentiate between GSM and UMTS, the size of the circles corresponds to the power classes of the base stations. The data has been taken from [56]. Only one base station is closer than 250 m to the ground station.

In contrast, Figure 3.5 shows base stations near the TU Wien Ground Station in the 4<sup>th</sup> district of Vienna. Seven base stations are closer than 250 m to the ground station, seven other stations are directly visible from the ground station – they are in line of sight. Squares have been used to mark the directly visible base stations.

Figure 3.6 shows additional interferer measurements in the spatial domain I made on the roof of the institute at the location of the S-band antenna system. The figure shows the received signal power as a function of azimuth  $\varphi$ , elevation  $\vartheta$  and frequency  $f$ . Each of the strips covers the full spatial range in azimuth, the elevation range from  $0^\circ$  to  $10^\circ$  and a 100 MHz frequency band. The pseudo colors used give qualitative information on the received power covering a power range of some 60 dB like in Figure 3.3. The  $360^\circ$  panoramic photo taken from the same position at the bottom of the figure covers an elevation from approximately  $-25^\circ$  to  $25^\circ$ . The numbers above the photo correspond to the numbers used in Figure 3.5 for the base stations. The figure again shows the strong interfering GSM 1800 and UMTS downlinks but now correlates the measurements with the base station locations in the spatial domain.

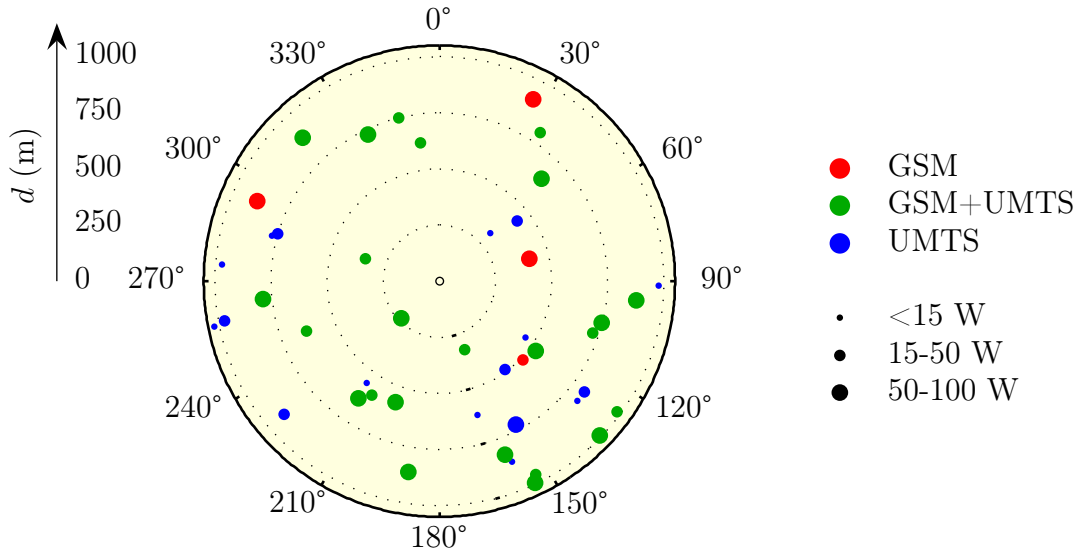


Figure 3.4: GSM and UMTS base stations within 1 km of the Vienna Ground Station for MOST in 18<sup>th</sup> district. The empty space in the north is the Türkenschanzpark (data source: [56]).

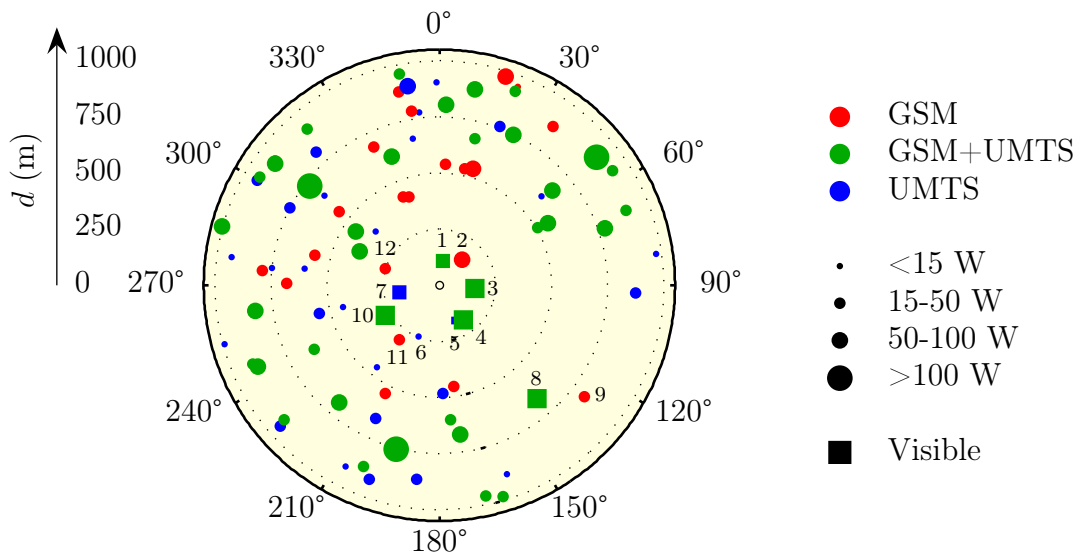


Figure 3.5: GSM and UMTS base stations within 1 km of the new TU Wien Ground Station. The empty space in the south-east is the gardens of Schloss Belvedere. The numbers are also used in other figures (data source: [56]).



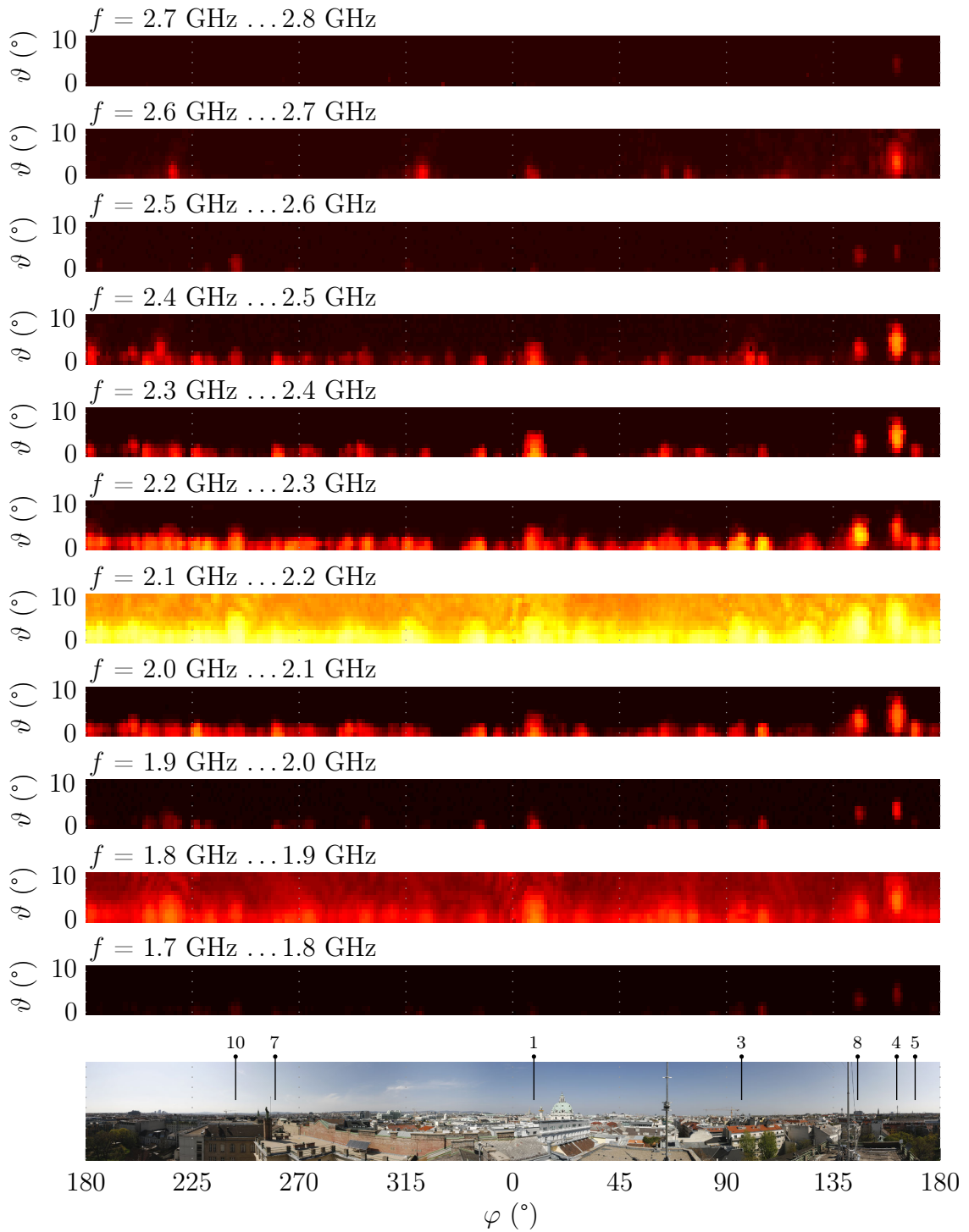


Figure 3.6: Radio interferers plotted vs. azimuth, elevation and frequency. Each subplot is a  $10^\circ$  elevation strip covering a frequency band of 100 MHz. The numbers used as markers in the photo correspond to the numbers of the base stations in Figure 3.5.

### 3.2.2 Radio Horizon

The choice of the location of the TU Wien Ground Station in the city of Vienna, rather than on some elevated location outside the city, limits the radio horizon of the ground station. That is, buildings in the vicinity and mountains in the outskirt areas of the city prohibit communication below some elevation angles depending on the azimuth. To avoid outage of communication because of structures or buildings close to the ground station, the antenna system has been elevated some 6 m above the roof, which is some 34 m above the ground. Detailed measurement results on the radio horizon of the TU Wien Ground Station are presented later in Section 6.2.

## 3.3 Ground Stations in Education

Not only satellites are well suited for the training of students – ground stations offer an even better learning basis for students in telecommunications because they are easier accessible than satellites. For examples of ground stations, satellite laboratories in education or other ground stations dedicated to single educational satellite missions see [6, 7, 38, 57, 58]. Possible experiments for students with the TU Wien Ground Station are treated later in Section 4.4.

## 3.4 Ground Station Networks and GENSO

Each satellite needs at least one possibility of communication with Earth to deliver the data obtained in space. So, at least one ground station is necessary per satellite. Further ground stations extend the communication duration with a satellite if placed at the correct locations on Earth. The idle times of a ground station between passes and the costs for multiple ground stations per mission can be decreased if several ground stations can be shared between several satellite missions. This idea leads to ground station networks. Otherwise, if several ground stations are available in different locations in a ground station network, the data received from several of them can be combined to increase the signal quality and to yield less outage [9, 11, 37, 59, 60].

One of these ground station network is the Global Educational Network for Satellite Operations (GENSO). Figure 3.7 gives a coarse overview of the system. A special software package written in the Java programming language enables the remote use of ground stations within GENSO if supported by the satellite mission. The GENSO layer on the mission side, adapts the data packets from the specific satellite

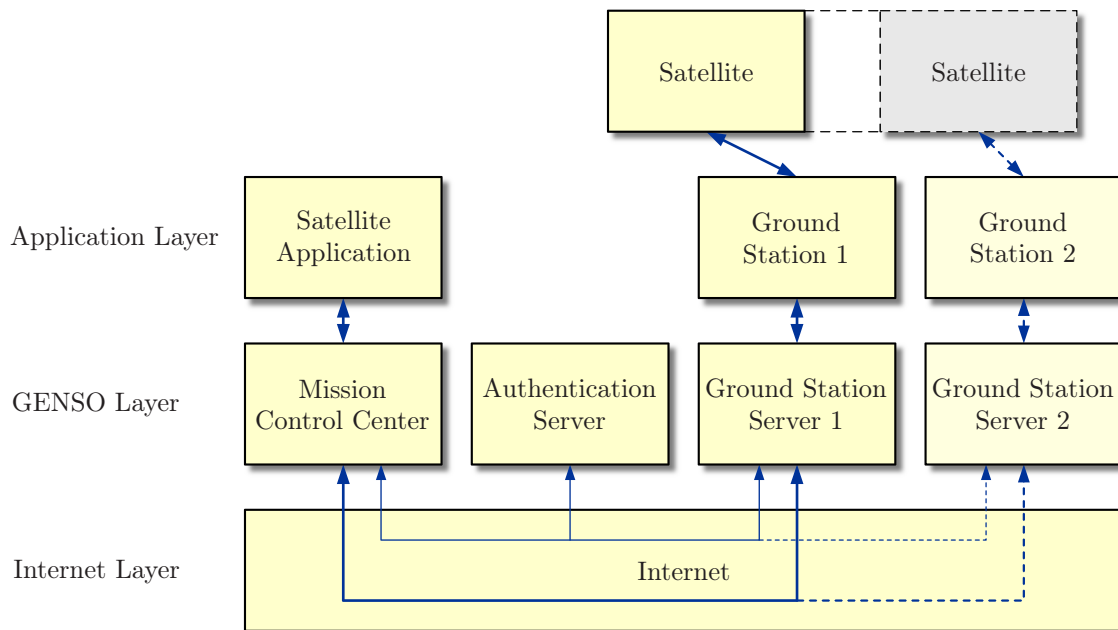


Figure 3.7: The GENSO layout with two ground stations working on one satellite [11, 36].

application to GENSO. At the ground station, this software – together with drivers for the ground station hardware and the hardware itself – performs the actual communication with the satellite. A central authentication server negotiates the data exchange between the mission control centers and the ground stations. On the one hand, because there are no requirements on the hardware or even the frequency bands in GENSO, GENSO is open to a multitude of satellite missions. On the other hand, this flexibility has the risk of not finding many partners in the network. A strong emphasis has been placed on amateur radio ground stations and amateur radio frequencies (see Table 2.1), which reduces the number of open parameters [11, 61, 62].

### 3.5 Vienna Ground Station for MOST

In 2002, a ground station in the 18<sup>th</sup> district of Vienna has been built by our institute dedicated to MOST [8]. This ground station is known as the Vienna Ground Station for MOST. It only supports the necessary S-band for up- and downlink and the protocols required for MOST. The TU Wien Ground Station builds upon this experience [63]. For example, several components of the TU Wien Ground Station’s S-band uplink described in Section 5.3 are adapted from those used at the Vienna Ground Station for MOST [8].

# Chapter 4

## TU Wien Ground Station Concept

Using the knowledge gained in Chapters 2 and 3, this chapter introduces the concept for the TU Wien Ground Station which enables multi-mission support and eases the use of the ground station in education. The concept builds upon a segmented approach, described in Section 4.1, open and extensible interfaces, described in Section 4.2, and virtualization, described in Section 4.3. Details on the use of the TU Wien Ground Station in education are given in Section 4.4.

In Chapter 2, I have shown that there is a huge diversity in satellites' communication parameters. The TU Wien Ground Station has been designed with flexibility in mind in order to adapt to many different satellites. However, the group of satellites has been limited to LEO satellites. Furthermore, a few satellites have been highlighted in Chapter 2 which are the most interesting for the ground station. In Section 4.5, I come back to these satellites and show how the overall concept fits together with the satellites.

Building on the concept described in this chapter, Chapter 5 will detail the realization of the ground station.

### 4.1 Segments of the Ground Station

To communicate with many different satellites, great flexibility is demanded from a ground station. Therefore, the TU Wien Ground Station is divided into modular subsystems. By definition of clear and open interfaces between each of the subsystems, I gain the flexibility to not only support multiple missions, but also to adapt to future missions by only adding some mission specific subsystems [64].

As visible in Figure 4.1, the ground station is divided into three segments, namely the segments for

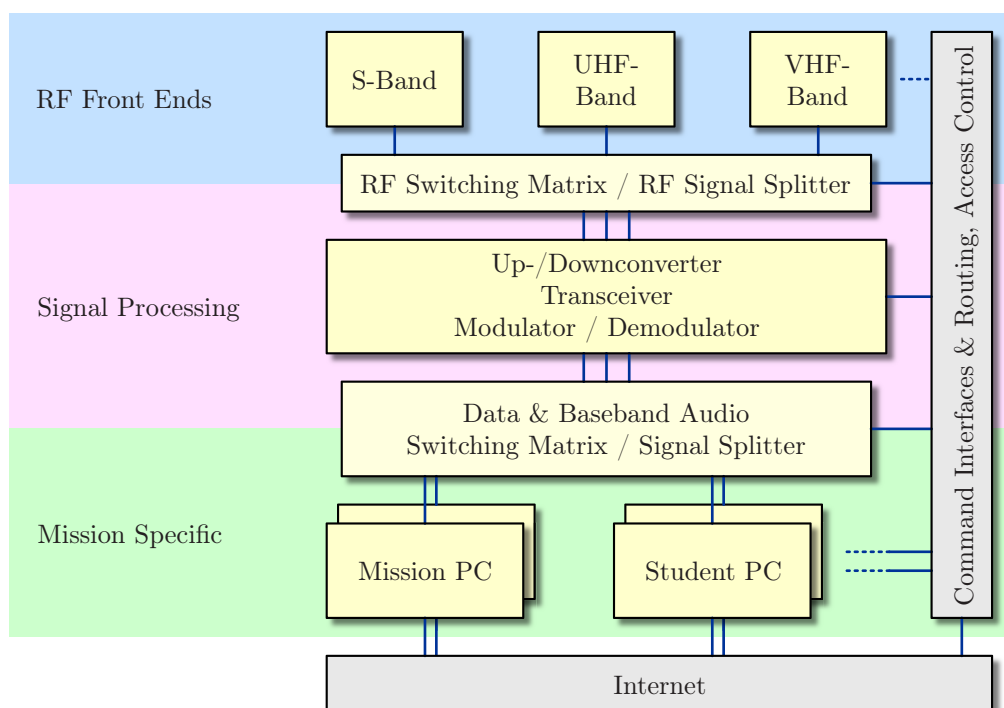


Figure 4.1: The three segments of the TU Wien Ground Station.

- the frequency-band-specific RF *front ends* including the antennas and their rotators,
- the RF *signal processing* components and converters between analog and digital domain, like transceivers, modulators, demodulators and terminal node controllers (TNCs) and
- the *mission or experiment specific data processing components* usually realized with personal computers (PCs).

Comparing this segmentation with other work, the *front ends* and the *signal processing segment* correspond to the “Tx/Rx Pipeline” in [10, 65], while the *mission specific data processing components* subsume the “Session Group” and some portions of the “Master Group” therein.

In the following, I will call a chain of components for a specific transmit or receive scenario “pipeline”, adopting the notation from [10]. Different transmit or receive pipelines can then be formed using different combinations of subsystems. Details are given later in Section 4.5.

Between each segment and also between some of the components inside each segment, signal switches or signal splitters are necessary. Here, the term “signal” includes for example RF signals, serial or parallel digital data, audio signals and

commands or status information. The switches and splitters allow to route signals flexibly for easy extension of the ground station to new missions or requirements. Where possible, splitters are used instead of switches because this allows for concurrently feeding signals to several subsequent components. This enables for example parallel processing and storage of data on the one hand, while monitoring the signal quality on the other hand. In addition, this allows comparing subsystems by comparing the signals after each path.

By adding *front ends*, further frequency bands can be made accessible. Adding components to the *signal processing segment* typically adds another modulation scheme or another data representation form required for a specific mission. Such a new feature is then available to all other missions as well. Finally, support for a new mission typically calls for an additional PC in the *mission specific segment*.

Spanning all three segments, various *command interfaces*, *command routing and access control components* are necessary. This extra block is responsible for actually setting up a transmit or receive pipeline, depending on the requirements and privileges of the respective mission.

#### 4.1.1 RF Front Ends

The RF front ends are the frequency-band specific components of the ground station. They are responsible for receiving and transmitting the signals from/to the satellite and for converting them to/from some common intermediate frequency (IF). The front ends of the TU Wien Ground Station were designed to support the satellites highlighted in Chapter 2. The respective frequencies are listed in Table 4.1 and Figure 4.2. Figure 4.2 shows the up- and downlink frequencies of CoRoT, MOST and BRITE Constellation.

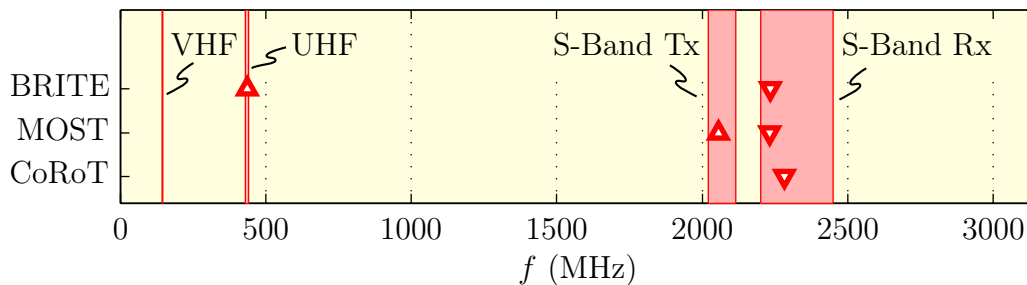


Figure 4.2: The four RF front ends of the ground station and selected satellite's up- and downlink frequencies.

Name	Start MHz	Stop MHz	Direction	Description in Sections
VHF	144	146	up/down	5.4, 5.5.6
UHF	430	440	up/down	5.4, 5.5.1 to 5.5.5
S-Band Tx	2025	2110	up	5.1, 5.3
S-Band Rx	2200	2450	down	5.1, 5.2

Table 4.1: Border frequencies of the four RF front ends of the TU Wien Ground Station with their designated transmission direction. The last column references the sections where the particular front end is described.

The VHF RF front end has been included because of amateur radio satellite services. The signals around 145 MHz are directly used by the signal processing segment. The front end can either transmit or receive at one time.

The UHF RF front end is used both by amateur radio satellites and by BRITE Constellation. Again, the signals near 435 MHz are directly used by the signal processing segment without up- or downconversion. Similar to the VHF RF front end, the UHF front end has to be switched either into transmit or into receive mode. BRITE Constellation utilizes the UHF front end for its uplink.

The S-band transmit RF front end covers the frequency segment for space operations from 2025 MHz to 2110 MHz (see also Figure 3.3). Its IF is in the UHF band around 435 MHz. This front end is used for the MOST uplink.

Because of CoRoT and MOST, the S-band receive RF front end includes the frequency range for space operations from 2200 MHz to 2290 MHz. It also includes amateur radio satellite services from 2400 MHz to 2450 MHz. It can only be used for reception, but it can be combined with any other RF front end – including the S-band transmit front end – for full duplex operation. Its IF for the space operation frequency band is in the VHF band around 140 MHz.

The RF front ends also include the antenna systems with their rotators.

### 4.1.2 Signal Processing Segment

The signal processing segment contains components, which can be shared among different missions. Of course, the minimum features of this segment are indicated by the particular missions. Therefore it includes the modulators and demodulators necessary for CoRoT, MOST and BRITE Constellation.

For amateur radio satellites and GENSO, the signal processing segment downconverts (and partially demodulates) the signals to baseband frequencies – also called audio frequencies (AFs). The resulting signals can then be processed by the sound card of a PC or a modem inside a TNC.

### 4.1.3 Mission Specific Segment

The mission specific segment contains all components which cannot be shared among missions because they are too specific. Typically, we find here components for the higher data processing layers like TNCs or computers which control the data flow between the ground station and the satellite.

### 4.1.4 Control and Supervisory Block

Spanning all three segments, a common control and supervisory block provides various command interfaces, command routing facilities and access control among the components. This extra block is responsible for actually setting up the respective transmit or receive pipeline before each satellite pass (as described later in Section 5.8.3).

It monitors the ground station's components, logs performance data and periodically runs performance tests. This block also provides interfaces to the outside world over the Internet and is responsible for the remote access to the ground station.

## 4.2 Ground Station Interfaces and Multi-Mission Support

Between the segments, clear and open interfaces are defined. The interfaces between the front ends and the signal processing segment are coaxial connectors which carry the RF signals with defined power levels at some IF. For the digital data, Ethernet or signals compliant to RS-232 or EIA-530 are used. The Ethernet connections are realized in a ground-station-internal local area network (LAN).

Most of the interfaces do not carry payload data from the satellite mission, but transfer commands to and from the control block to the components for setup and supervision. Figure 4.3 illustrates the interfaces of the control block and the mission specific segment of the ground station.



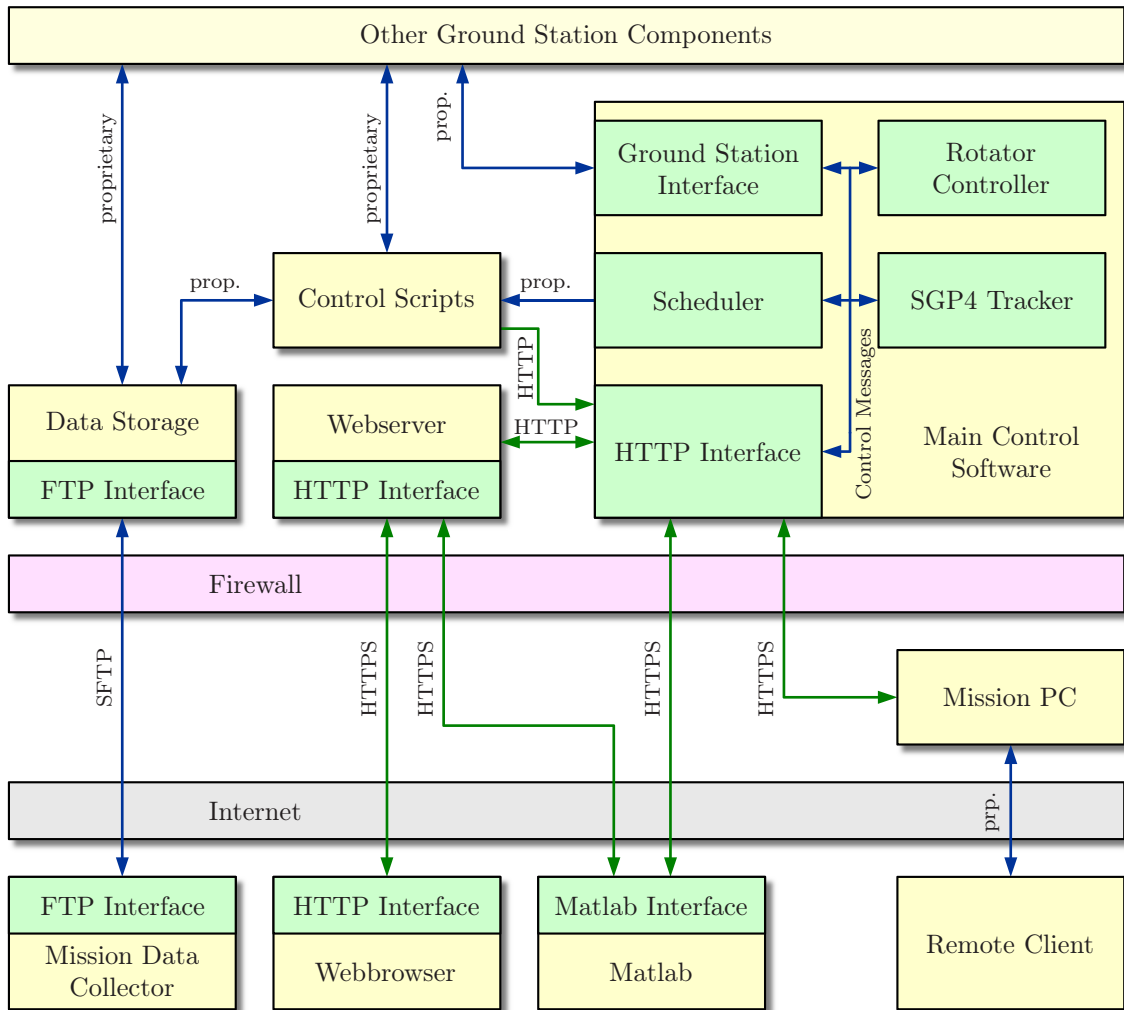


Figure 4.3: Block diagram illustrating the control interfaces of the ground station.

- At the heart of the control block, there is the *Main Control Software* described in detail in Sections 5.7, 5.8 and 5.9. It contains – among others – blocks for controlling the rotator, tracking satellites and scheduling tasks.
- The *Data Storage* and the *Mission PC* belong to the mission specific segment described in Section 5.6. They can be behind or in front of the firewall and their interfaces are also mission dependent.
- There are two webservers – one built into the Main Control Software, the other running on a separate PC for the sake of robustness. While the built-in webserver heavily interacts with the ground station by means of *Control Scripts*, the standalone webserver is only used for remote access.
- The proprietary links between some of the components utilize mostly Ethernet, RS-232 or EIA-530.

The webbrowser interface and the Matlab interface realized with these two webservers are described in the next sections.

### 4.2.1 HTTP Interface

Where possible the hypertext transfer protocol (HTTP) standard or its encrypted version, HTTP over secure socket layer (HTTPS), are used inside the ground station and when connecting to the outside world (see green lines in Figure 4.3).

There is a webserver built into the *Main Control Software*. It accepts commands which are then translated into actions for the ground station. The command structure is described in Section 5.7. Mission PCs are only allowed to send commands to the ground station via this interface. As a result, the interface controls the authorization of the specific missions. The webserver also acts as an information broker and provides status information to others.

### 4.2.2 Matlab Interface

The Matlab interface builds upon the HTTP interface. It provides Matlab functions for communication with the ground station's

- rotators (azimuth, elevation, position, tracking source),
- front ends (selection, signal routing, frequency, data rates),
- modulators and demodulators (data, mode, status information) and
- further supporting components.

The Matlab functions translate the specific tasks into HTTP requests which are sent to the internal webserver of the ground station. The functions interpret the answers received back into Matlab data [66].

Lots of the measurements from Chapters 5 and 6 have been conducted using this Matlab interface.

#### 4.2.3 Remote Access to the Ground Station

Remote access to the ground station is possible over the Internet. Three different scenarios have to be distinguished and are implemented:

- Remote access for the missions is handled mission specific and is described in Section 5.6.
- Remote access from operation personal for supervision or control of the ground station is realized with different graphical user interfaces (GUIs) utilizing a web-browser (see Section 5.7.4).
- Further remote access is possible using flexible interfaces like the Matlab interface, or over virtual private network (VPN) when a more direct access is required.

### 4.3 Virtualization and Ground Station Networks

The modular and layered approach used for the ground station eases virtualization. Commands are sent by the mission PCs to the components only via the webserver inside the *command interface* block. This block allows for hardware abstraction, i.e. it presents hardware to other components in their expected way. For example from the viewpoint of the mission PC, there is a dedicated, mission specific hardware setup [10].

The flexibility gained by virtualization also enables easy inclusion of the ground station into ground station networks like GENSO or others (see Section 3.4 and [7, 9, 10, 59]). By means of virtualization the ground station network is presented with the hardware it expects.

## 4.4 The TU Wien Ground Station in Education

One of the objectives of the TU Wien Ground Station is to serve the education of students. This is facilitated by the modular structure of the ground station and by the open interface approach between the components and especially between the segments.

In a first phase, students can experience a live, real world satellite link. They can insert a probe – e.g. a spectrum analyzer or a serial data analyzer – at any interface between two components and sample the received or transmitted signals. Attenuators or noise generators can be temporarily inserted into the pipelines to systematically degrade the overall ground station performance to demonstrate its behavior under varying conditions.

In a second phase, data recordings of satellite passes can be used in a playback scenario by students to simulate a satellite. By this, the operation of a ground station can be learned. The approach has similar objectives as [67].

In a third phase, students can set up a separate PC in parallel to the actual mission PCs. In this setup they can tap the receive or transmit pipeline at any given point and receive the same data as the mission PC receives or supervise the data the mission PC transmits. Figure 4.4 illustrates this for an example scenario, where students build their own modem and design a TNC in software. While keeping the ground station up and running, students can run their experiment without interfering with the mission. By using the mission data output as a reference feedback, students are even able to judge their own results quantitatively.

In a further scenario, students can substitute components of the ground station – be it hardware or software – by self designed, pre-tested versions. For example the modem could be replaced by a software defined radio (SDR) like in [68]. Inspired by an earlier work [69], a diploma student and I have investigated this scenario for the ground station in a recent diploma thesis [70].

Last but not least, several students have been involved in the actual construction of the ground station, e.g. in student projects or during their master thesis. Six master theses have been written in support of the ground station and have been supervised by me [69–74]. A seventh is currently in progress.

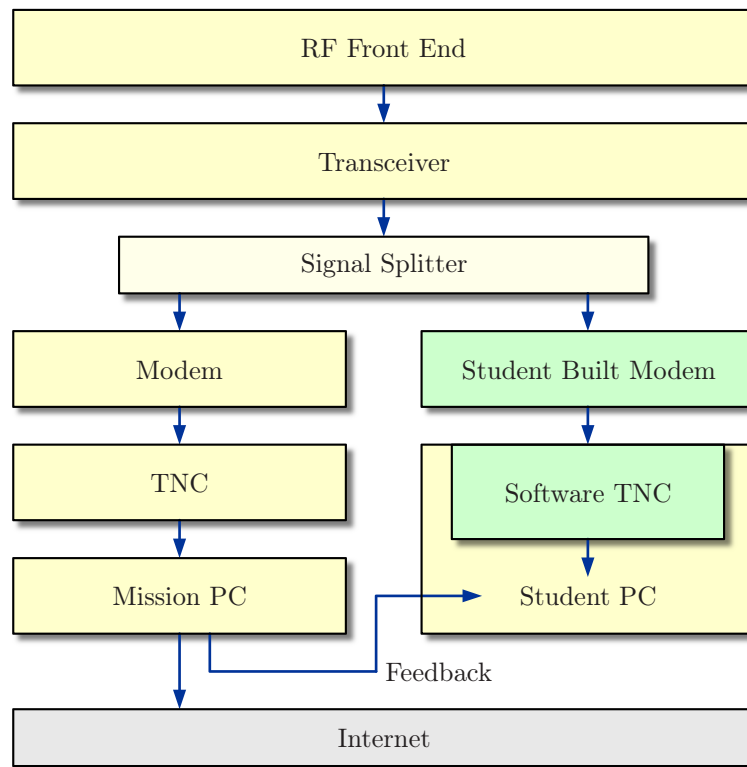


Figure 4.4: Block diagram illustrating a parallel pipeline for a student's experiments.

## 4.5 Pipelines for Different Missions

Each satellite mission requires a different pipeline for communication with the respective satellite. A pipeline is a specific chain of components from the three segments used for transmission or reception to/from a satellite. A pipeline is formed (i.e. is set up and initialized) before a satellite pass (see [10] and Section 5.8.3).

### 4.5.1 CoRoT Pipeline

The CoRoT downlink in S-band uses the S-band receive RF front end. The signals are downconverted to an IF of 140 MHz and demodulated with a commercial satellite modem. The modem is connected to the CoRoT TNC where the data is stored in files which are later collected by CNES.

### 4.5.2 MOST Pipeline

The MOST uplink in S-band uses the S-band transmit RF front end. The commands to the satellite are transferred from the mission control center in Canada to the mission specific PC in Vienna over the Internet. After conversion to a serial data stream by the MOST TNC, the data is modulated and upconverted into S-band.

MOST uses the S-band receive RF front end for receiving data from the satellite. The signal is demodulated with the same or a similar commercial satellite modem. A switch connects the modem to the MOST TNC. After that, the data is directly sent to Canada where upon delivery an acknowledge response is issued for the satellite. The communication is full duplex, MOST only transmits upon receiving an uplink signal.

### 4.5.3 Future Pipeline for BRITE

Since BRITE will be launched by the end of 2012 or begin of 2013, the pipeline for BRITE Constellation is not ready yet, although the components have been selected and characterization measurements are presented in Chapter 5.

The satellites forming BRITE Constellation all use the same frequencies. For the uplink, they utilize the UHF front end. For the downlink the S-band receive RF front end is used. Similar to MOST, a mission PC and a BRITE specific TNC are used for data processing. No separate upconverters are necessary for BRITE because the signals generated by the TNC and modulated by the UHF/VHF radio are already at the correct UHF frequencies. BRITE is operated in full duplex mode similar to MOST.

### 4.5.4 Proposed Interaction with GENSO

Since GENSO does not represent a single satellite mission, but rather a generic network of satellite ground stations, there is no predetermined configuration and several different pipelines have to be available to support potential satellites. However, typical satellites utilize the amateur radio VHF, UHF or S-band for up- and downlink. Full duplex operation in GENSO is preferably using different frequency bands for up- and downlink.

For starters, one UHF/VHF transceiver will be available. The radio directly supports the VHF and UHF bands. Either one can be used for uplink and/or downlink.

For some satellite missions of the GENSO project, the audio connectors of the radio are then directly connected to the sound card inputs or outputs of a PC to perform the analog to digital and digital to analog conversion. This allows – for small bandwidths and low data rates (e.g. some 5 kHz and 9600 bps) – very flexible signal processing, because processing is easily definable by software on the PC. It also allows for direct storage or remote transfer of the captured data. Further processing can be performed offline and/or remotely.

For other satellite missions, the pipeline could include a TNC with modems. The TNC is responsible for the HDLC (high-level data link control) and/or AX.25 protocol processing and relays the data to/from the PC, typically over a serial RS-232 connection.

# Chapter 5

## Realization of the TU Wien Ground Station

As indicated in Figure 5.1, the TU Wien Ground Station is structured in modular building blocks. There are

- the antennas for different frequency bands (Sections 5.1 and 5.4)
- mounted on a rotator (Section 5.9),
- the corresponding RF front ends (Sections 5.2, 5.3 and 5.5),
- the demodulators and modulators (Sections 5.2.10, 5.3 and 5.5),
- the mission specific components (Section 5.6) and
- the control software of the ground station with its scheduler (Sections 5.7 and 5.8).

Each of the blocks can be related to one or two of the segments described in Section 4.1 and Figure 4.1. All components have been selected to fulfill the requirements already devised in the previous chapters. The following sections recapitulate these requirements and give the realized solution and the characterization of the components selected.

### 5.1 S-Band Antenna System

The S-band antenna system consists of a 3.7 m parabolic reflector with a feed assembly used for both the receive and the transmit RF front end respectively. The feed assembly is discussed in Section 5.2. Measurements are also given there. The setup is mounted on an azimuth/elevation rotator to track the satellites, which is discussed in Section 5.9.1. For a photograph see Figure 7.2 in Chapter 7.

The parabolic dish is a CKD 12 by SAMI and has been selected as optimum choice for the ground station in terms of size, weight, quality, availability and price. It



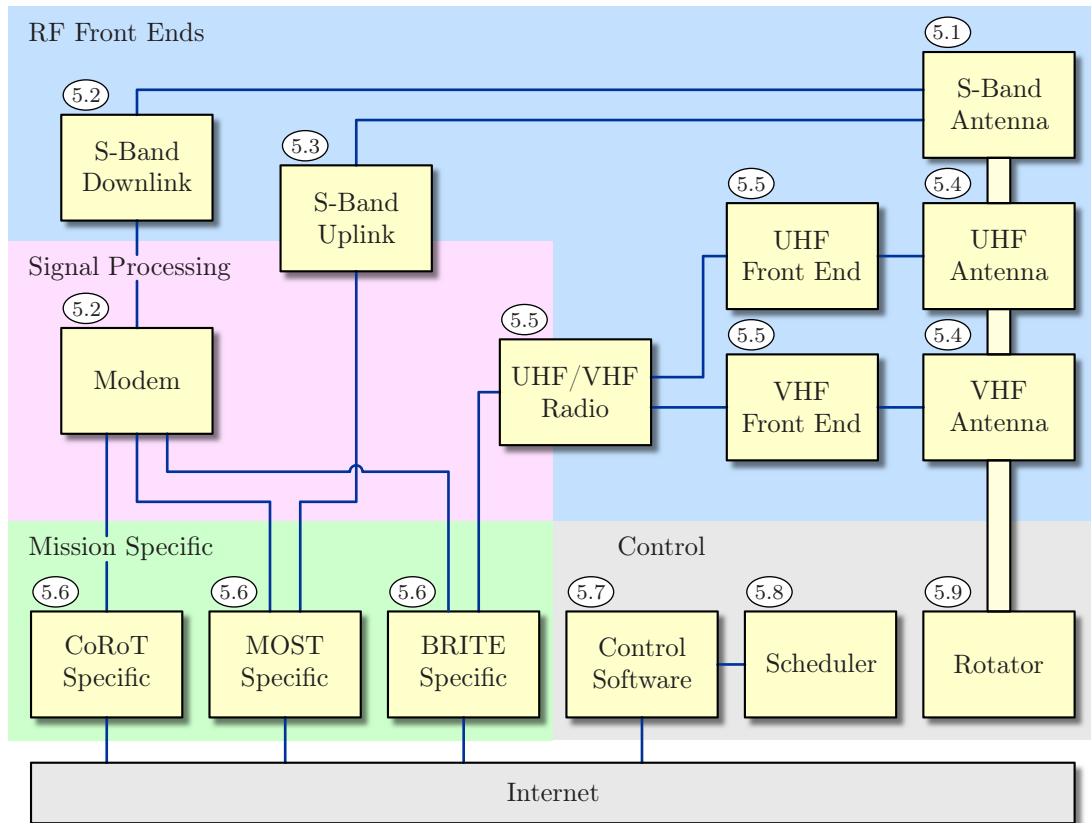


Figure 5.1: Block diagram of the TU Wien Ground Station. The circled numbers reference the corresponding sections of the text.

is mostly made of aluminum ribs and aluminum mesh. The openings in the mesh are in the order of 1.5 mm, which is small with respect to the used wavelength (approximately 13 cm in the S-band). Consequently, the openings do not severely degrade the performance of the reflector. Using a mesh instead of a solid metal sheet reduces the weight of the dish considerably. Furthermore, the openings allow the wind to pass through and therefore reduce the wind cross section of the antenna.

The CKD 12 is a prime focus antenna – the feed is mounted in its center without any further secondary reflector [52]. By this, the antenna is rotationally symmetric, which is desirable due to the changing pointing direction during a pass. When outside a satellite’s pass, the antenna is parked pointing to the zenith, i.e.  $\vartheta = 90^\circ$ . The antenna with a focal distance  $f_a$  and a diameter  $D$  has a ratio  $f_a/D$  of 0.4. This relatively shallow shape results in a low wind load of the antenna when parked.

The gain of an aperture antenna depends on its reflector area  $A$  and its efficiency  $\eta$  with respect to the squared wavelength  $\lambda$ . In case of a parabolic dish antenna it depends on the efficiency  $\eta$  and the squared quotient of the reflector diameter  $D$  divided by the wavelength  $\lambda$  [75, 76]

$$G_{\text{ant}} = G_{\text{R1}} = \frac{4\pi A}{\lambda^2} \eta = \left(\frac{\pi D}{\lambda}\right)^2 \eta. \quad (5.1)$$

The 3.7 m parabolic dish has an efficiency of 0.57 and a gain of about 36 dBi in the S-band according to the manufacturer.

## 5.2 S-Band Downlink

The S-band receive RF front end is designed to receive signals between 2.20 GHz and 2.45 GHz. The signals are downconverted to an IF of about 140 MHz. This downlink front end is used for the CoRoT, MOST and BRITE satellites. Also described in this section are the satellite modems which belong to the signal processing segment.

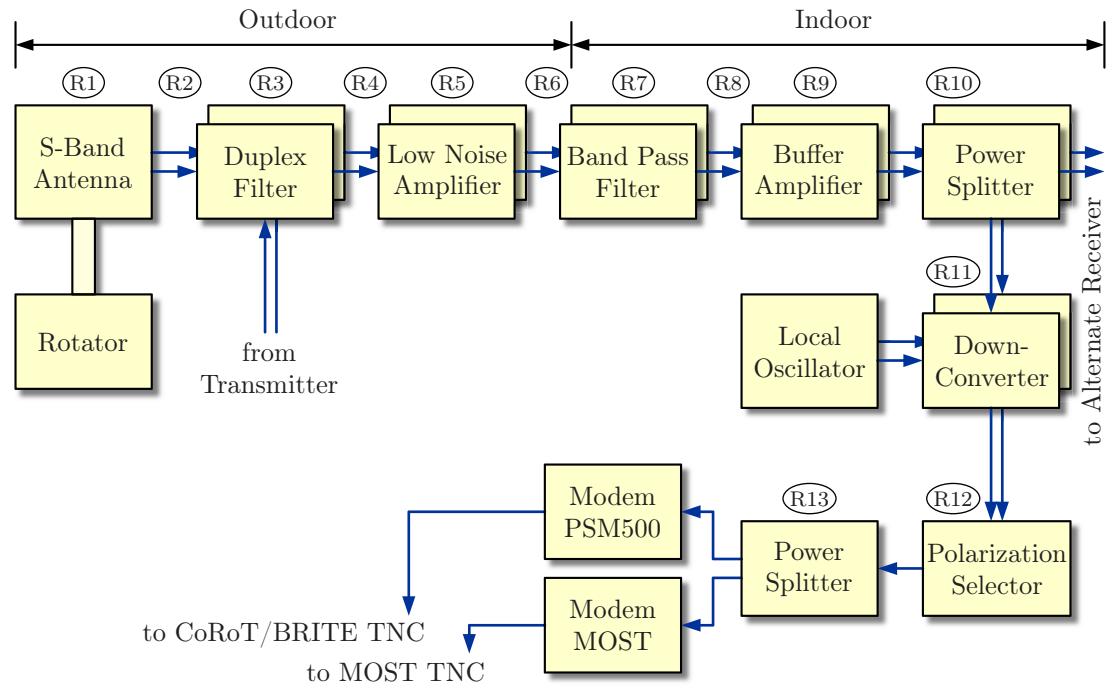


Figure 5.2: Block diagram of the S-band receive RF front end. The circled numbers correspond to the component index  $i$  in Table 5.1.

Figure 5.2 shows the elements of the front end. The antenna block consists of the 3.7 m parabolic dish and the feed. The parabolic dish has already been described in Section 5.1. The feed is dual linearly polarized (LP) and is described in this section. The feed assembly contains – apart from the feed itself – duplex filters and LNAs. The following components in the signal path are two band pass filters (BPFs), buffer amplifiers, power splitters and a dual-downconverter. The buffer amplifiers are necessary to adjust the power levels adequately. The power splitters allow to connect an alternate receive pipeline or allow for an easy measurement access. After the downconverters a polarization selector combines the two signals with LP states to a single signal with either left hand circular polarization (LHCP) or right hand circular polarization (RHCP). The last components shown in Figure 5.2 are two modems which demodulate the analog received signal.

### 5.2.1 Link Budget

Following the block diagram in Figure 5.2, Table 5.1 lists all the components of the S-band receive front end. The components are indexed from R1 to R13 in both the figure and the table.

The components are interconnected by coaxial cables. In the link budget, the cables at the antenna side of the front end – with bigger impact on the overall noise figure of the system – are listed explicitly with their own component index, while the other cables are only implicitly included by their losses in the respective subsequent component.

Table 5.1 gives the respective gain  $G_i$  and noise figure  $F_i$  for each of the components, anticipating their detailed description in the following sections. Gains and noise figures for active devices are taken from their datasheets, while for passive devices (e.g. cables) the noise figures  $F_i$  are calculated from their losses or attenuations  $L_i$  [1, 50, 52] by

$$F_i = L_i = 1/G_i. \quad (5.2)$$

The cumulative gain  $G_{\text{cum},i}$  from the system's input to the output of each component  $i$  is given by

$$G_{\text{cum},i} = \prod_{i=1}^n G_i. \quad (5.3)$$

The gain of each component has been chosen not to overload the input of the subsequent component regarding its maximum input power  $P_{\text{in,max}}$ , its 1 dB compression point  $P_{1\text{dB}}$  and its 3<sup>rd</sup> order intercept point  $IIP_3$ .

Each of the components has also been chosen to optimize the overall  $G/T_s$  of the S-band receive front end. Table 5.1 lists  $G/T_{s,i}$ , which is explained later in this

section together with  $G/T_s$ . The goal is to guarantee a minimum  $G/T_s$  required by the satellites (see Appendix D and Table 5.1).

### Graphical Representation of the Link Budget

Figures 5.3 and 5.4 give a graphical representation of the link budget for the down-link signals of CoRoT and MOST. The two blue lines together with the shaded area show the upper and lower limit of the expected signal power. The red line shows the thermal noise level.

The signal power  $P_i$  is calculated by

$$P_i = P_{\text{rx}} G_{\text{cum},i}, \quad (5.4)$$

where  $P_{\text{rx}}$  refers to the expected received signal power.

$i$	Component Name	$G_i$ dB	$F_i$ dB	$G_{\text{cum},i}$ dB	$G/T_{s,i}$ dB/K
R1	S-band antenna & feed	36.4		36.4	17.5
R2	Semi-rigid cable	-0.1	0.1	36.3	17.2
R3	Duplex filter	-0.3	0.3	36.0	16.2
R4	Semi-rigid cable	-0.1	0.1	35.9	15.9
R5	Low noise amplifier	31.2	0.5	67.1	14.6
R6	Cables 40 m	-6.2	6.2	60.9	14.5
R7	Band pass filter	-0.5	0.5	60.4	14.5
R8	Cable	-0.6	0.6	59.8	14.5
R9	Buffer amplifier	19.1	2.6	78.9	14.5
R10	Power splitter	-3.2	3.2	75.7	14.5
R11	Downconverter	29.2	0.8	104.8	14.5
R12	Polarization selector	-2.3	2.3	102.5	14.5
R13	Power splitter	-3.0	3.0	99.5	14.5
	- $G/T_s$ required for CoRoT				8.2
	- $G/T_s$ required for MOST				9.9

Table 5.1: Values for the link budget of the S-band receive RF front end.  $G_{\text{cum},i}$  and  $G/T_{s,i}$  refer to the output of the corresponding component with index  $i$ .

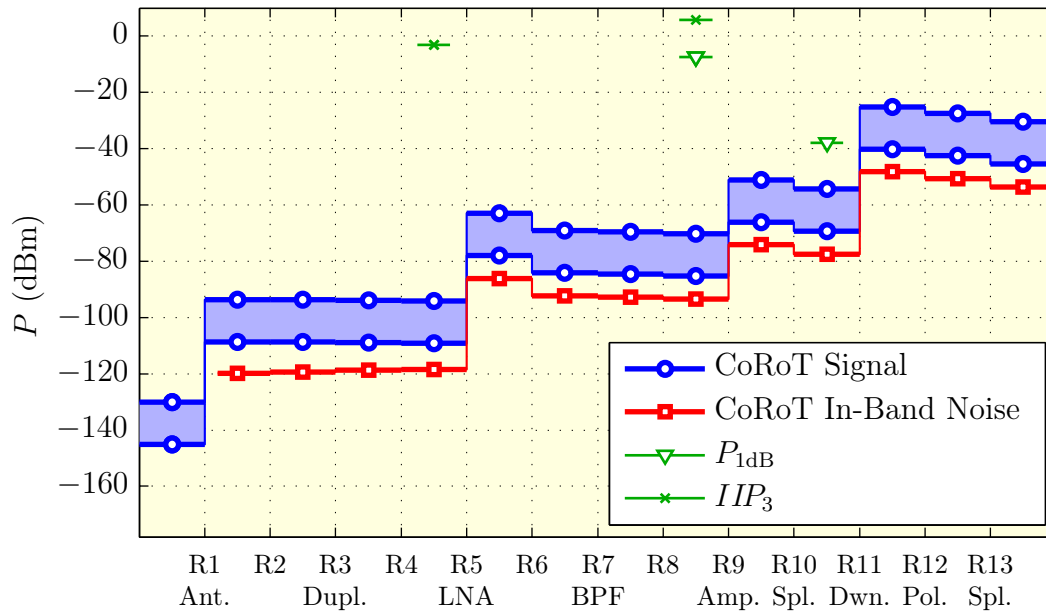


Figure 5.3: Signal power and in-band noise power for the CoRoT receive pipeline. The numbers on the abscissa correspond to the component index  $i$  in Table 5.1.

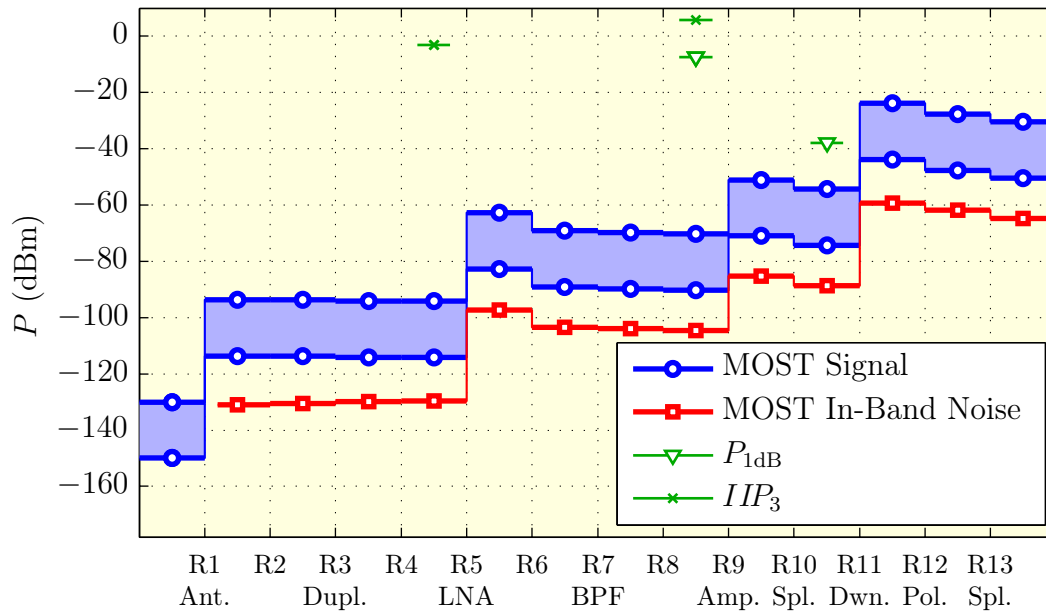


Figure 5.4: Signal power and in-band noise power for the MOST receive pipeline. The numbers on the abscissa correspond to the component index  $i$  in Table 5.1.

The change in the signal levels between the input (i.e. left) side and the output (i.e. right) side is described by

$$P_i = P_{i-1} G_i \quad (5.5)$$

with the gain  $G_i$  of the corresponding component  $i$ . For the calculations,  $P_{\text{rx}}$  is used as derived in Appendix D. For CoRoT levels between  $-145$  dBm and  $-130$  dBm are used in Figure 5.3, respecting lower and higher elevation angles as well as bigger path losses that exceed the values used for the calculations in Appendix D. Similarly, levels between  $-150$  dBm and  $-130$  dBm are used for MOST in Figure 5.4.

The in-band noise power  $N_i$  at each component's output is calculated based on the bandwidth  $B_i$  occupied by the signal, the system's noise temperature  $T_{s,i}$  and the cumulative gain  $G_{\text{cum},i}$  [52]

$$N_i = k_B T_{s,i} B_i G_{\text{cum},i}. \quad (5.6)$$

The quotient between the signal power and the noise power is the signal to noise ratio (SNR)

$$\text{SNR} = \frac{P_i}{N_i}. \quad (5.7)$$

The SNR is proportional to  $G/T_{s,i}$ .

Furthermore, in Figures 5.3 and 5.4, for some components, green markers are added to indicate their 1 dB compression point  $P_{1\text{dB}}$  and their 3<sup>rd</sup> order intercept point  $IIP_3$ , both referred to the component's input.

### Figure of Merit $G/T_s$

The ‘‘figure of merit’’  $G/T_s$  of a radio receiving system is a measure for its ability to receive low level signals effectively. It is well suited for the characterization of the ground station's receive RF front end because it is independent of the received signal strength. Therefore,  $G/T_s$  neither depends on the satellite's transmit power nor on its distance to the ground station [1, 52, 77].

$G/T_s$  is calculated at one point of the system – typically the antenna's output. In Table 5.1, the values given for  $G/T_{s,i}$  correspond to  $G/T_s$  which would be obtained if all components following component  $i$  would be omitted. This value of course changes when further components are included.

For  $G/T_s$  we need the antenna's gain and the noise temperature of the system  $T_s$ .

$$G = G_{\text{ant}} = G_{\text{R1}} \hat{=} 36.4 \text{ dBi} \quad (5.8)$$

$$T_s = T_{\text{ant}} + T_{\text{rx}} \quad (5.9)$$

For the system's noise temperature in turn we need the antenna's noise temperature  $T_{\text{ant}}$  and the composite noise temperature of the receive front end  $T_{\text{rx}}$ .

The antenna's noise temperature is the temperature the antenna "sees". It is a composite of the cold sky's temperature  $T_{\text{sky}}$  which is assumed 10 K, other influences along the signal path and ohmic losses of the antenna and its feed. The most prominent contributions along the path are rain and clouds in the atmosphere. Rain has a temperature of 280 K and clouds of 260 K [2, 8, 75, 78]. Because of the ohmic losses, the physical temperature of the antenna  $T_{\text{ph}}$  also contributes to the overall noise temperature of the antenna [77, 79, 80]

$$T_{\text{ant}} = \left( \frac{T_{\text{sky}}}{L_{\text{rain}}} + T_{\text{rain}} \left( 1 - \frac{1}{L_{\text{rain}}} \right) \right) \eta_{\text{ohm}} + T_{\text{ph}} (1 - \eta_{\text{ohm}}). \quad (5.10)$$

Assuming rain with a rain attenuation  $L_{\text{rain}}$  of 1 dB, an ambient temperature  $T_{\text{ph}}$  of 290 K and an ohmic efficiency  $\eta_{\text{ohm}}$  of 95% we obtain

$$T_{\text{ant}} = 76.8 \text{ K}. \quad (5.11)$$

For the receiver's noise temperature, we need the noise figure of each of the component and the cumulative gain of each of the preceding components [52]. We start by obtaining the component's equivalent noise temperature  $T_i$  from the respective noise figure  $F_i$

$$T_i = T_0 (F_i - 1) = 290 \text{ K} (F_i - 1) \quad (5.12)$$

using the standard temperature  $T_0$  of 290 K.

The receiver's composite noise temperature is then calculated as [52, 76, 81]

$$T_{\text{rx}} = T_{\text{R2}} + \frac{T_{\text{R3}}}{G_{\text{R2}}} + \frac{T_{\text{R4}}}{G_{\text{R2}} G_{\text{R3}}} + \cdots + \frac{T_n}{G_{\text{R2}} G_{\text{R3}} \cdots G_{n-1}} = 78.1 \text{ K}. \quad (5.13)$$

This results in a calculated

$$G/T_s = 28.2 \text{ K}^{-1} \hat{=} 14.5 \text{ dB/K}. \quad (5.14)$$

for the S-band receive RF front end of the TU Wien Ground Station. Measurements show a value of 13.8 dB/K (see Section 6.5).

### 5.2.2 S-Band Feed

The feed of the S-band RF front end is a dual LP FPP2DL-20-S from mWave Industries, LLC. It has been selected because of its frequency band from 1.5 GHz to 2.5 GHz and fits the  $f_d/D$  ratio of 0.4 of the 3.7 m parabolic dish (see Section 5.1). Its dual LP configuration allows reception and transmission in two orthogonal polarization states. The resulting two signals can be combined later to form RHCP or LHCP (see Section 5.2.9). Figure 5.5 shows the feed with its two sub-miniature version A (SMA) connectors.

To get the pattern of the S-band antenna system, the following measurement has been taken [66]: The antenna was pointed to the Sun at an azimuth  $\varphi_{\text{Sun}}$  and an elevation  $\vartheta_{\text{Sun}}$ . Then, an area around the Sun was scanned with the antenna, pointing it to  $\varphi = \varphi_{\text{Sun}} + \Delta\varphi$  and  $\vartheta = \vartheta_{\text{Sun}} + \Delta\vartheta$ . Figures 5.6 and 5.7 give the results. In Figure 5.6, two cuts, one in the horizontal plane (i.e. only  $\Delta\varphi$  changed) and one in the vertical plane (i.e. only  $\Delta\vartheta$  changed), are shown. Figure 5.7 shows the corresponding pseudo color plot, with the full width at half maximum (FWHM) beamwidth (i.e. the 3 dB beamwidth) marked by a blue line.

The measurement shows, that the antenna is almost perfectly aligned. The FWHM beamwidth  $\theta_{\text{ant}}$  is  $3.1^\circ$ .

### 5.2.3 Duplex Filters

Right after the feed, there are two duplex filters – also called diplex filters [50, 52]. These filters are responsible for separating two frequency bands to allow for transmission and reception at the same time. They separate or combine the uplink frequency band (from 2.0 GHz to 2.1 GHz, see Section 5.3) and the downlink frequency band (from 2.2 GHz to 2.45 GHz). They further reduce the influence of out of band interferers at the receiver input to avoid blocking in the subsequent LNAs.

The duplexers directly follow the feed in the receive pipeline. Therefore, they have a strong influence on the overall noise figure of the system. Still, they are necessary to mitigate the strong interferers of the city (see Section 3.2). They are custom made types from Miteq and have been optimized for a very low insertion loss  $L_{R3}$  of 0.3 dB on the one hand and for a high suppression (minimum 60 dB) of the nearby UMTS signals on the other hand.

Figure 5.8 shows a photograph of one of the two duplex filters, while Figure 5.12 implicitly shows the transfer function of the duplexers.



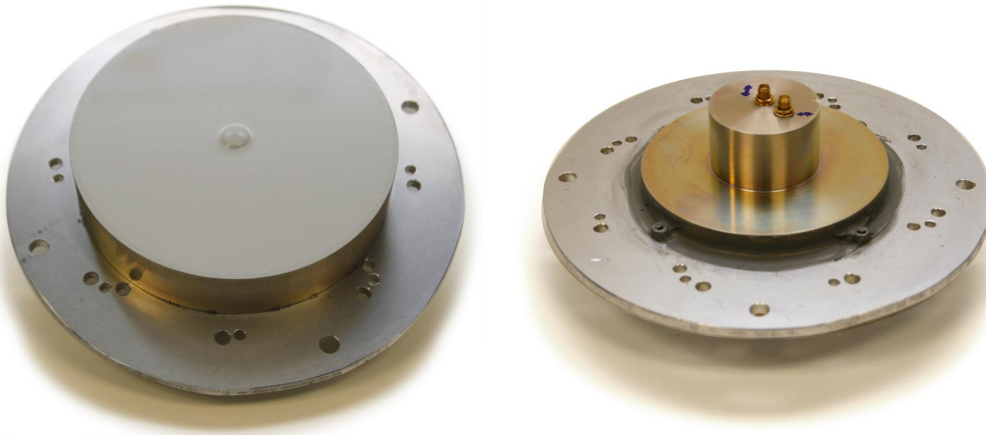


Figure 5.5: Front and back of the dual LP S-band feed usable from 1.5 GHz to 2.5 GHz. On the back, there are two SMA connectors. The holes are for mounting and to allow condensed water to trickle out.

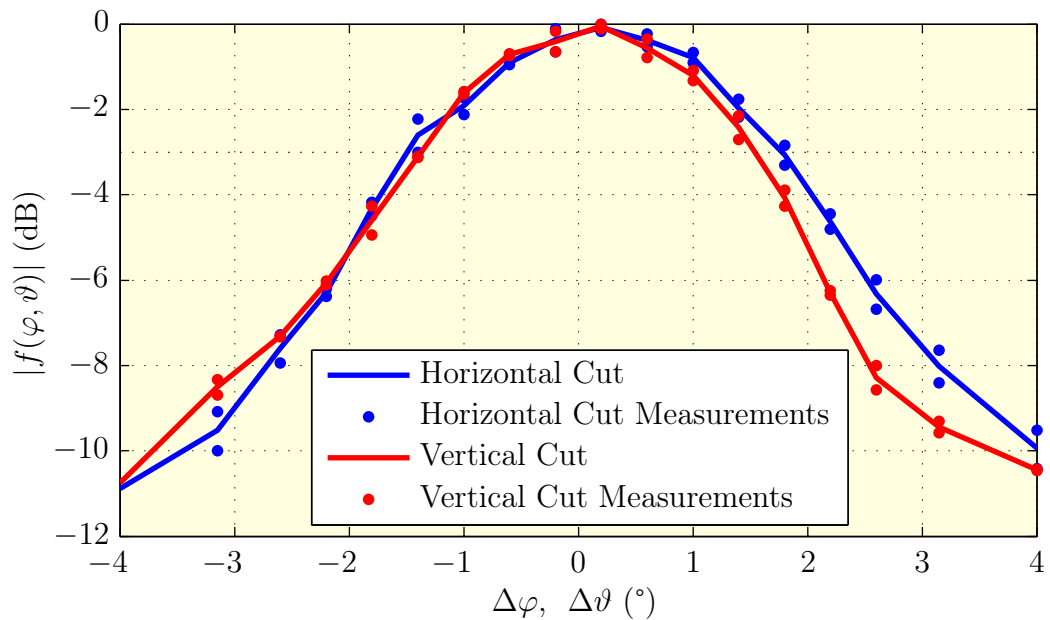


Figure 5.6: Cut through the radiation pattern of the 3.7 m parabolic dish and S-band feed in the azimuth and the elevation plane.

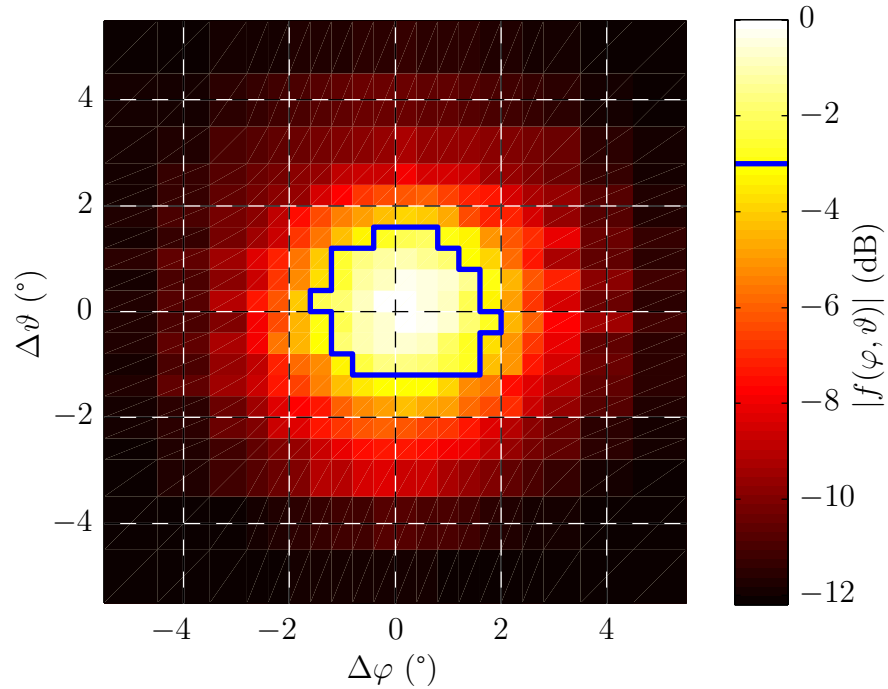


Figure 5.7: Pseudo color plot of the radiation pattern of the 3.7 m parabolic dish and S-band feed measured at 2.23 GHz. The blue line indicates the 3 dB beamwidth.



Figure 5.8: The duplex filters used in the S-band RF front end to separate the receive and the transmit frequency bands.

### 5.2.4 S-Band LNAs

To keep the overall noise temperature  $T_s$  low and to improve the received signal level, low noise amplifiers (LNAs) are placed as early in the receive pipeline as possible. Two KU LNA 222 AH from Kuhne Electronic – shown in Figure 5.9 – with a gain  $G_{R5}$  of about 31 dB are used. They have SMA connectors and use a separate input for the power supply. They are supplied with 12 V and consume about 90 mA each.

In Figure 5.10 the gains of both LNAs are plotted as a function of frequency. The receive center frequencies of MOST and CoRoT are marked with extra vertical lines. For further calculations, the gain at the arithmetic mean of the two center frequencies is used. Both LNAs have a noise figure  $F_{R5}$  of 0.5 dB and an  $IIP_3$  of  $-3$  dBm.

Because of the high gain of the LNAs the subsequent components do not have such a high impact on the overall  $T_s$  anymore.

### 5.2.5 S-Band Feed Assembly/LNB

To keep the attenuation of the cables connecting the feed, the duplex filters and the LNAs low, these components have been mounted together into a single S-band feed assembly – also called low noise block (LNB).

Figure 5.11 shows a block diagram of the parabolic reflector antenna together with the components of the LNB. All four RF ports connecting to the outside are of N type. The figure also shows circled numbers from 1 to 3 for the first LP signal path and from 4 to 6 for the second signal path. The numbers are later used as designators for the measurements in Figure 5.12.



Figure 5.9: LNA used in the S-band receive RF front end.

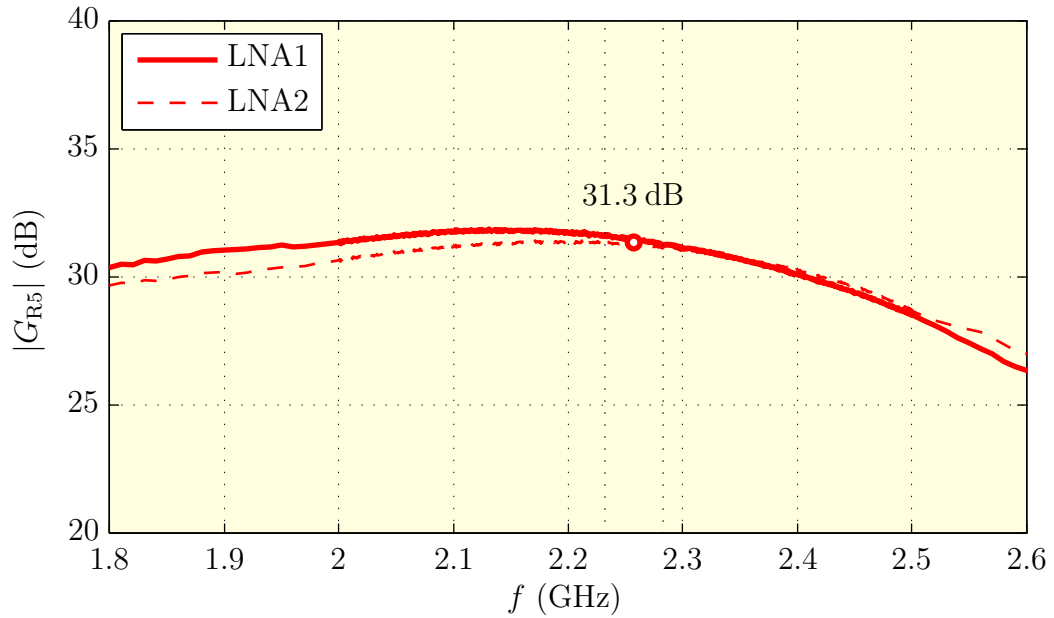


Figure 5.10: Gain measurement results for the S-band LNAs.

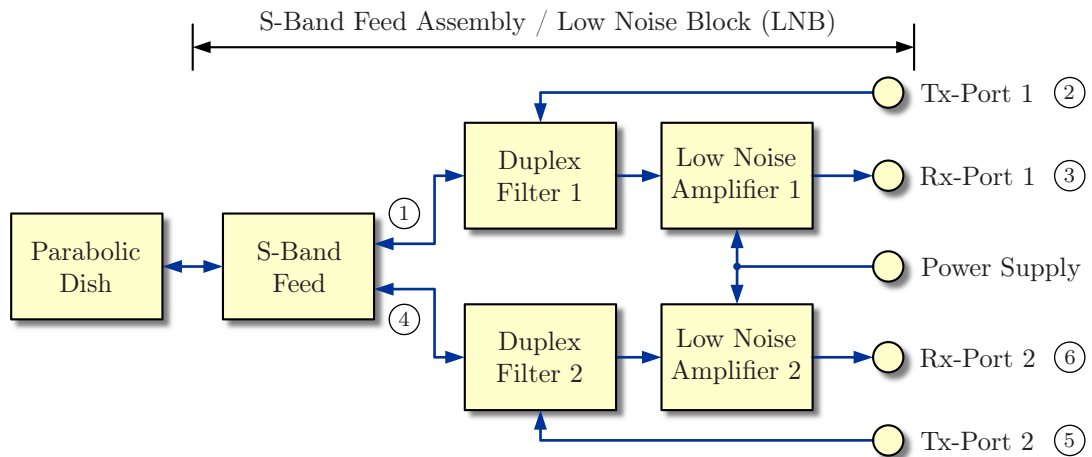


Figure 5.11: Block diagram of the S-band feed assembly illustrating the measurement labeling in Figure 5.12.

All connections inside the LNB are made with UT141 semirigid cables and SMA connectors. These cables offer lower insertion losses than most flexible cables with similar dimensions. To obtain an overall impression of the frequency response of the LNB, measurements have been taken on the complete assembly. The results are given in Figure 5.12.  $S_{ij}$  are the transmission coefficients of the six-port from input port  $j$  to output port  $i$  [76]. It can be observed that the overall gains ( $S_{31}$  and  $S_{64}$ ) of the receive path are 30.4 dB. The losses of the transmit paths ( $S_{12}$  and  $S_{45}$ ) are 1.0 dB (see Section 5.3). The difference in the frequency response between the two LP signal paths is due to the slightly different tuning of the duplex filters.

The duplex filters and the LNAs are mounted in a cylindrical structure on top of the feed. Figure 5.13 shows this assembly without the cover. The shape has been chosen to reduce the cross section affecting the received/transmitted waves. The cylindrical cover can be removed along its rotation axis. When properly mounted, the overall assembly is almost watertight. However, four small canals have been milled into the bottom plate to allow for condensed water to trickle out of the assembly. Desiccant bags have also been placed inside the assembly.

Figures 5.14 and 5.15 show the S-band feed assembly mounted in the center of the parabolic dish. Four threaded rods – best visible in Figure 5.15 – allow for movement of the assembly along the rotation axis of the dish in order to reach the correct focal distance  $f_d$  with the feed.

The LNB is connected with about 10 m of Ecoflex 10 cables and about 30 m of RFA 1/2" and RFA 7/8" to the indoor components of the TU Wien Ground Station. The flexible Ecoflex 10 cables are routed first along the struts holding the feed, then along the backside of the dish and finally in a loop dangling down the rotator to allow for the movement of the dish. Due to the repeated bending during a satellite pass, these cables suffer from increased wear which requires them to be replaced regularly. In contrast, the RFA 1/2" and RFA 7/8" cables are rigid and fixed-installed. The interconnections between the flexible and the rigid cables are equipped with lightning and surge protections. The combination of the cables in front and behind the lightning protection is subsumed in R6 in Figure 5.2 and Table 5.1.

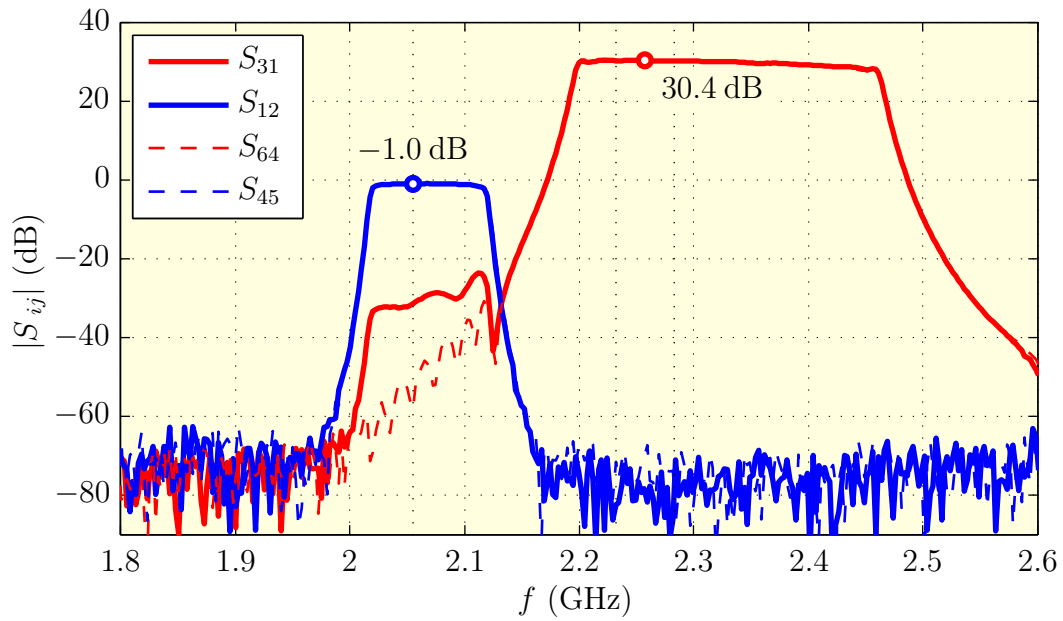


Figure 5.12: Gain measurement results from the S-band feed assembly. The port naming scheme is given in Figure 5.11.

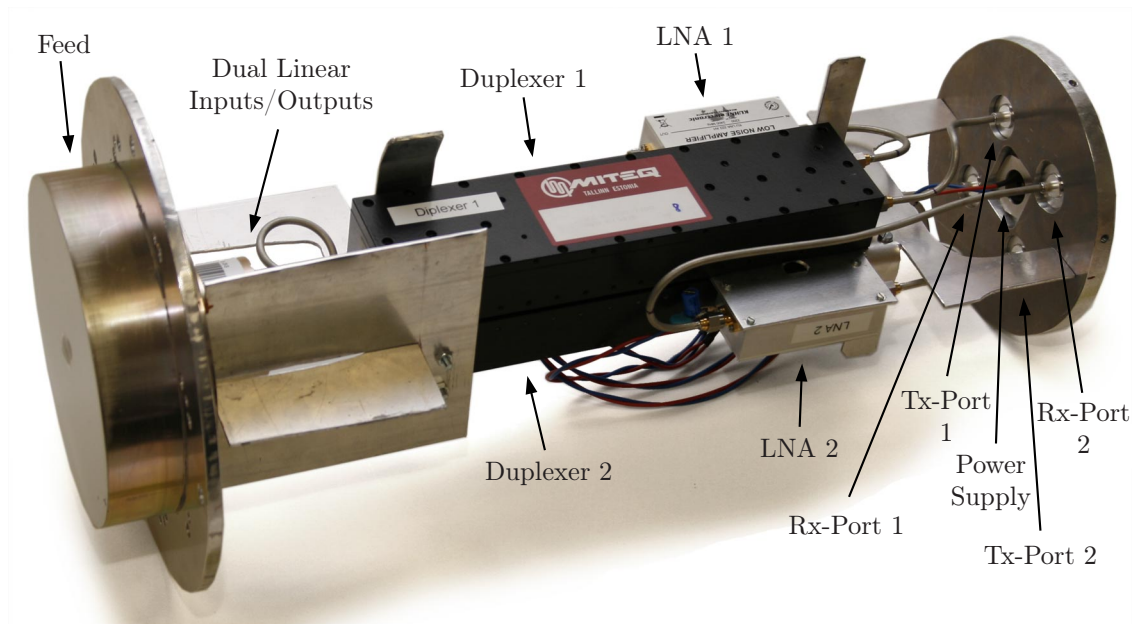


Figure 5.13: The S-band feed, the duplex filters and the LNAs assembled to form the S-band LNB.

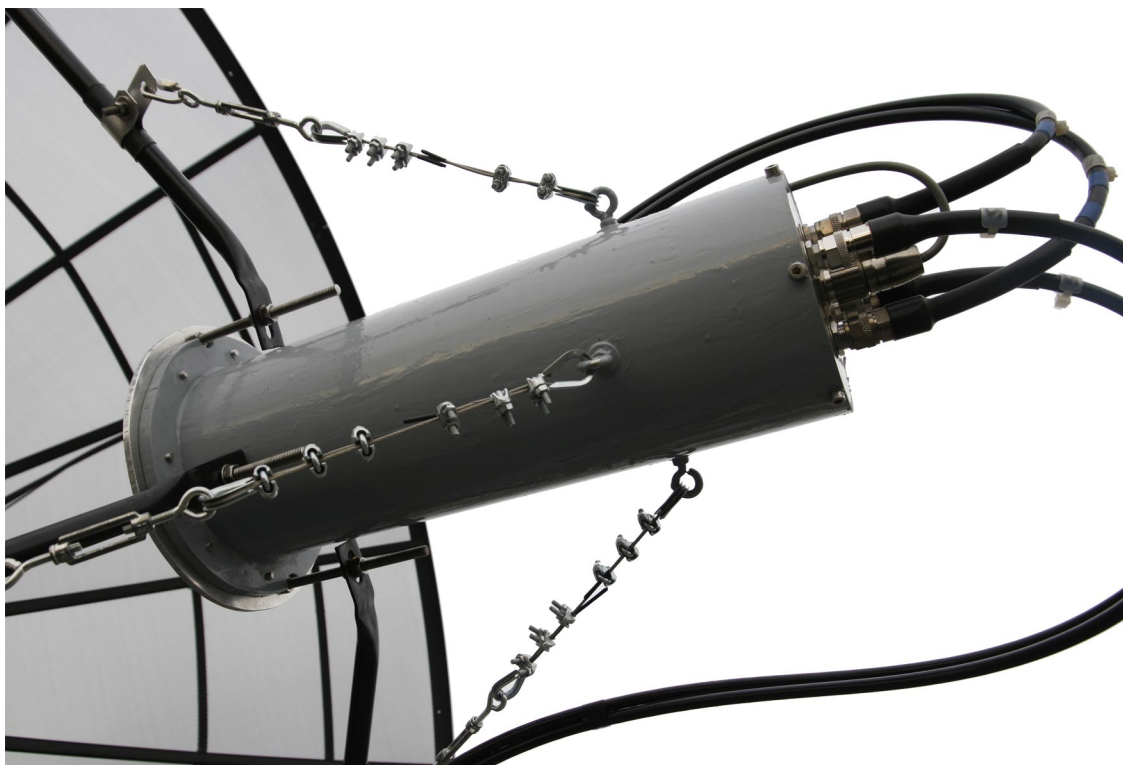


Figure 5.14: The S-band LNB outdoors with the Ecoflex 10 cables connected.

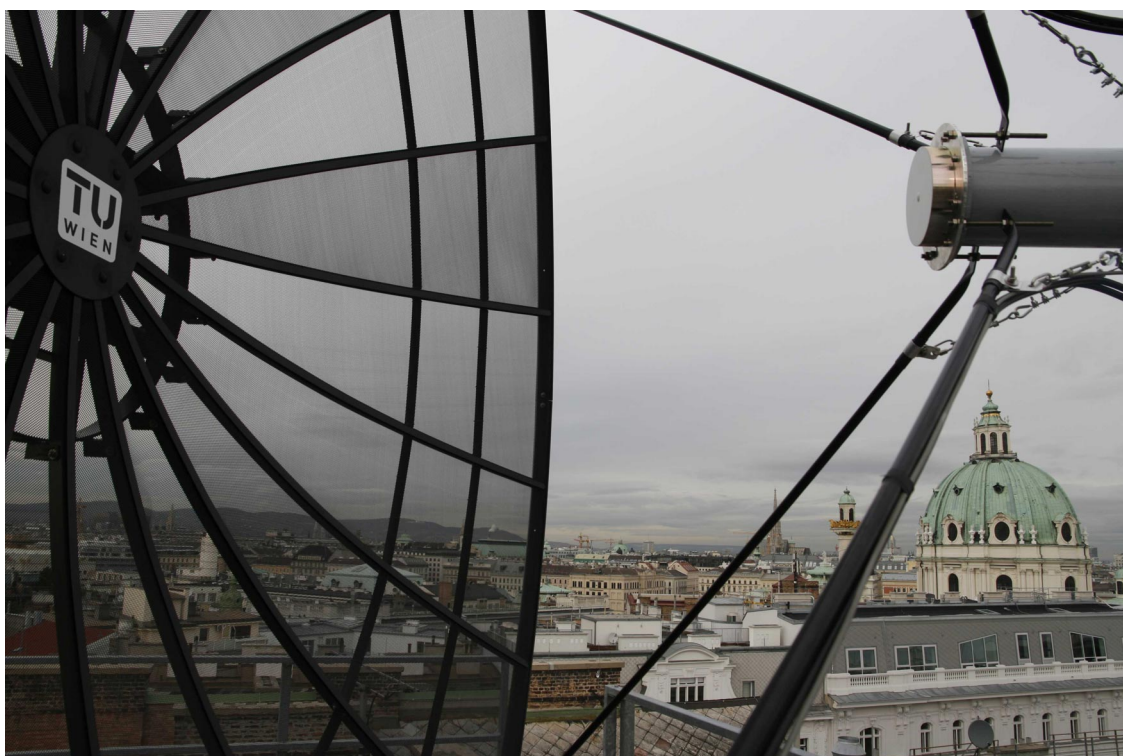


Figure 5.15: The S-band LNB mounted in the focus of the 3.7 m parabolic dish.

### 5.2.6 Bandpass Filters

Inside the building, the two output signals of the LNB reach the set of indoor components. There, the very first components are two BPFs which suppress out-of-band interferers like UMTS or LTE signals. As visible in Figure 5.16, inter-digital filters with five poles are used. Figure 5.17 shows the measurement results of the two filters. The filters are custom made like the duplex filters. They are optimized for high suppression of out-of-band interferers. UMTS signals for example are suppressed by some 60 dB.

The man made noise data measured and presented previously in Chapter 3, Figures 3.3 and 3.6, were obtained without the duplex filters and without the BPFs.

### 5.2.7 Buffer Amplifiers and Alternate Receiver Output

To increase the signal level for the downconverters, additional buffer amplifiers are necessary. Two broadband ZX60-3018G+ amplifiers from MiniCircuits are used which offer about 20 dB gain (see Figure 5.18). They are operated far below their 1 dB compression point and their 3<sup>rd</sup> order intercept point.

To allow for easy measurement access and for extension by alternate receive pipelines, two 3 dB power splitters ZX10-2-42 from MiniCircuits are used to make the two LP received signals additionally accessible via two complementary N connector ports.

### 5.2.8 Dual Downconverter

A dual downconverter is used to convert from the RF band down to the IF. The two downconverters from Kuhne Electronic are driven with one shared local oscillator (LO) of 2410 MHz. Because only one shared LO is used, the phase relation between the two LP receive signals is preserved. In the spectrum, the frequency of the LO lies above the frequency band of the received signal. Consequently, the received spectra are inverted in the IF domain, leading to the resulting output frequencies

- for CoRoT:  $f_{\text{IF,CoRoT}} = 127.6$  MHz and
- for MOST:  $f_{\text{IF,MOST}} = 178.1$  MHz.

The downconverter utilizes passive diode ring mixers but uses built-in amplifiers to achieve an overall conversion gain  $G_{\text{R11}}$  of 30.6 dB (see Figure 5.19). The 1 dB compression point was measured at  $-38$  dBm input power.





Figure 5.16: The BPF used in the S-band receive RF front end.

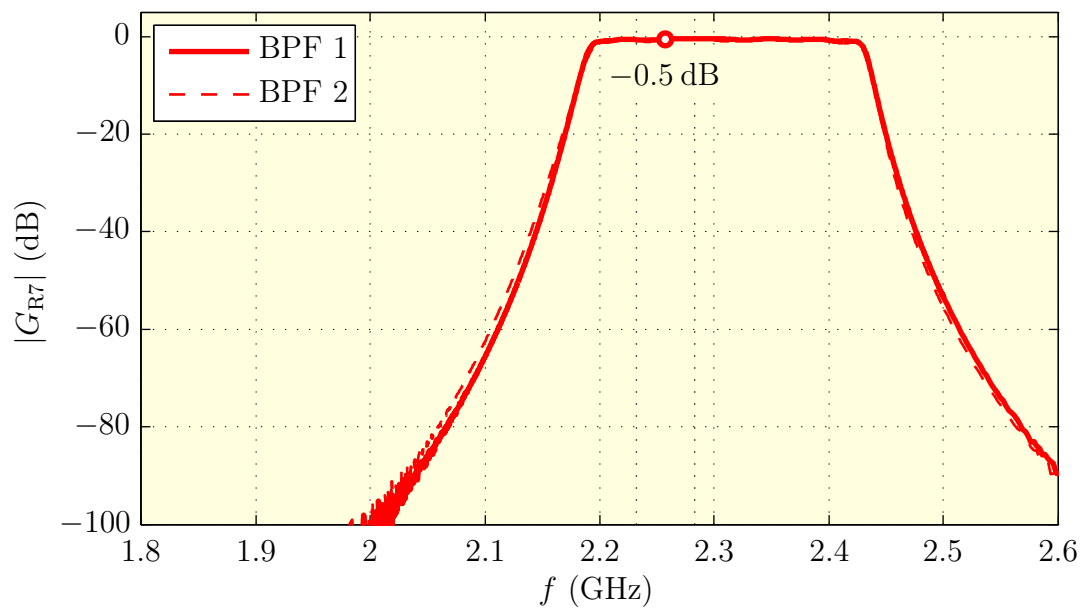


Figure 5.17: Insertion loss of the BPFs in the S-band receive RF front end.

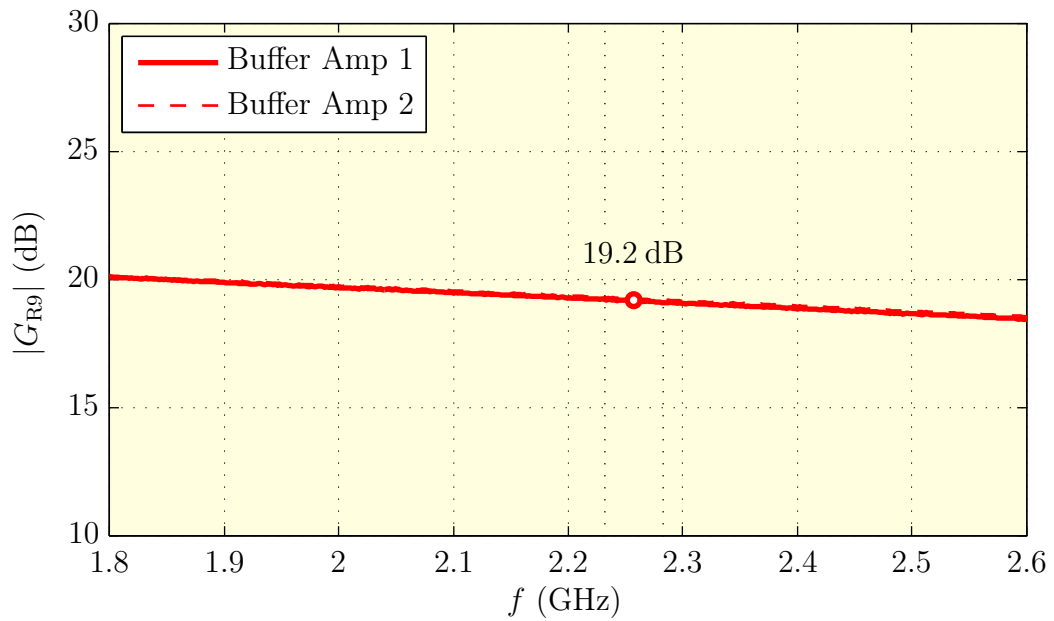


Figure 5.18: Gain measurement results of the buffer amplifiers used in the S-band receive RF front end before the downconverter.

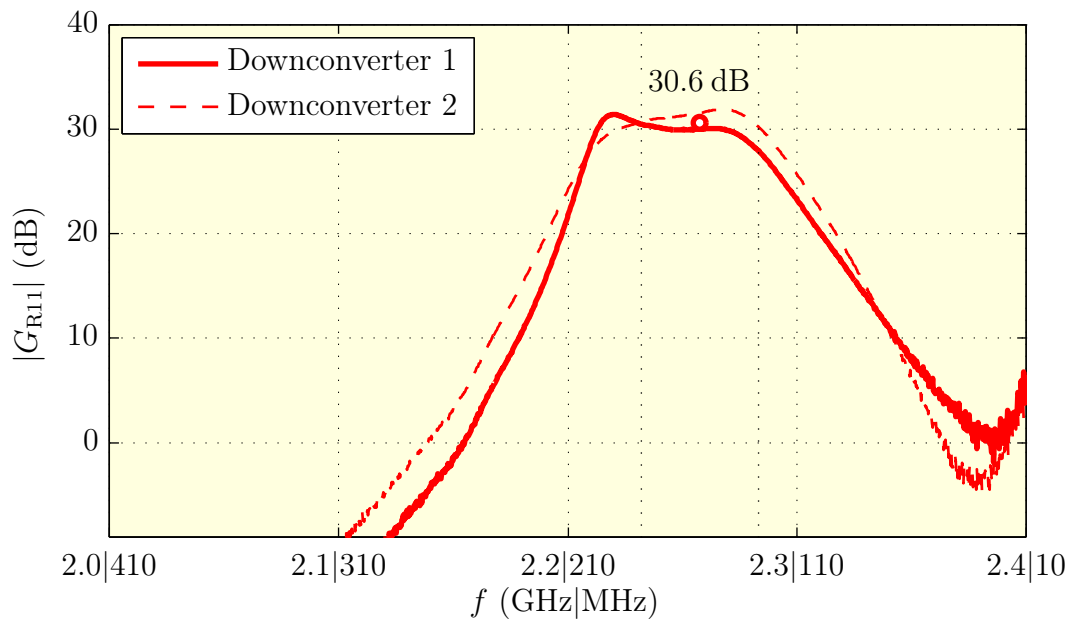


Figure 5.19: Gain measurement results of the downconverters from S-band to 140 MHz IF used in the receive RF front end.

### 5.2.9 Polarization Selection

The polarization selector combines the two received LP signals into a single CP signal with selectable rotation. Internally, the circuit depicted in Figure 5.20 uses two  $90^\circ$  hybrids and two power combiners to generate two signals with LHCP and RHCP respectively from the two signals at the SMA inputs 1 and 2. A gold wire relay then connects one of the two generated signals to the output SMA connector 3. Right near the inputs and after the power combiners four sub-circuits realize power detectors for the input and possible output signals. These could be used to select LHCP or RHCP automatically.

Several measurements have been performed to characterize the polarization switch. First, Figure 5.21 shows the magnitude of  $S_{31}$  and  $S_{32}$  for both states of the switch. The two pairs of measurements utilizing either the  $0^\circ$  or the  $90^\circ$  branch of the hybrids are almost identically in magnitude. The changes in the magnitudes of the frequency responses are caused by the hybrids.

Second, Figure 5.22 gives the phase difference between port 1 and 2 at the output for either polarization state.

Third, in Figure 5.23 two signals with equal power  $|a_1|^2 = |a_2|^2$  but different phase are injected at port 1 and 2 respectively. For two of the four measurements the impressed phase difference corresponds to the selected state of the selector – a co-polarized input signal is applied. For the other two measurements, the phase difference is exactly the opposite of the selected polarization state – the measurement is performed with a cross-polarized input signal. The results are given as a ratio between the output power  $|b_3|^2$  and the input power  $|a_1|^2$  at input port 1. In the co-polarized case we get 3 dB attenuation, while in the cross-polarized case we get at least 20 dB isolation in the relevant frequency range.

### 5.2.10 Satellite Modem

After the signal conditioning and downconversion to the IF of about 140 MHz in the S-band receive RF front end, the signal is demodulated in a commercial satellite modem. The modem is not part of the RF front end segment but is part of the shared signal processing segment, although it is described in this section.

The modem is a PSM-500 by Datum Systems. The modem can demodulate (and modulate) various modulation schemes, including BPSK, QPSK and several quadrature amplitude modulation (QAM) types at bit rates up to 29.5 Mbit/s. Furthermore, different forward error correction (FEC) variants are implemented including a Viterbi decoder and Reed-Solomon codes. The modem supports IFs in the

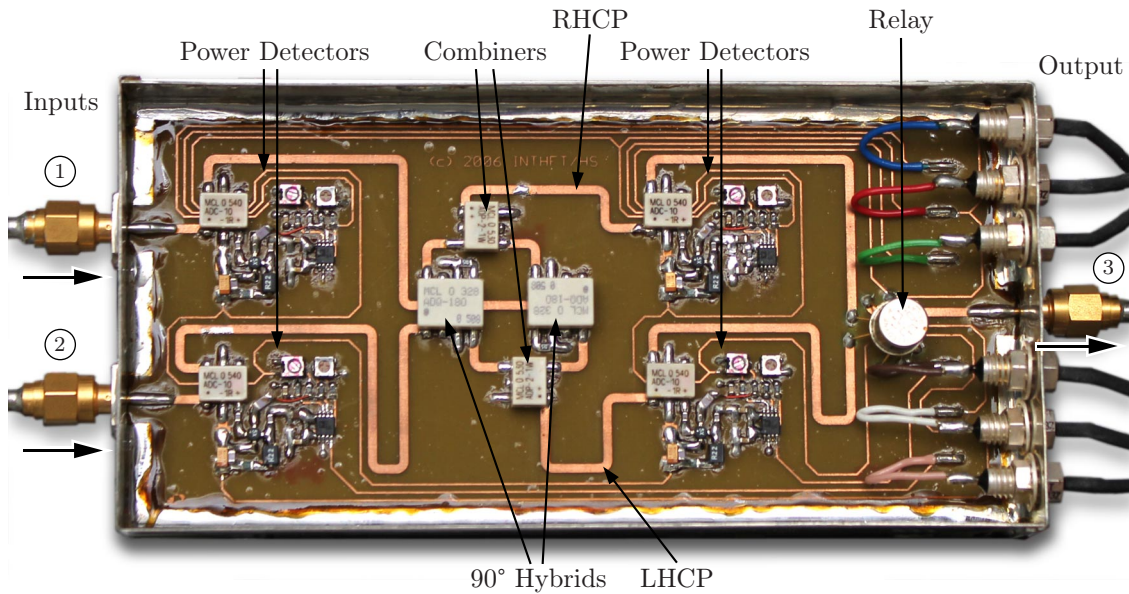


Figure 5.20: The power combiner circuit used to form a single CP signal out of two orthogonal LP signals at the end of the S-band receive RF front end.

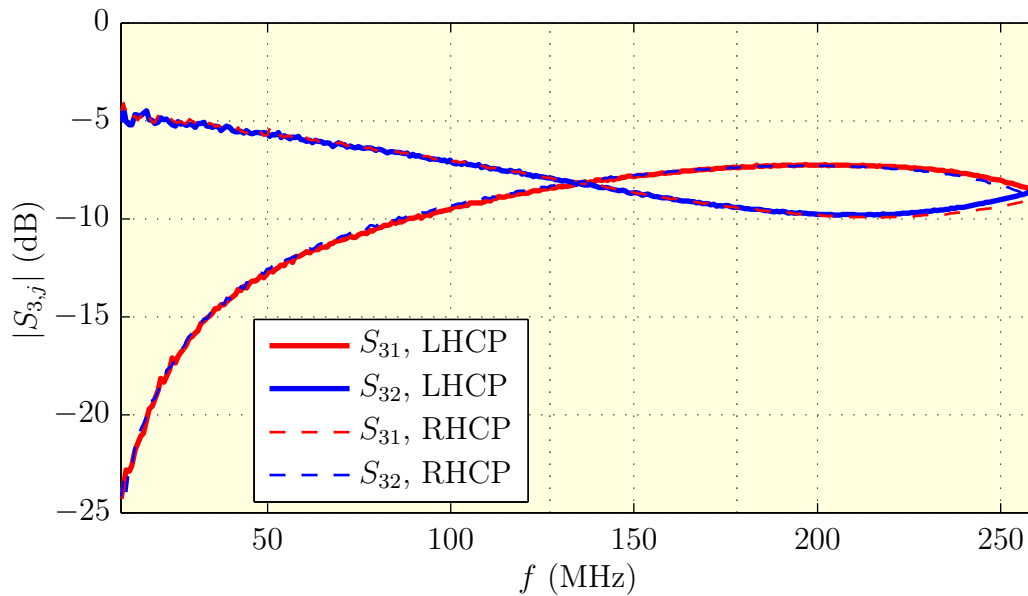


Figure 5.21: Frequency response of the polarization selector from the two input ports 1 and 2 to the output port 3. Both the LHCP and the RHCP mode are shown.

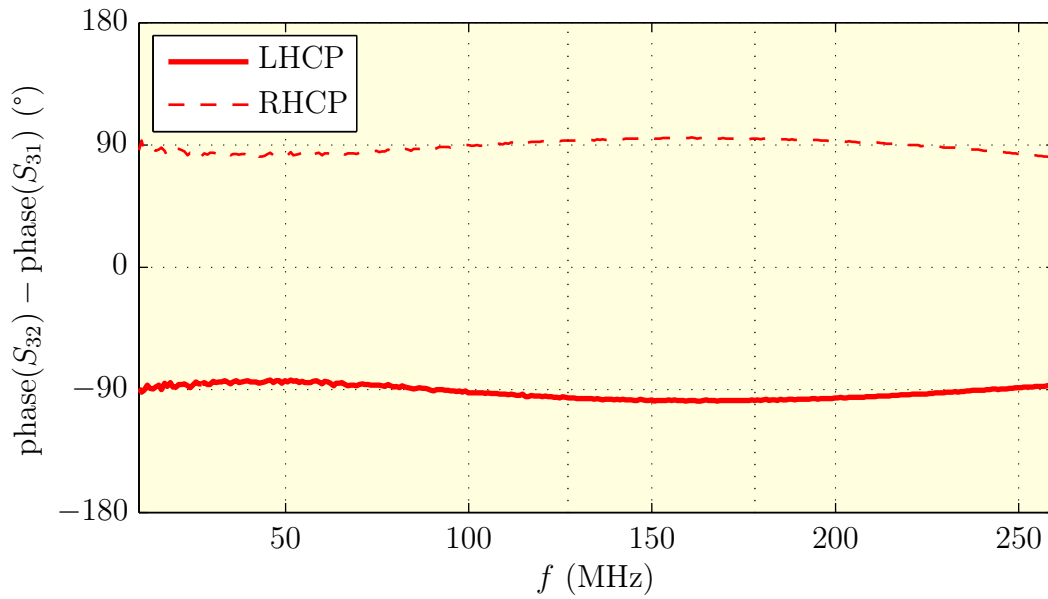


Figure 5.22: Phase difference between the two input ports 1 and 2 with respect to the output port 3 of the polarization selector in LHCP and RHCP mode.

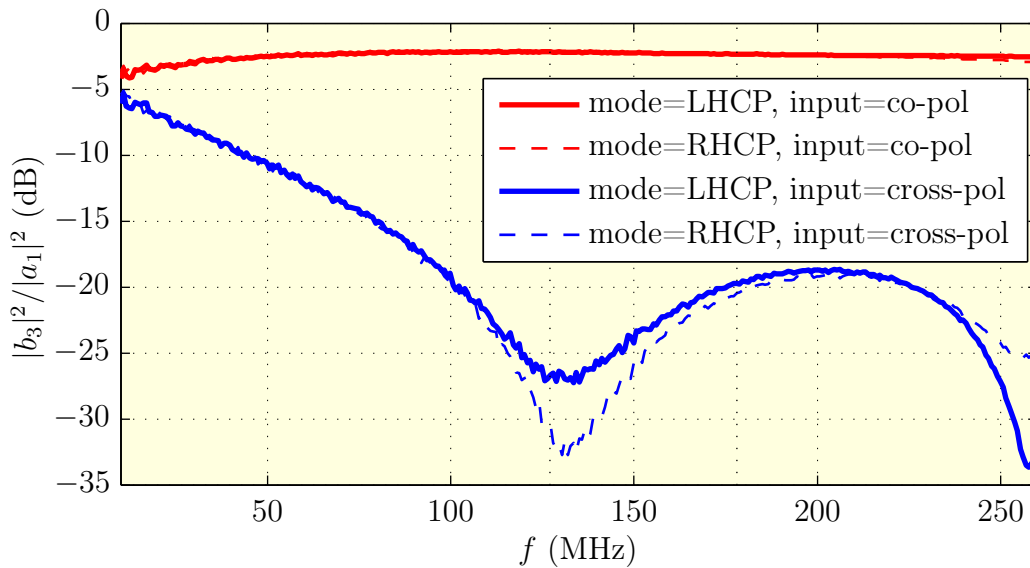


Figure 5.23: Relation between the output power at port 3 and the input power at port 1. The input signal at port 2 has the same power level as the signal at port 1, but its phase is shifted by  $+90^\circ$  or  $-90^\circ$  to form either a signal with LHCP or with RHCP.

range from 100 MHz to 180 MHz. This results in S-band frequencies from 2230 MHz to 2310 MHz with the downconverters described in Section 5.2.8.

The modem has a synchronous serial data output following the EIA-530 standard. Two differential line pairs with EIA-422 conforming signal levels are used for data and clock transmission respectively. The data output is currently exclusively used by CoRoT. A switching matrix for EIA-422 signals will later route the signals to either the CoRoT TNC or the BRITE TNC.

The modem is fully controlled by the ground station control software. A few seconds before the next satellite pass starts, the software sets up the correct receive frequency, data rate, modulation and FEC schemes. Furthermore, the control software queries and records status parameters like the received signal strength indicator (RSSI), the Doppler correction value or the estimated bit error rate (BER) of the modem during a pass. Because the modem determines the RSSI value even when no data is received, it can be used as a test receiver for noise figure measurements with the Sun (see Section 6.5).

As shown in Figure 5.2, there is a second modem which is dedicated to MOST. It is an older PSM-4900 by Datum Systems.

## 5.3 S-Band Uplink

The S-band transmit RF front end is responsible for transmitting between 2.00 GHz and 2.10 GHz. The uplink basically consists of a GMSK modulator at 435 MHz, an upconverter and a power amplifier (PA). This uplink is used for MOST.

### 5.3.1 Link Budget

Following the block diagram in Figure 5.24, Table 5.2 lists all the components of the S-band transmit front end. The components are indexed from T9 down to T1 in both the figure and the table.

Similar to Section 5.2.1, the coaxial cables interconnecting the components are not always listed explicitly in the link budget. Especially, for attenuators, the given attenuation also includes the loss of the cables they are connected to.

Table 5.2 gives the respective gain  $G_i$  for each of the components obtained either from their datasheets or by measurement. With these figures, for each output port of the components  $i$ , the cumulative gain  $G_{\text{cum},i}$  and the output power  $P_{\text{out},i}$  is calculated by

$$P_{\text{out},i} = P_{\text{out},T9} G_{\text{cum},i}. \quad (5.15)$$

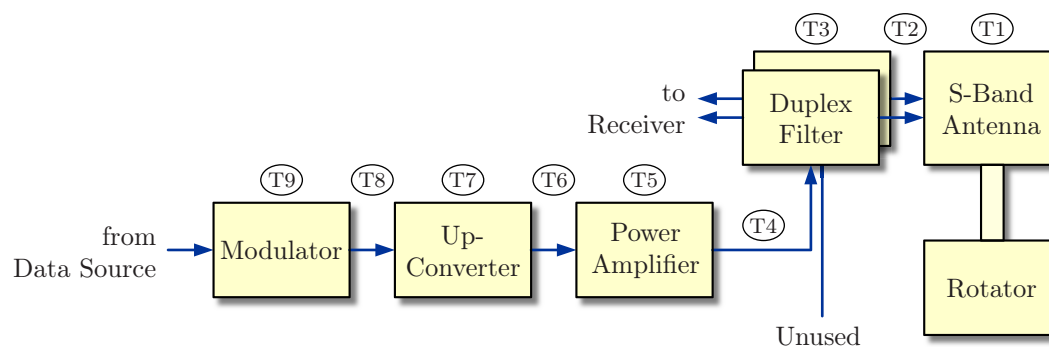


Figure 5.24: Block diagram of the S-band transmit RF front end. The circled numbers correspond to  $i$  in Table 5.2.

$i$	Component Name	$G_i$ dB	$G_{cum,i}$ dB	$P_{out,i}$ dBm	$P_{1dB,i}$ dBm	$IIP_{3,i}$ dBm	$P_{in,max,i}$ dBm
T9	Modulator			20.3			
T8	Attenuator	-24.5	-24.5	-4.1			27.0
T7	Upconverter	19.0	-5.5	14.9	9.5		17.0
T6	Attenuator	-18.5	-24.0	-3.6			
T5	Power amplifier	49.6	25.6	46.0	-2.8	7.0	
T4	Cables 40 m	-4.4	21.3	41.6			
T3	Duplex filter	-0.3	21.0	41.3			50.0
T2	Semi-rigid cable	-0.4	20.6	40.9			
T1	S-band antenna & feed	35.5	56.1	76.4			47.8
-	$EIRP$ required for MOST			69.5			

Table 5.2: Values for the link budget of the S-band transmit RF front end.

The last power level  $P_{\text{out},T1}$  in the table is the  $EIRP$  of the ground station. The goal is to reach at least the  $EIRP$  required for MOST, which is calculated in Appendix D. Furthermore, the input power at the 1 dB compression point  $P_{1\text{dB}}$  and the 3<sup>rd</sup> order intercept point  $IIP_3$  as well as the maximum input power  $P_{\text{in,max}}$  is given where available.

Figure 5.25 gives a graphical representation of the link budget for the uplink signal of MOST. The blue lines show the signal power, while the green markers denote the various maximum and minimum input levels from Table 5.2.

In the chain of modulator, upconverter and PA, two attenuators T8 and T6 have been inserted to adjust the overall output power. Two duplex filters are present, because they are required in the downlink for the reception of CP signals. In the uplink only one of these paths is realized, resulting in LP. The transmit input of the second duplexer is left unused, but could be used for transmission of CP signals.

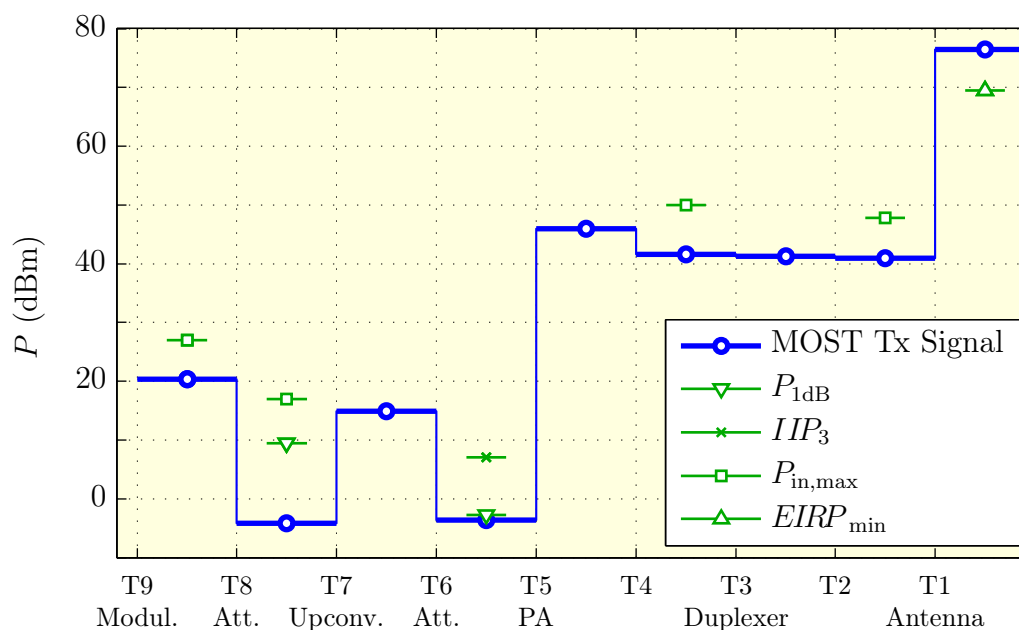


Figure 5.25: Signal power and  $EIRP$  for the MOST transmit pipeline. The numbers on the abscissa correspond to  $i$  in Table 5.2.



### 5.3.2 Modulator

The first component of the S-band RF front end is an UHF FM transceiver – a TRX4S by SYMEK GmbH. At its data input, it requires pre-shaped baseband data with a rate of 9600 Baud. Based on this, the modulator generates a frequency modulated UHF near 435 MHz. According to the pre-shaping used in the signal processing segment, the overall modulation of this UHF signal is GMSK. The transceiver originally can be used only at coarsely stepped frequencies. It has been modified to allow for fine Doppler frequency correction [8]. The output stage of the modulator has been disabled, resulting in about 20 dBm output power. The modulator provides three input ports, one for the pre-shaped input data, one for the coarse and one for the fine selection of the transmit frequency.

### 5.3.3 Upconverter

A custom built upconverter by Kuhne Electronic is used for the conversion from 435 MHz to the final S-band transmit frequency of 2055 MHz [8]. A 2490 MHz LO is used, leading to an inverted transmit spectrum. A 25 dB attenuator T8 in front of the upconverter and a 18 dB attenuator T6 after the upconverter adjust the overall transmit power.

Figure 5.26 gives the measured conversion gain  $G_{T7}$  of the upconverter. Due to its internal amplifiers, the upconverter has 19.0 dB gain at the MOST uplink frequency. The 1 dB compression point has been measured at 9.5 dB input power.

The upconverter is not meant to support the whole transmit S-band from 2.0 GHz to 2.1 GHz but is tailored for MOST. To deploy this band fully, a replacement of the upconverter would be necessary.

### 5.3.4 Power Amplifier

A power amplifier by EMPOWER RF Systems, Inc., provides 46 dBm output power for transmission. Originally developed for 1.9 GHz, it has been re-tuned by the manufacturer to support higher frequencies, including MOST [8]. It is operated near its saturation point, which is fine for GMSK and FM.

Figure 5.27 shows the gain  $G_{T5}$  of the amplifier as a function of frequency, which is 49.6 dB at 2055 MHz. The data in Figure 5.28 has been measured at 2055 MHz and shows the gain as a function of input power. The 1 dB compression point is measured at  $-2.8$  dBm input power. The actual input power used is  $-3.6$  dBm.

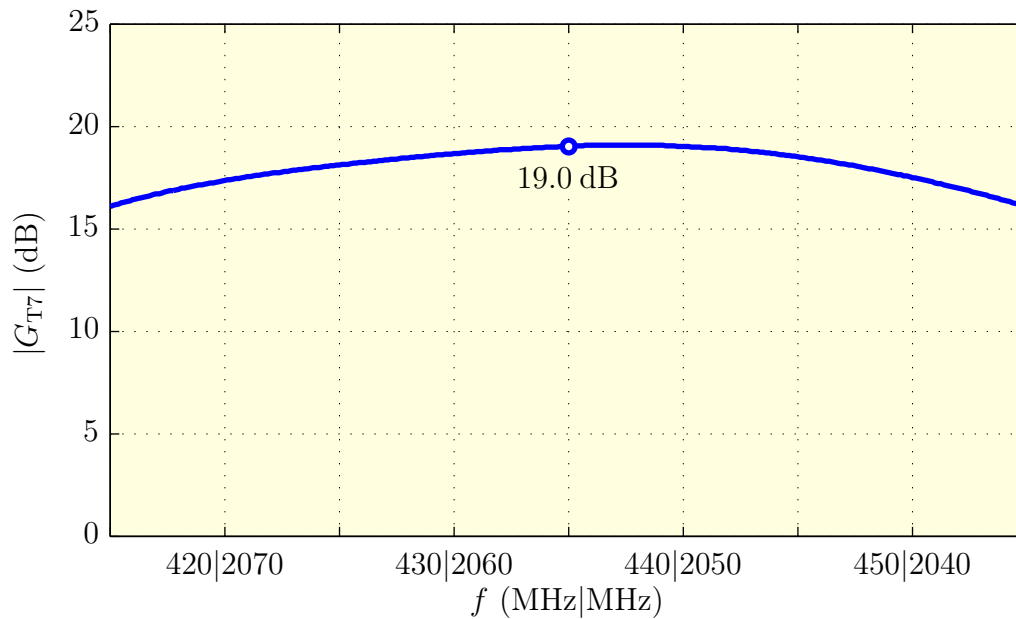


Figure 5.26: Conversion gain of the S-band upconverter. The frequency axis simultaneously shows the input frequency IF and the output frequency RF. The LO has a frequency of 2490 MHz.

For supervision, the PA has a power detector output. At this sense output, a voltage between 0 V and 5 V is available. The measurement is shown in Figure 5.29 on top.

A 28 V power supply provides the PA with the necessary power. The idle current consumption is 2.5 A and increases to 7.6 A at 46 dBm output power. The measurement of the current as a function of output power is shown in Figure 5.29 at the bottom.

The PA is mounted on an aluminum heat spreader equipped with three fans for cooling. Thermal over temperature switches are used to protect the PA in case of failure of the fans or too high ambient temperatures.

Low loss RFA  $7/8$ " cables and short flexible Ecoflex 10 cables connect the PA to the transmit input of the LNB. Although low loss, the cables still attenuate the signal by 4.4 dB. To increase the *EIRP* of the ground station, the PA could be moved outside into an enclosure on top of the antenna mast. To compensate for the attenuation introduced by the cables in front of the PA in this scenario, the attenuator at the upconverter's output could then be decreased. This keeps the output power of the PA constant, but decreases the losses between PA and antenna.

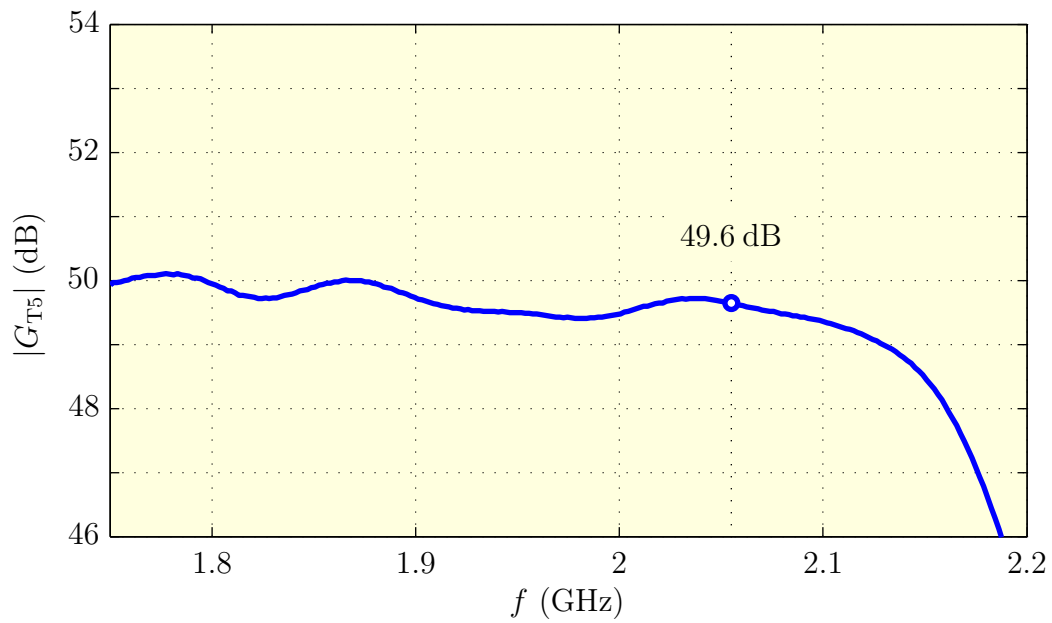


Figure 5.27: Gain of the power amplifier as a function of the frequency  $f$ .

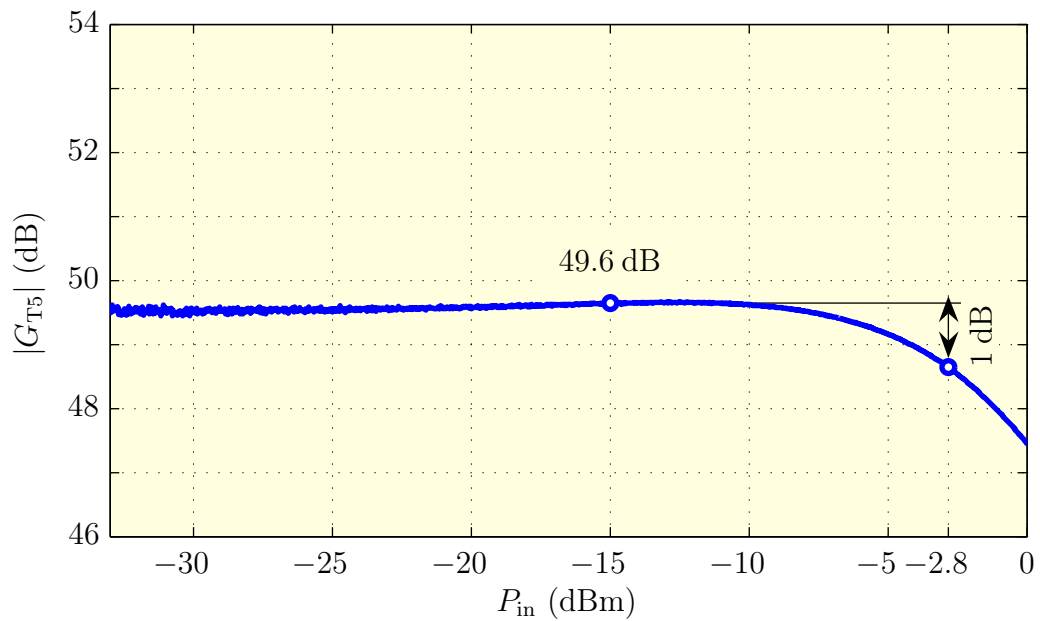


Figure 5.28: Gain of the PA as a function of input power indicating the 1 dB compression point.

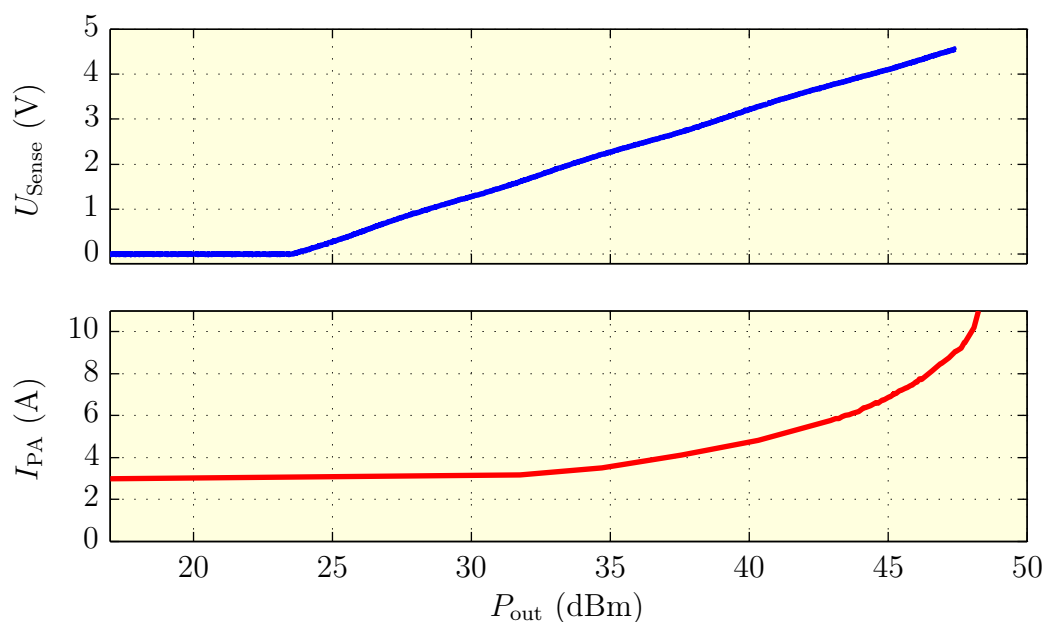


Figure 5.29: Output power sense voltage and current consumption of the PA.

Because the LNB has a dual linear input, a second identical PA could be deployed to increase the *EIRP* of the ground station. This would further enable transmission of CP signals.

### 5.3.5 MOST Output Signal

This sections gives the measurement results on the MOST output signal. The output spectrum has been measured at the PA’s output and is displayed in Figure 5.30.

MOST uses two different uplink and downlink frequency pairs – designated “Channel A” and “Channel B”. Each pair is assigned to one of the two transceivers (see Section 2.2). Figure 5.30 shows the output spectrum at both transmit frequencies. The 30 dB bandwidth has been measured as 141 kHz, the 60 dB bandwidth is 255 kHz.

Furthermore, the spectrum has been scanned for spurious emissions (spurs). Table 5.3 lists these spurs with their respective frequency, measured at the PA’s output. The levels are given in dBc – that is relative to the carrier power level. Most of the spurs are due to the LOs inside the modulator and the upconverter. We can observe harmonics of the internal crystal oscillators. The harmonics are used

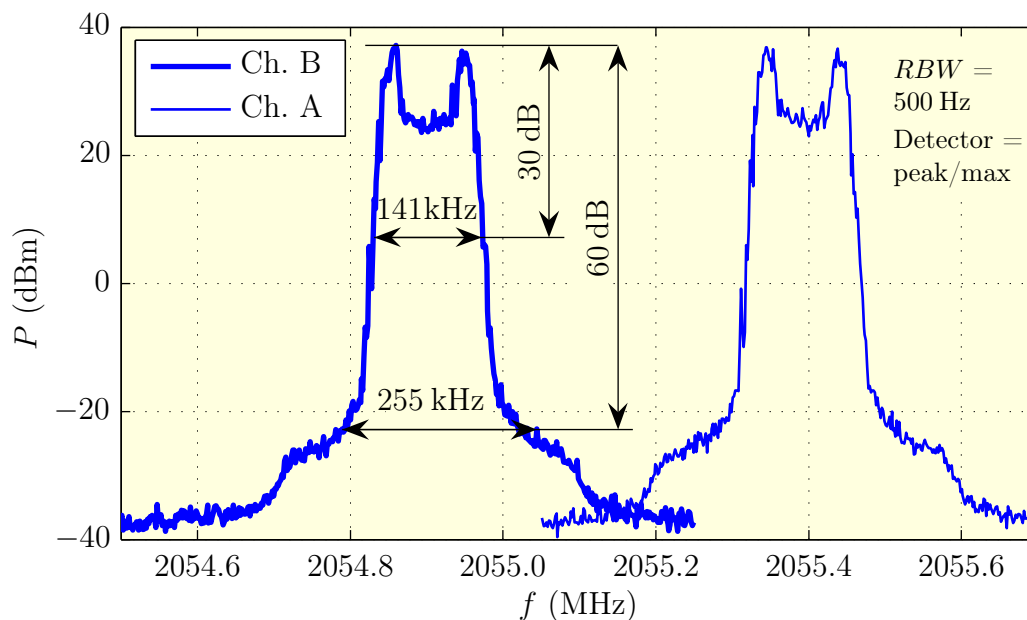


Figure 5.30: Output spectrum of “Channel A” and “Channel B” of the MOST S-band uplink signal measured at the PA output.

$f$ MHz	$P_{\text{out},T5}$ dBc	$P_{\text{out},T3}$ dBc	$P_{\text{out},R10}$ dBc	Type
2035.4	-62.7	-62.8		a) intermodulation
2037.8	-79.4	-79.5		a) LO feed through
2072.6	-63.3	-63.3		a) intermodulation
2075.0	-48.6	-48.7		a) LO feed through
2198.5	-61.4	-135.2		a) LO feed through
2490.0	-75.9	-166.3		a) LO feed through
2055.2			-128.4	b) crosstalk to Rx

Table 5.3: a) Spurious emissions in the MOST uplink signal measured at the PA output (T5 in Figure 5.24), the resulting value after the duplex filter (T3 in Figure 5.24) and b) the crosstalk to the S-band downlink (measured at R10 in Figure 5.2).

to yield the final LO signals. At the PA's output we can also observe 3<sup>rd</sup> order intermodulation products between the transmit signal and harmonics of the crystal oscillators.

For Table 5.3, I also calculated the resulting signal power at the antenna feed's input – i.e. after T3 – by including the frequency response of the duplex filters. All spurs are at least 48 dB below the actual transmit signal. All spurs outside the frequency band for satellite operations from 2.00 GHz to 2.10 GHz are more than 135 dB below the carrier.

Table 5.3 also lists the crosstalk of the transmitted signal to the receive pipeline at 2055 MHz. This measurement includes crosstalk in the components as well as back reflection at the parabolic dish antenna. It has been measured after R10 as  $-128.4$  dBc before the downconverters of the S-band receive RF front end.

## 5.4 UHF/VHF Antenna System

The UHF/VHF antenna system will consist of two UHF and two VHF Cross-Yagi antennas mounted next to the S-band parabolic dish. Since the UHF and the VHF front ends are not involved in the operation of CoRoT and MOST, they are not operational at the time of writing. This section and the following Section 5.5 however describe the UHF/VHF front ends and its antennas. The sections are based upon an earlier experimental setup and measurements on this [72].

The two UHF Cross-Yagi antennas are two WX7036 antennas manufactured by WiMo Antennen und Elektronik GmbH for the 70 cm band (435 MHz). These are dual LP 18 element Yagi antennas with a gain  $G_{U1}$  of 16.2 dBi and 3.4 m length each. The two antennas will be mounted in a stacked configuration on one side of the S-band dish. The signals of the two antennas are combined with a coaxial power combiner. An extra gain of 2.8 dB is assumed for this setup. Figure 5.31 shows one of these antennas on the left hand side of another rotator.

The two VHF Cross-Yagi antennas are two WX214 antennas manufactured by WiMo for the 2 m band (145 MHz). These are dual LP 7 element Yagi antennas with a gain  $G_{V1}$  of 12.2 dBi and 2.6 m length each. The two antennas will be mounted in a stacked configuration on the other side of the S-band dish opposite the two UHF antennas. Again 2.8 dB gain is assumed. Figure 5.31 shows one of these antennas on the right hand side.

For the antenna cabling, again Ecoflex 10 cables are used. These connect the outdoor components among each other as well as to the lightning protection. They have been chosen – besides from their low loss – because of their low weight and their flexibility. The flexibility is necessary to allow for the movement of the rotator.



Figure 5.31: Photo of an early test setup of one VHF and one UHF Cross-Yagi antenna completed with LNA and polarization selector mounted on a second azimuth/elevation rotator.

After the lightning protection, RFA  $\frac{1}{2}$ " cables are used to reach the indoor part of the ground station.

## 5.5 UHF/VHF Front Ends

The UHF and VHF RF front ends are quite similar in structure. As Figures 5.32 and 5.37 show, they differ only regarding the PA. The UHF/VHF RF front ends share a common radio. The radio itself allows full duplex operation. Therefore, UHF can be used for transmission while at the same time, VHF is used for reception, or vice versa. The UHF/VHF RF front ends can also be combined with one of the S-band RF front ends. The UHF RF front end will be used as an uplink for BRITE. The VHF RF front end is for future use (see Sections 2.4 and 2.5).

In the following sections, the UHF RF front end is explained in detail. In Section 5.5.6 the differences of the VHF front end are given.

### 5.5.1 UHF Link Budgets

The BRITE uplink requires an  $EIRP$  of 2 kW (see Appendix D). This requirement has been used for the link budget calculations of the UHF front end. Table 5.4 gives the gain  $G_{tx,i}$  of each of the components shown in Figure 5.32 in transmit mode of the front end. For a set output power of 5.4 W of the radio,  $P_{out,i}$  is listed in addition. The same information is illustrated graphically in Figure 5.33.

Furthermore, Table 5.4 lists the gain  $G_{rx,i}$  and the noise figure  $F_i$  of each of the components in receive mode. In receive mode, the bypass switches of the LNA and the PA are in reversed state.

The components U1 to U3 of the antenna system have already been discussed in Section 5.4.

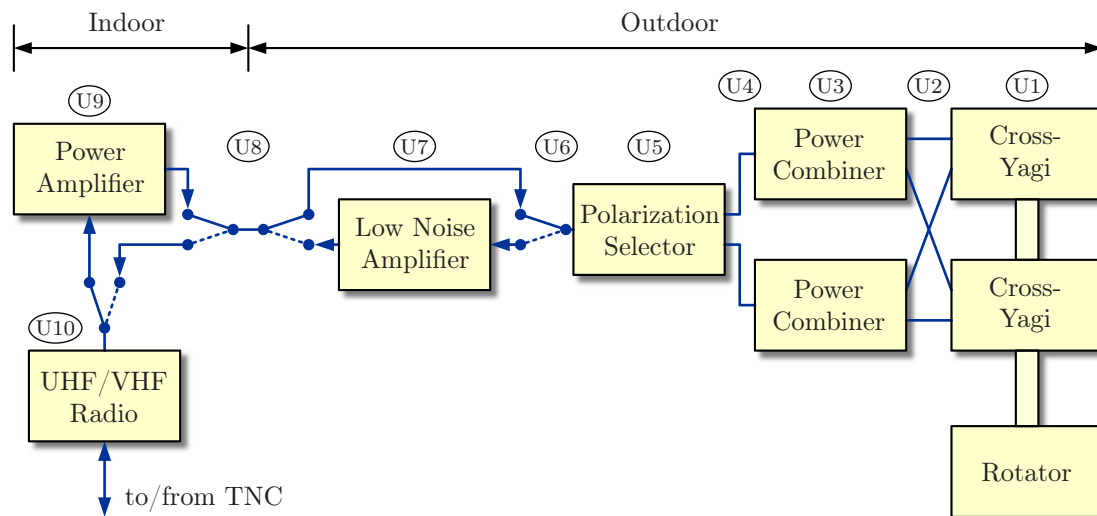


Figure 5.32: UHF RF front end used for transmission and reception.



$i$	Component Name	$G_{tx,i}$ dB	$P_{out,i}$ dBm	$G_{rx,i}$ dB	$F_i$ dB
U10	UHF radio		37.3		
U9	Power amplifier with bypass	12.6	50.0	-0.5	0.5
U8	Cables 40 m	-2.0	48.0	-3.4	3.4
U7	LNA with bypass	-1.7	46.3	20.9	0.9
U6	Cable	-0.2	46.1	-0.2	0.2
U5	Polarization selector	-0.6	45.5	-0.6	0.6
U4	Cable	-0.3	45.2	-0.3	0.3
U3	Power combiner	-0.5	44.7	-0.5	0.5
U2	Cable	-0.2	44.5	-0.2	0.2
U1	Yagi antenna group	19.0	63.5	19.0	0.0
-	$EIRP$ required for BRITE		63.0		

Table 5.4: Values for the up- and downlink budget of the UHF RF front end.

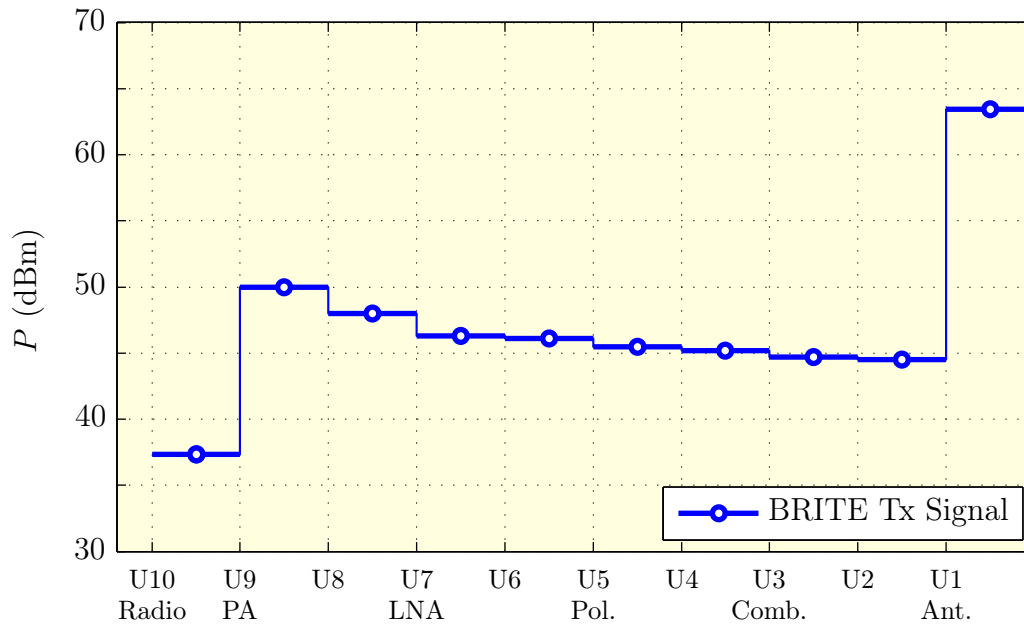


Figure 5.33: Power levels of the UHF RF front end used for the communication to BRITE.

### 5.5.2 UHF Polarization Selector

When receiving, the first component following the Yagi antenna group is the polarization selector by WiMo. It combines the dual LP signals, applying the correct phase shifts which depend on the user's choice. By this, either one of the two LP states or LHCP or RHCP are obtained [72]. For consistency with the manufacturer's datasheet, the two LP states are called horizontally (HLP) and vertically linear polarized (VLP), although the antennas are tilted by  $45^\circ$  and thus do not receive literally horizontally and vertically polarized waves. The antennas are mounted that way, because then, none of the Yagi's elements are parallel to the mounting structures.

In transmit mode, the polarization selector similarly distributes the transmit power for the two Cross-Yagi antennas of the antenna group.

Figure 5.34 shows the measured phase difference between the two antenna ports 1 and 2 with respect to the ground station port 3. The required phase shift of  $\pm 90^\circ$  is adequately realized. The two dipoles of each Cross-Yagi antenna are not located exactly at the same position along the main beam axis, but they are slightly shifted. This introduces a phase shift which is compensated by the cabling and the polarization selector. This has been accounted for in the measurements.

Figure 5.35 shows the resulting insertion losses caused by the polarization selector in the different states for co-polarized input signals on top and for cross-polarized input signals at the bottom. The figure shows the transmission coefficients calculated as the ratio between the power received at port 3 ( $|b_3|^2$ ) and the power provided to the selector at ports 1 and 2 ( $|a_1|^2 + |a_2|^2$ ). The mean insertion loss for co-polarized signals in the CP modes is 0.6 dB.

### 5.5.3 UHF LNAs

After obtaining a single receive signal out of the two dual polarized signals, an LNA increases the signal level in receive mode [72]. A SP-7000 from SSB-Electronic has been chosen. It offers about 20 dB gain with a noise figure of 0.9 dB.

Figure 5.36 shows the gain measurement of the UHF LNA. The gain  $G_{rx,U7}$  has been measured to be 20.3 dB at the BRITE uplink frequency. The 1 dB compression point is reached at  $-12.7$  dBm input power, the 3<sup>rd</sup> order intercept point at  $-2.2$  dBm input power per tone.

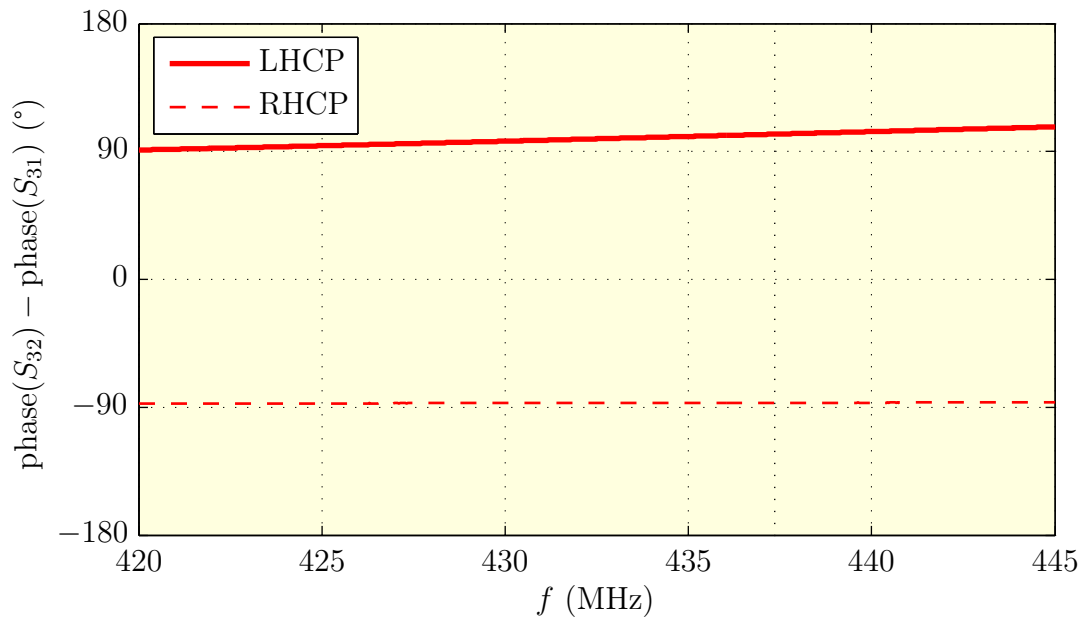


Figure 5.34: Phase differences in the CP modes of the polarization selector used in the UHF RF front end.

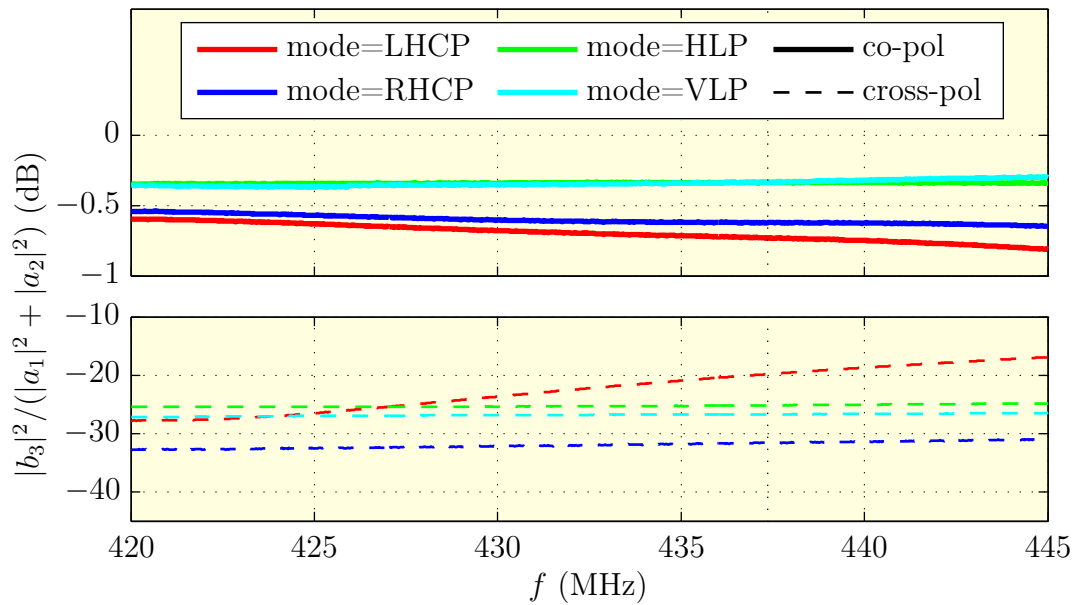


Figure 5.35: Gain of the polarization selector used in the UHF RF front end for its different states for co- and cross-polarized input waves.

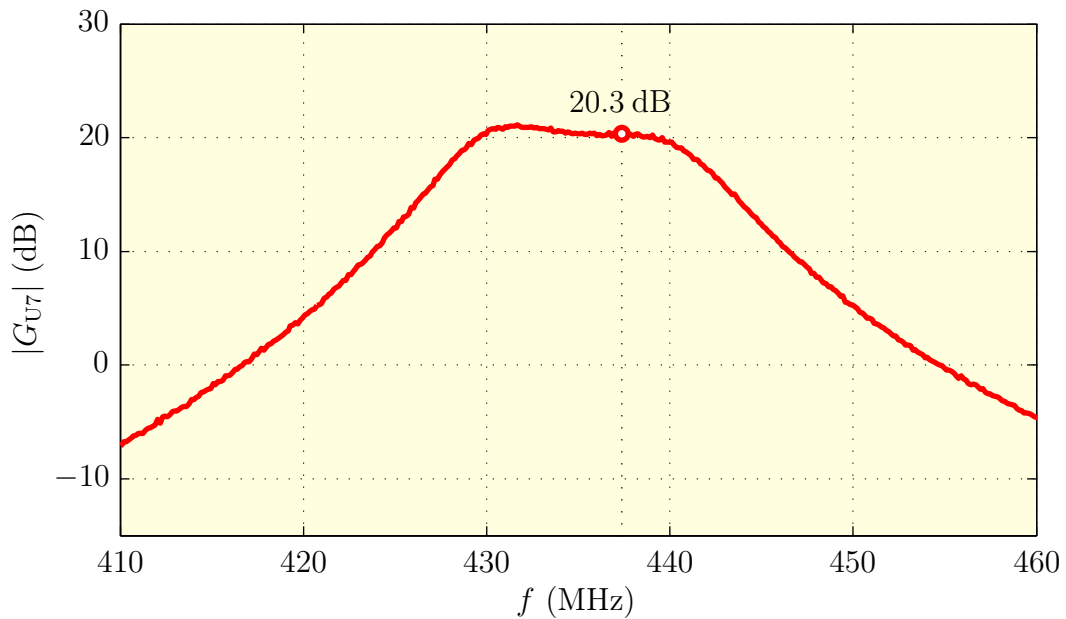


Figure 5.36: Gain of the LNA used in the UHF RF front end.

The UHF LNA has a built-in automatic transmit/receive bypass switch. In transmit mode, the LNA is bypassed by its internal relays, which results in an insertion loss of 0.3 dB.

### 5.5.4 UHF Power Amplifier

To reach the transmit power required for the BRITE uplink, a power amplifier is necessary. A ULA-100 by RM Costruzioni Elettroniche, Italy has been selected. It offers the required 100 W output power and has a gain of about 13 dB. It needs a maximum supply current of 22 A at a voltage of 13 V.

To further increase the *EIRP*, the PA can be – similar to the S-band PA – moved outside the building and mounted inside an enclosure on top of the antenna mast. This would yield additional 2 dB.

### 5.5.5 UHF/VHF Radio

As transceiver, an Icom IC-910H has been chosen. The radio offers single side band (SSB) modulation and FM in both the amateur radio UHF band from 430 MHz to 440 MHz and the amateur radio VHF band from 144 MHz to 146 MHz. In full

duplex mode, the radio can simultaneously use UHF for transmission and VHF for reception or the other way around. The frequency can be tuned in 1 Hz steps, which allows for fine Doppler correction. The maximum output power is 75 W at UHF and 100 W at VHF [71, 72].

When transmitting GMSK, the radio receives the pre-shaped analog baseband signal from the modem inside the TNC and converts it to a frequency modulated RF signal. The transmit frequency is controlled via a serial interface from the ground station control software or the TNC.

When receiving, the radio forwards the received analog baseband signal to the modem inside the TNC.

### 5.5.6 Differences in the VHF Front End

The VHF RF front end is very similar in structure to the UHF front end. This section lists the differences and gives the measurement results for the components of the VHF front end.

Figure 5.37 shows the block diagram of the VHF RF front end. It differs from the UHF front end in the missing PA for transmission, since the used UHF/VHF radio itself already offers an output power of 100 W. Table 5.5 lists the gains  $G_{tx,i}$  and output powers  $P_{out,i}$  for the components in transmit mode and the gains  $G_{rx,i}$  and noise figures  $F_i$  of the components in receive mode. Again, the LNA is bypassed with internal relays when transmitting.

The VHF polarization selector is similar to the UHF polarization selector. Figure 5.38 gives the measurements on the phase shifts for the LHCP and RHCP states.

Figure 5.39 gives the eight resulting insertion losses for the four different settings for co-polarized and for cross-polarized waves. A mean attenuation of 0.3 dB is measured for the two CP states.

The LNA used in the VHF front end is a SP-2000 by SSB-Electronic. It offers 21.4 dB gain with a noise figure of 0.8 dB at 145 MHz. Figure 5.40 gives the measurement of the gain as a function of frequency. The 1 dB compression point has been measured at  $-13.3$  dBm input power, the 3<sup>rd</sup> order intercept point is at  $-4.5$  dBm input power per tone. When not receiving, the LNA is bypassed by two internal relays, resulting in an insertion loss of 0.1 dB.

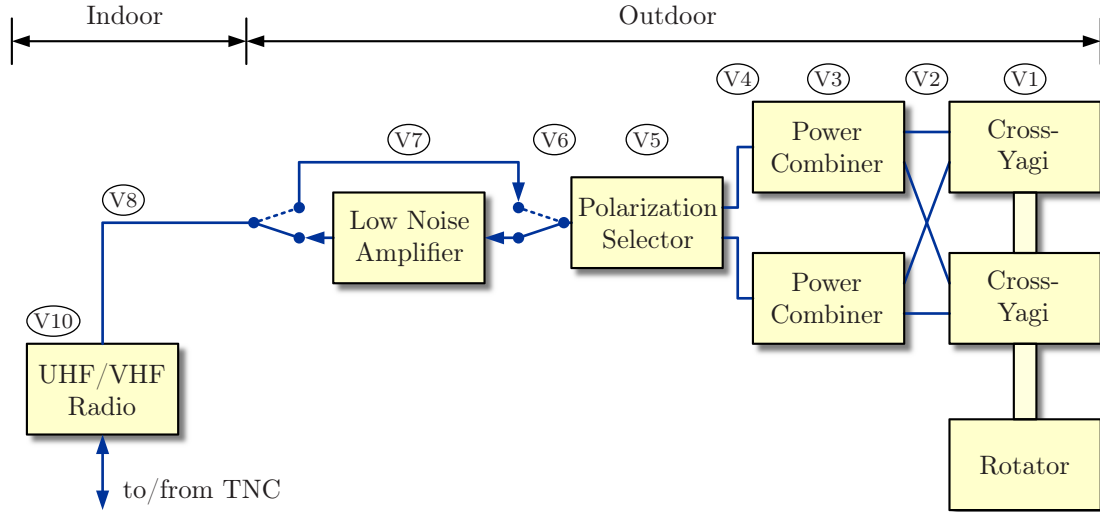


Figure 5.37: VHF RF front end used for transmission and reception.

$i$	Component Name	$G_{tx,i}$ dB	$P_{out,i}$ dBm	$G_{rx,i}$ dB	$F_i$ dB
V10	VHF radio		50.0		
V8	Cables 40 m	-1.5	48.5	-2.1	2.1
V7	LNA with bypass	-0.9	47.5	21.4	0.8
V6	Cable	-0.1	47.4	-0.1	0.1
V5	Polarization selector	-0.3	47.1	-0.3	0.3
V4	Cable	-0.2	46.9	-0.2	0.2
V3	Power combiner	-0.5	46.4	-0.5	0.5
V2	Cable	-0.1	46.2	-0.1	0.1
V1	Yagi antenna group	15.0	61.2	15.0	0.0

Table 5.5: Values for the up- and downlink budget of the VHF RF front end.

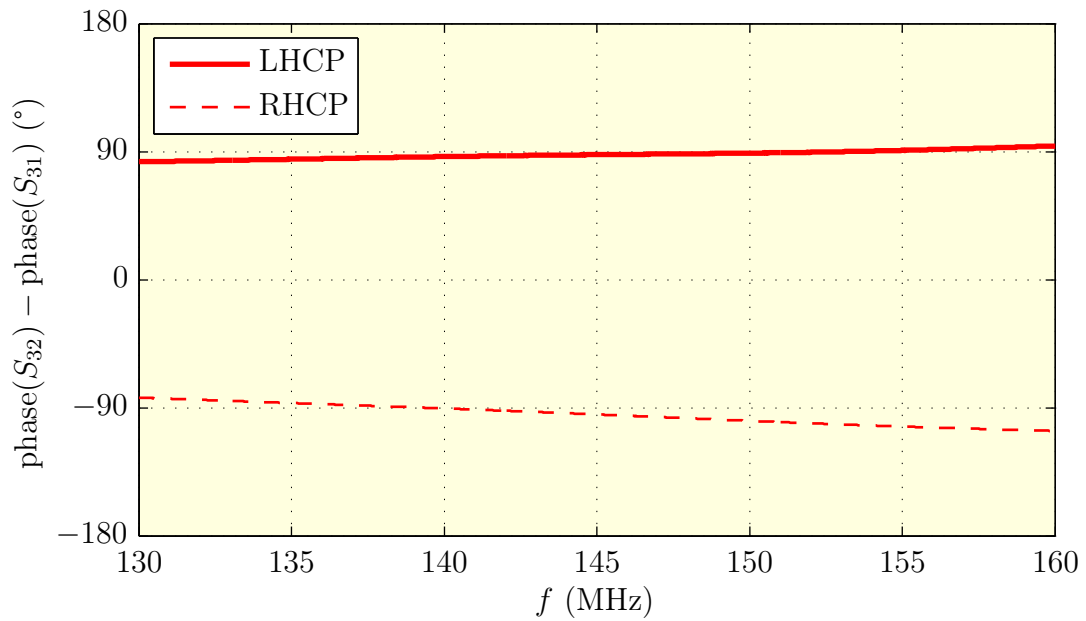


Figure 5.38: Phase differences in the CP modes of the polarization selector used in the VHF RF front end.

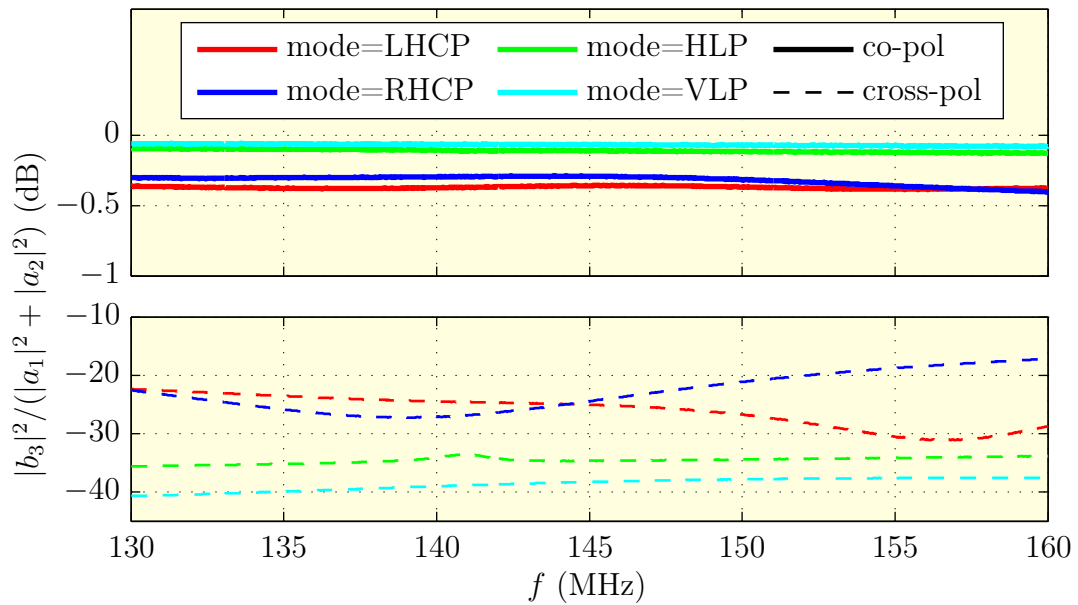


Figure 5.39: Gain of the polarization selector used in the VHF RF front end for its different states for co- and cross-polarized input waves.

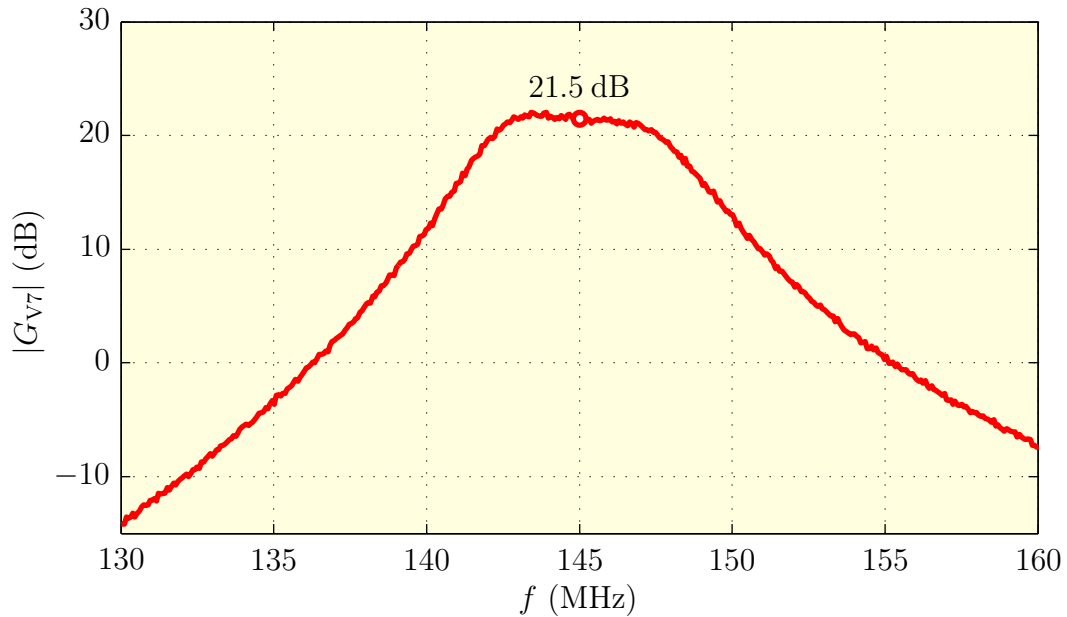


Figure 5.40: Gain of the LNA used in the VHF RF front end.

## 5.6 Mission Specific Segment

The RF front ends and the general signal processing segment perform all data treatment steps common for communication with a satellite. In contrast, the mission specific segment contains all components which cannot be shared among different satellite missions. These are mostly responsible for the data processing on the higher layers of the communications protocol. Typically, we find here TNCs and mission specific control software.

A TNC is responsible for generating a binary data stream when transmitting. In the other direction, the TNC packetizes the binary data stream when receiving. It removes the outer, bottom protocol layers and possibly performs decryption of the data.

### 5.6.1 CoRoT TNC and Data Storage

The CoRoT mission adheres to the CCSDS standards for communications with Earth [15]. A dedicated CCSDS decoder is used as TNC. Upon receiving a CCSDS data stream, it autonomously performs the separation of the virtual channels inside



the stream and stores each of the channels in a separate file with a maximum size of 10 MB. The gross data rate of the downlink is some 800 kbit/s. If no data is received for more than two minutes, the TNC resets its data processor and closes all open files.

The CoRoT specific data storage synchronizes itself with the CCSDS decoder five minutes after the end of a CoRoT pass. The files recorded during the pass, are transferred to a file transfer protocol (FTP) server. CNES periodically retrieves the data from this data storage via the secure file transfer protocol (SFTP) over the Internet (see *Data Storage* and *Mission Data Collector* in Figure 4.3).

The CoRoT data storage is also used by CNES to book passes with the ground station and to share updated two line elements (TLEs) of the CoRoT satellite. These datagrams are processed automatically by CoRoT specific software (see *Control Scripts* in Figure 4.3). Further software periodically cleans up the data storage and, after a certain time, removes data that has already been transferred. The data storage is implemented using Linux on virtualized hardware.

### 5.6.2 MOST TNC and Computer

The MOST satellite's communication with Earth follows the AX.25 protocol [82]. The AX.25 protocol encapsulates the commands and data transmitted between the satellite and the ground station inside datagrams and forms binary sequences for transmission [42]. A MOST proprietary TNC is used for this purpose. Following the original AX.25 TNC definition, it includes a baseband modulator. It therefore has an analog output for the uplink signal. For reception, it connects to the EIA-530 output of the satellite modem (see Section 5.2.10). The data rates are 9.6 kBaud for the uplink and 38.4 kBaud for the downlink.

A separate ground station computer (see *Mission PC* in Figure 4.3) is used to run the MOST ground station software [8]. This is a computer separated from the main ground station control system for robustness reasons. At the moment the computer is a physical one, in a future step the computer will be moved to virtualized hardware.

### 5.6.3 BRITE TNC and Computer

For BRITE, the satellite communication uses the nanosatellite protocol (NSP). This communication protocol is like the one used with MOST based on the AX.25 protocol [6]. Again, a BRITE proprietary TNC is used, which is a successor of the

TNC used for MOST and has similar inputs and outputs. However the data rates are 4 kBaud for the uplink and up to 256 kBaud for the downlink.

Similar to MOST, the BRITE ground station software uses a dedicated computer for robustness reasons. The computer hardware is a virtualized one.

## 5.7 TU Wien Ground Station Control Software

For controlling the TU Wien Ground Station, I have developed a special software. Its main tasks are

- hardware control (see Sections 5.7.2 and 5.9.1),
- satellite tracking (see Section 5.9.2),
- task scheduling (see Section 5.8) and
- interaction with operation personal (see Section 5.7.4).

I have written the software object oriented in the C++ programming language for a multi-threaded MS Windows environment using a few external complementary libraries. The software operates in near real-time and acknowledges that Windows environments do not offer true real-time capabilities. Special care has been taken to make it easily expandable in the future and freely configurable by means of configuration files.

Figure 5.41 shows a block diagram of the internals of the TU Wien Ground Station Control Software and its interaction with the outside. Each of the blocks corresponds to an instance of a C++ object dedicated to a specific task. The blocks are connected to each other and pass messages to each other using a common unified interface (see Section 5.7.1). The connections are set up during startup but can be modified at runtime.

The blocks are organized in the following groups:

**Satellite tracking:** *Rotator, SGP4 Tracker, Parker, Manual Coordinate, Switch, Selector*, see Section 5.9

**Hardware control:** *Wind Sensor, Modem*, see Section 5.7.2

**Pass and task scheduling:** *Action Scheduler, Pass Scheduler, Launcher*, see Section 5.8

**Background support:** *Shutdown, Difference, Logger*, see Sections 5.8 and 5.9.1

**User interface:** *Display, Text GUI, Webserver*, see Section 5.7.4

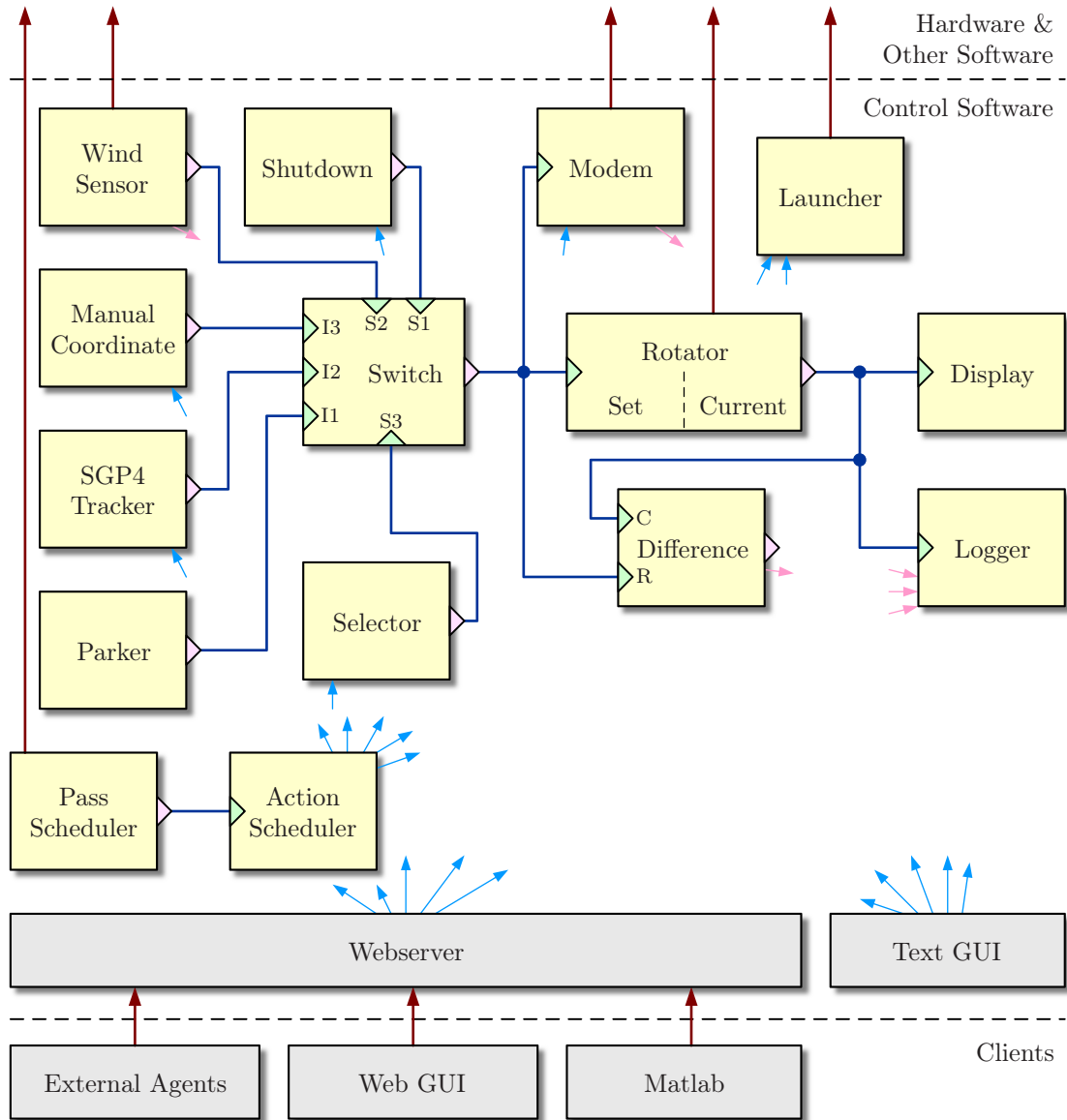


Figure 5.41: Block diagram illustrating the modules of the TU Wien Ground Station Control Software and their interaction. The light blue arrows symbolize *write actions*, the light red arrows symbolize *read requests*.

### 5.7.1 Inter-Block Messaging

The control software uses multi-threading for operation. While the main thread is responsible for the main message loop and the *Text GUI*, most of the blocks have a dedicated worker thread in the background for their respective actual tasks. The background threads communicate internally asynchronously with their block's main thread or can (again asynchronously) request a main thread notification via the main message loop. The main message loop is constructed similarly to the standard Windows message queue loop.

Two types of messages are passed between the blocks:

1. synchronous notifications with data packages (dark blue lines in Figure 5.41)
2. actions and simple messages (light blue and light red arrows in Figure 5.41)

#### Synchronous Notifications with Data Packages

When the main thread part of a block is given control by the message loop, it can notify its connected peers with special data packages. These data packages include

- new azimuth and elevation coordinates,
- a timestamp when these coordinates are valid,
- a range rate,
- a status text and
- the originator of the data package.

The main purpose of these notifications is the update of the connected peers with new direction information of the satellite. Because each coordinate is accompanied with a timestamp, the receiving block knows when the coordinates are valid. A block can, for example, be informed five seconds before the satellite reaches a certain position. The ground station internally only uses coordinated universal time (UTC). However, for presentation of timestamps to the user, they are often converted to local time on the user's client.

The range rate  $v_{\text{rr}}$  is the speed by which the satellite moves away from the observer, i.e.

$$v_{\text{rr}} = \frac{\vec{v} \cdot \vec{r}}{|\vec{r}|}, \quad (5.16)$$

where  $\vec{r}$  is the vector from the observer to the satellite and  $\vec{v}$  is the velocity vector of the satellite, both in a geocentric equatorial inertial (GEI) coordinate system.

The range rate directly relates to the Doppler shift  $\Delta f_{\text{Doppler}}$  by

$$\Delta f_{\text{Doppler}} = -\frac{v_{\text{rr}}}{c} f, \quad (5.17)$$

using the transmit frequency  $f$  and the speed of light  $c$ .

Each data package is also accompanied with a status text. This is, for example, the name of the satellite whose coordinates are advertised. Mostly, this is used for displaying information to the user or for recording in a logfile.

There are blocks which mainly emit coordinates, like the *SGP4 Tracker*, which outputs updated coordinates of the satellite it tracks. Then, there are blocks which mainly wait for coordinate input, like the *Display*, which informs the user utilizing the program's status header. Last but not least, there are blocks which both receive and transmit notification data packages, like the *Rotator*, which accepts new set coordinates on the one hand and informs other blocks of the current pointing direction of the parabolic dish on the other hand.

When there is more than one receiver port in a block, the ports can have names, and then, notification connections from other blocks can be made to a specific port. Here, the originator field in the notification data package is used to identify the destination port. The *Switch* for example distinguishes between alternate coordinate inputs (I1, I2 and I3) and selection inputs (S1, S2 and S3). The latter determine which one of the alternate coordinate inputs is forwarded to the output and which are ignored.

The second main purpose of these synchronous notifications is to inform the block's peers of a state update. The *Pass Scheduler* for example informs the *Action Scheduler* of a new pass scheduled by a notification data package and triggers a schedule update there. Most fields of the data package are ignored then.

Worker threads of blocks can asynchronously request a notification by the main thread.

## Actions and Simple Messages

Beside the synchronous notifications with data packages, there are other, even more powerful means for communication between blocks and for the control of blocks. These are called *actions* and are grouped in read actions, write actions and control actions. They are symbolized by light red arrows for the read actions and light blue arrows for the write and control actions in Figure 5.41.

There are two read actions to query key/value pairs from blocks, and two write actions to modify key/value pairs in the blocks. Their four action codes are called

`int`, `str`, `setint` and `setstr` respectively. Together with a key from a predefined list of named keys, the actions can either transport `integers` or `strings`. Most blocks only support very few keys. Reading an `integer` with some certain key corresponds to a different parameter of a block than reading a `string` with the same key from the very same block. The same applies to write actions. These four actions are called simple messages.

The read actions are performed immediately by the blocks involved. The write and control actions are normally queued in the main message queue and are processed by the main message loop one after the other.

Actions can be requested by each of the blocks, by the *Text GUI* or by the *Webserver*. Typically, write and control actions are requested by the *Action Scheduler* block or by the *Webserver*. The read actions are mostly used by the *Web GUI* via the *Webserver*.

Read actions can query the block's current azimuth and elevation coordinates, its internal timestamp, its range rate, its status, or when accompanied with a key, they can read a simple message from a block.

In turn, write actions to a block can set its current coordinates, timestamp, range rate or status, or can send a simple message to a block.

Control actions are used to connect blocks to each other, or to remove such connections. They can start or stop a block and can shutdown the control software. After a shutdown, the ground station control software is automatically restarted after a few seconds, thus allowing a full reset of the controller.

## 5.7.2 Hardware Control

Three of the main blocks are used to directly control hardware components. These are the *Wind Sensor* and the *Modem* block – described here in this section – and the *Rotator* block described in Section 5.9.1.

### Wind Sensor

The *Wind Sensor* block is connected to the wind sensor through a serial connection. The RS-232 signal from the wind sensor is first converted to TCP data and is available to the control software over a virtual serial port. The block captures the datagrams sent periodically by the wind sensor and decodes them. Other blocks can then read the current wind speed by simple read actions.

If the wind speed increases over 45 km/h, the block asserts wind mode. It stays in wind mode for a minimum of 10 minutes. If the wind speed has decreased below 40 km/h by then, wind mode is canceled. Otherwise, the block waits till the wind speed has sufficiently decreased. The two thresholds and the retention time are configurable. When wind mode is asserted, the block informs the *Switch* block, which puts the rotator into parking position (see Section 5.9.1).

If no datagrams of the wind sensor are detected for a too long period, the block also asserts wind mode. This ensures safety in case of sensor failure.

The *Logger* block periodically polls the *Wind Sensor* block and records the wind speed and wind state in a logfile. See Figure 6.10 in Chapter 6 for an example. There, the red portions in the top diagram show the periods when the ground station is turned off because of wind mode.

## Modem

The PSM-500 modem (see Section 5.2.10) is controlled by the *Modem* block. Upon receiving a short message with a configuration name, the block sets up the modem into the requested state. A state vector consists of parameters like the modem's IF, modulation scheme, bit rate and FEC settings.

The *Modem* block can also automatically shift the selected IF of the modem to compensate Doppler shift. The IF shift is calculated by equation (5.17) from the range rate supplied by other blocks.

The block periodically requests status information from the modem and stores it internally. Status information includes the demodulators state (locked, unlocked or failure), the signal power, the signal quality (SNR and BER) and the receiver offset (i.e. Doppler shift). These parameters in turn can be polled by other blocks or logged by the *Logger* block to a file. For an example record of the signal power during a pass, see Figure 6.3 in Section 6.2.

### 5.7.3 Built-In Webserver

The *Webserver* built into the ground station control software is its most versatile interface. By means of HTTP requests an entity can completely read the status of the ground station and control it (see also Section 4.2.1). This enables feedback from external modules (see Section 5.8), remote control (see e.g. Section 4.2.2) and powerful user interaction (see Section 5.7.4).

The built-in webserver responds in two different ways depending on the uniform resource locator (URL) requested. On the one hand it responds to action requests and on the other hand it simply transfers files to the client like a traditional webserver. The latter feature is used to host the *Web GUI*.

The client can encode several action requests within the URL of a single HTTP request. Each request consists of the number of a block it should operate on. The blocks are given numbers in the setup files of the control software. Furthermore, each action request specifies an action code. For the key/value pairs of the blocks, these are `int` and `str` for reading and `setint` and `setstr` for writing (see Section 5.7.1). Depending on the action, there can be further parameters like a key name or a value. For each action request, the webserver first checks if the user logged in is authorized to request the specific action. There is also a public mode, when no user is specified by the client. If authorized, read action requests are processed immediately and write and control actions are put onto the main message queue and processed there. If not authorized, action requests are silently dropped.

The webserver uses a separate working thread for the HTTP requests. The read requests are therefore processed asynchronously to the rest of the control software. The server also offers encrypted communication using HTTPS.

### Authorization of Actions

Each action request is checked for authorization before being processed. Authorization is defined in a setup file. The setup file contains elements to define groups of users, hosts and commands respectively.

Users are specified by a user name and a password and are assigned to groups. If no user is specified by the client during the HTTP request, a predefined default public user is assumed for the connection.

Single hosts are specified by their internet protocol (IP) address. Networks are specified by their IP address and network mask.

Command groups consist of a combination of action code, block number and parameters. For each of these, wildcards can be used. So a command group could for example consist of all read actions (`int` and `str` on any block with any key name) or of any command to one of the blocks.

In the authorization setup file, there are rules allowing or denying a specific combination of user group and host group to perform a specific command group. Again wildcards can be used for user, host or command groups.



### 5.7.4 User Interfaces

The ground station offers different means of interaction with the users of the ground station. Different user interfaces allow for the daily operation of the ground station, for long term quality tracking, for automated measurements, for maintenance tasks, for trouble shooting and many more tasks.

#### Text GUI

The most basic GUI is the *Text GUI* shown in Figure 5.42. The figure shows both the *Display* block and the *Text GUI*. The *Display* block receives coordinates and status text from its peers and displays them in the title line of the application window. In the figure, the antenna points to 6.4° above the horizon in approximately north-north-west direction. The *Text GUI* code is part of the main message loop of the ground station control software. It displays one or two lines per block. The color of the line represents, whether the line corresponds to the input (red) or the output (green) port of a block. Two lines are shown if input and output port are relevant in a block. Blue color is used if the block works mainly manually. The *Text GUI* allows for basic visualization of the control software state and for maintenance interaction with the ground station. Using the keyboard, the user can open or close a block or enable or disable notification routes between blocks. The keyboard commands are translated into actions and simple messages here.

#### Web GUI

The *Web GUI* shown in Figure 5.43 is built upon the *Webserver* of the ground station control software (see Section 5.7.3). I have completely written it in the hypertext markup language (HTML) and the JavaScript programming language. It is executed in the user's web browser. The individual script files are stored along the control software and are delivered to the client via the control software's internal webserver. The *Web GUI* is structured in widgets, each using a horizontal block on the user's screen. The figure shows a few basic status widgets on top and more advanced visualization widgets on the bottom.

The *Web GUI* periodically polls the status of the control software over its HTTP interface by submitting read actions. The results are then nicely formatted in the user's web browser. Each widget refreshes its content automatically. The refresh period depends on the widget's content and the control software's state.

Upon entering a user name and password, the *Web GUI* also allows for write and control actions being submitted to the control software. This allows to set the

```

2012-03-25T09:32:40.075 <UTC+02> selection: 00:00
09 S4 09 S1 09 S2 09 S3 11 R 12 R 08 S2 08 S1 18 T 07-11 14-06 05-01
>01 Winter 1.95 343.61 +006.68 MOST 0 -0.2 0.1 1.37
<01 Winter -0.01 344.08 +006.40 00JK=F -0.8 0.0C /t~m~e~t~mtem 0.13
>04 LoggerSmpl -0.01 344.08 +006.40 4,1,5,12,14,16,17,20 00JK=F -0.8 0.13
<05 Flipper 1.95 343.61 +006.68 MOST 0.7 45283 -3.7801 :2 0.22
<06 Switch 1.95 343.61 +006.68 3:MOST 0.7 45283 -3.7801 :0,0.3 0.22
<07*Player -5:32:39 000.00 +000.00 34 0.00 [S7] 2.31
<08 SwFlipper -4:04.8 *2 99.99
<09 GUISwitch -4:02.0 *3 1.83
<11 InpManual -4:02.8 359.33 +000.00 Input 99.99
<12 InpDelta -9:59:59 000.00 +000.00 Input 0.00
>13 LoggerSmpl 0.00 292.50 +010.30 14,26 0.33
<14 Windsensor 0.00 13.7/21.6km/h 292 +14.2C 0.33
<15 Parker 0.00 345.00 +090.00 Parking 0.00
<16 GUIDiff -6.85 -00.62 +000.11 00JKF= -0.2 0.0C fme~e~/t~m~e~t~m 0.00
<17 PSM500 -0.01 -295.6k -54.1m 19.5dB <1.0e-10 -++ MOST +00.0k 0.50
<19 SGP4 2.00 343.63 +006.67 MOST 0.7 45283 -3.7801 0.22
<20 PSM4900Mon -0.32 +06.1k -53dBm 14.7dB <1.0e-12 -++ c000 177.833 2.09
<21 Token -4:03.3 000.00 +000.00 Lamp 0 LNA 1 PSM 1 UGSPAPWR 1 UGS 0.92
<22 Sun -0.84 118.98 +025.90 Sun 1.11
<23 PassCalc 9:13.4 359.33 +011.81 *MOST 45283 11:38 259.07 0.00
<24 AutoAction 2:20.1 000.00 +000.00 53 UpdCNES [0] 99.99
>25 Launcher -9:59:59 000.00 +000.00 0.00
<26 PCHealth -1:01.4 000.00 +000.00 2970;7405305;2700;4000;666133;648 64.33
<27 Shutdown -9:59:59 off 0.00

```

Figure 5.42: Text interface of the TU Wien Ground Station tracking software.

rotator's coordinates manually or to disable one of the scheduled passes. Also, many of the ground station's hardware blocks can be turned on or off with one of the widgets.

The widgets can be freely arranged vertically on the screen. Even a two column mode is supported. Most of the widgets can be resized. The layout can be stored on the client and there are several predefined layouts.

## Advanced Web GUI

Figure 5.43 on the bottom and Figure 5.44 show two of the more advanced visualization widgets of the *Web GUI*. Most of the ground station status parameters are sampled periodically and automatically plotted in graphs. The green graph in Figure 5.43 shows the communication duration of the ground station with CoRoT and MOST in minutes per day. The dark green bars represent communication time missed because of shutdown of the ground station caused by strong wind. The black bars represent the total theoretical possible communication time for each day.

The two blue diagrams convey similar information, split by the two satellites and represented in percent relative to the theoretical possible communication time for each day.

## 5.7 TU Wien Ground Station Control Software

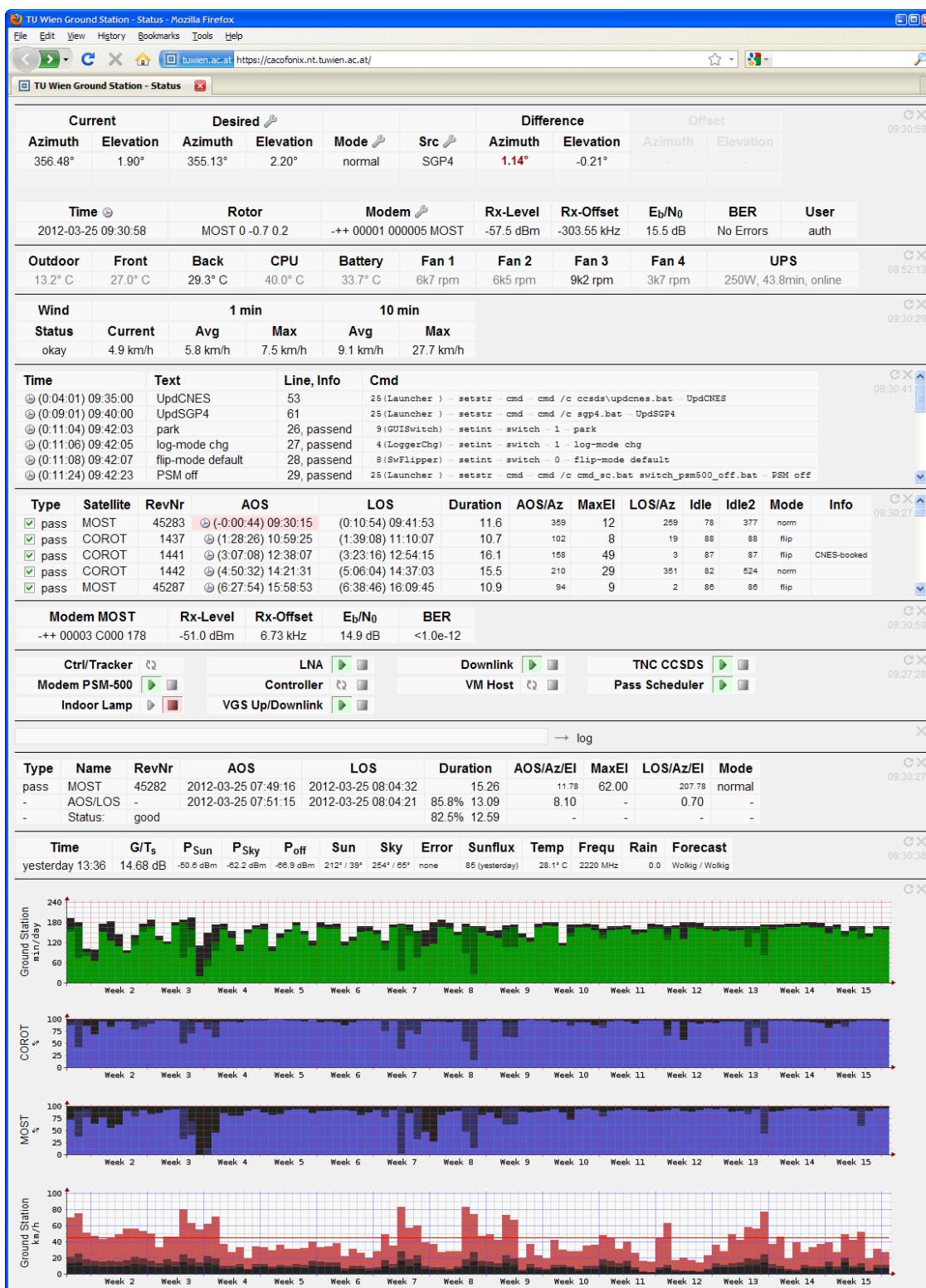


Figure 5.43: Web interface of the TU Wien Ground Station tracking software.

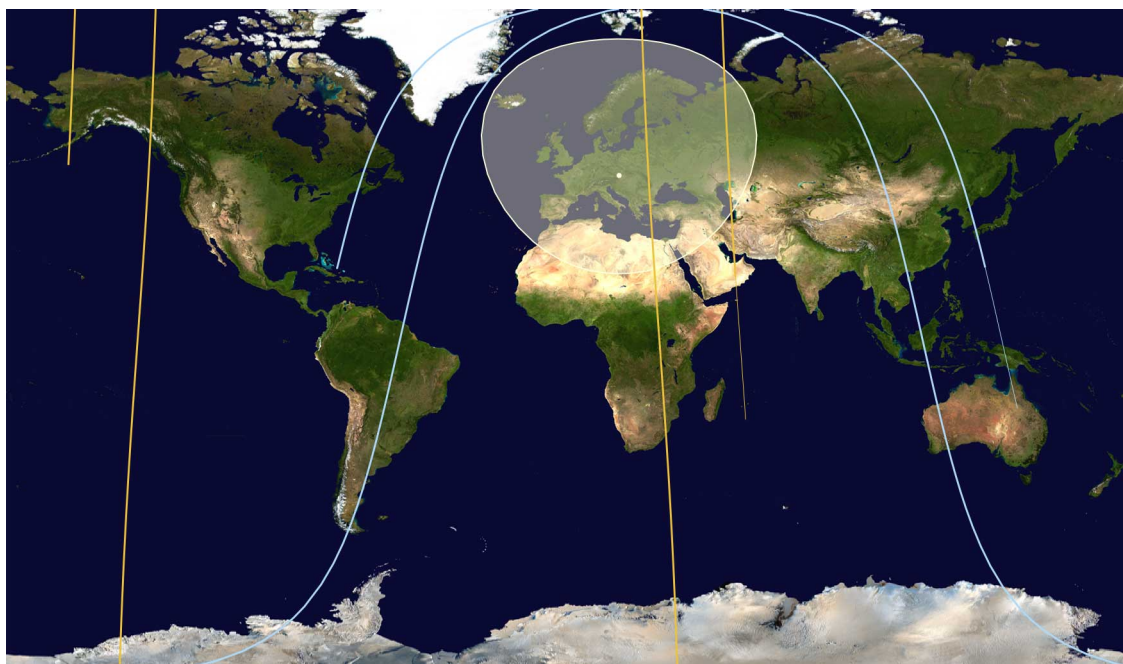


Figure 5.44: Visualization of the recent and future satellite's paths and the ground station's visibility region over the Earth in the online web interface using a photo of the Earth by NASA [83].

Finally, the red diagram in Figure 5.43 gives the maximum wind speed together with two averaged values for each day. The bright red line at 45 km/h is the wind mode threshold selected for the ground station.

Similar graphs exist for the traffic over the Internet, split up by each satellite or service. Furthermore, there are graphs for temperature, power consumption, tracking error, receiver offset frequency, received signal strength and BER, modem status and many more. The diagrams can be shown with different timescales on the abscissa, spanning a day, a few weeks or more than a year.

Figure 5.44 gives a graphical representation of the current and future satellite's positions as calculated from the *SGP4 Tracker* module (see Section 5.9.2). For each of the satellites tracked, the ground path is visualized with a line. These lines extend one and a half satellite orbits into the future and a bit into the past. The past is shown with a thinner line. To indicate the possible contact times, the visibility region of the ground station is shown shaded for a satellite with an altitude of some 800 km, a circular orbit and a minimum elevation of  $0^\circ$ .

## 5.8 Pass and Task Schedulers

The TU Wien Ground Station Control Software incorporates two schedulers with several further supporting blocks. The *Pass Scheduler* block calculates possible satellite passes over the ground station and resolves conflicts. The *Action Scheduler* block generates the actual action requests necessary during a pass or during a day for other reasons.

### 5.8.1 Pass Scheduler

The *Pass Scheduler* block calculates possible satellite passes over the ground station. As input it gets TLEs from a file (see Section 5.9.2). The TLEs are retrieved from different sources. For CoRoT, CNES periodically supplies updates. For MOST, TLEs from the North American Aerospace Defense Command (NORAD) are used which are periodically retrieved via CelesTrak.

The *Pass Scheduler* uses a simplified perturbations model 4 (SGP4) algorithm (see Section 5.9.2) to calculate the satellite passes over the ground station for the next three days for each of the satellites configured. The data calculated include expected acquisition of signal (AOS) and loss of signal (LOS) times  $t_{\text{AOS}}$  and  $t_{\text{LOS}}$ , azimuth  $\varphi_{\text{AOS}}$  and  $\varphi_{\text{LOS}}$  of AOS and LOS, maximum elevation  $\vartheta_{\text{max}}$  and duration of each pass. The passes are sorted chronologically and – if configured – some external program is called to set priorities among the satellites and passes. Currently, this external program takes into account the reservations for CoRoT passes by CNES and it skips passes with low maximum elevation  $\vartheta_{\text{max}}$ . After this external selection, the *Pass Scheduler* eliminates further conflicts, taking into account a setup time of the ground station of 120 s and a decommissioning phase of the ground station after each pass of 90 s.

The pass list is updated periodically every few hours, upon update of the TLEs or when requested. After each update, the *Pass Scheduler* notifies its connected peers.

### 5.8.2 Task Scheduler

The *Task Scheduler* automatically generates action requests and submits them to other blocks using the main message queue. It is configured with a specially tailored type of `cronfile`. Traditionally, `cronfiles` on Unix systems consist of multiple lines, each line containing a timing information and a job to process [84]. The timing information is a schedule, specifying at which minute, at which hour and/or at

which day a job has to be executed. Picking up on this, the *Task Scheduler* uses a similar style. The job information is replaced by an action request (see Section 5.7.1) with all its parameters separated by tab characters (ASCII 0x09). The last parameter is used as a descriptive text. For example the line

```
0 0-23/3 * * * → 25 → setstr → cmd → cmd /c updtle.bat → UpdTLE
```

is used to periodically update the TLEs every three hours at each day of the week. It utilizes an external script `updtle.bat` which is launched by the *Launch* block with the internal number 25.

The syntax of the `cronfile` is further extended to additionally support sequence blocks and satellite passes. Sequence blocks are a batch of actions which are processed one after the other. In the `cronfile`, their start time relative to the block start can be specified. The start time of each block is manually set by a write message to the *Task Scheduler* indicating the block's number. That way, single write actions can trigger complex, predefined, timed operations. The extension toward satellite passes is explained in the next section.

### 5.8.3 Tasks During a Satellite Pass

The syntax of the `cronfile` allows to define actions which execution is triggered by a satellite pass. For each action, one can specify the time relative to the start (AOS) or the end (LOS) of a pass. Actions can be conditionally limited to a specific satellite. The *Pass Scheduler* block informs the *Task Scheduler* block of an updated pass list. The *Task Scheduler* then polls the next satellite pass and uses its AOS and LOS times to queue the actions specified accordingly.

Figure 5.45 shows the sequence diagram of a CoRoT satellite pass. On the unscaled vertical time axis, the expected AOS and LOS are referred to by the symbols *s* and *e* respectively. The diagram lists the actions and the activation times of a few of the components involved in a pass.

About 2 minutes before a pass begins, the modem and the RF front end are switched on and initialized for CoRoT. 30 s after the pass they are switched off again.

98 s before CoRoT appears at the horizon, the rotator is assigned to move into the initial position. The position is given by the expected AOS azimuth and an elevation of 0°. Next – while the rotator starts moving – the rotator is connected to the *SGP4 Tracker* block (see Section 5.9.2). This block has already been set to track CoRoT. Because the *SGP4 Tracker* block emits negative elevation coordinates at that time, the rotator ignores them and moves steadily to the starting position. This takes

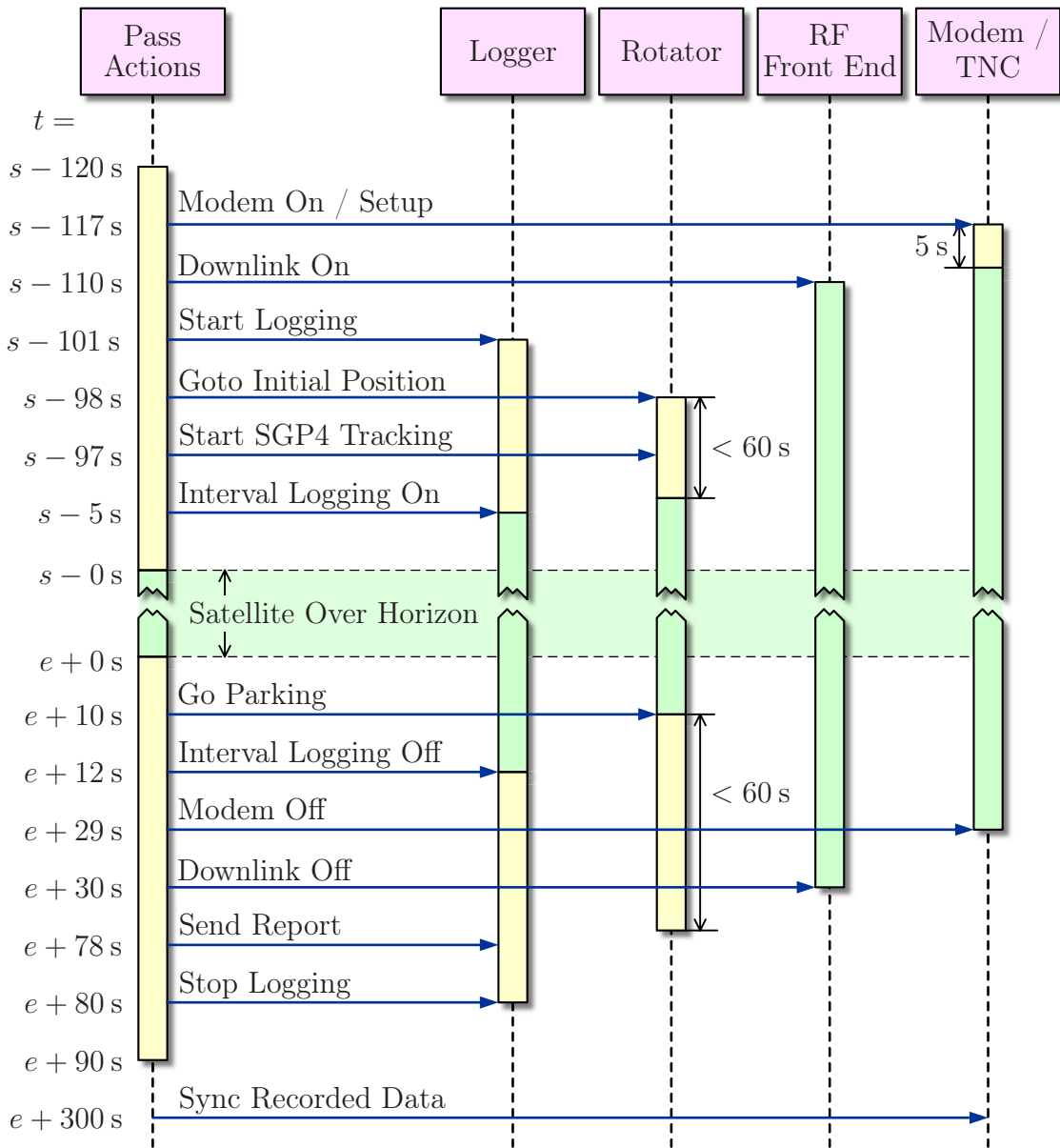


Figure 5.45: Sequence diagram for a CoRoT satellite pass.

some 60 s at maximum. 10 s after the pass, the rotator is connected with the *Parker* block which brings the antenna system back to 90° elevation.

In advance to a pass, the *Logger* block opens a new logfile and starts logging to it. The logfile is given a unique name including the current date, the satellite's name and revolution number. The *Logger* is configured to log several parameters including the received signal quality – whenever the rotator moves (see Section 5.9.1). Then, 5 s before the pass actually starts, the *Logger* is switch to interval logging mode, where it logs regularly 2 times per second.

This mode is turned off 12 s after the pass has ended. 78 s after LOS, the logfile and other data are analyzed automatically (see Section 6.2). A report is generated and sent to the operation personal via email. Finally, 80 s after LOS, logging is stopped again.

In case of CoRoT, a special synchronization process is scheduled 300 s after the pass to forward the data recorded to the CoRoT data storage (see Section 5.6.1). This is realized with a separate sequence block which is outside of the time scope of the pass, as seen from the *Task Scheduler* block (see Section 5.8.2).

## 5.9 Antenna Rotator and Satellite Tracking

The antenna systems are mounted on a single azimuth/elevation rotator (see Sections 5.1 and 5.4). The rotator and its control software are discussed in Section 5.9.1. During a satellite pass, the rotator points to the respective satellite. The corresponding SGP4 tracker is discussed in Section 5.9.2.

### 5.9.1 Antenna Rotator and Rotator Controller

The rotator is a combined azimuth/elevation rotator from Winter Maschienbau. It is mounted on top of a 6 m high mast on top of the roof of the Institute of Telecommunications, resulting in some 34 m height above ground. The rotator is equipped with an integrated pulse width modulation (PWM) motor driver and a position sensor with 0.1° resolution. The rotator operates with angular speeds up to  $v_\varphi = 7.5^\circ/\text{s}$  in azimuth and up to  $v_\vartheta = 2.0^\circ/\text{s}$  in elevation.

On top of the rotator the 3.7 m parabolic dish is mounted (see Section 5.1 and Figure 7.2). The UHF/VHF antennas will be mounted next to this dish. Previously, they where mounted on a secondary smaller rotator (see Figure 5.31 and [72, 73]). Beneath the rotator, there is a 4 m × 4 m platform, which allows for easy access to the antenna systems.



Initially, the pointing direction of the rotator has been calibrated roughly by visual inspection. After that, the antenna pattern has been measured to optimize the calibration of the pointing direction (see Section 5.2.2).

### Rotator Controller

I have programmed a rotator controller in the C++ programming language (see *Rotator* block in Figure 5.41). It is part of the TU Wien Ground Station Control Software and calculates the commands sent to the PWM motor driver through a RS-485 link. It accepts azimuth/elevation coordinates together with a timestamp and calculates the speed necessary to reach the requested position at the requested time. For typical passes the speeds are only a fraction of the maximum speed. For the azimuth direction, this results in start/stop operation at low speeds. The rotator controller has been optimized to avoid twitching in this situation. A finite state machine (FSM) is used to enable the various drive modes of the rotator.

Various other blocks interact with the *Rotator* block. The *Switch* block connects one of many alternate input sources to the *Rotator* block. One of the sources is a *Manual Coordinate* block, which receives the direction via user input or simple messages. Other sources are an *SGP4 Tracker* block (see Section 5.9.2), a *Parker* block and a block that tracks the Sun. Which of the sources is passed to the *Rotator* block is determined by the state of several blocks at the switch's selection inputs S1, S2 and S3. Input S1, which is connected to the *Shutdown* block, takes precedence and can force the selection of the *Parker* block if instructed by an external command. Next comes the *Wind Sensor* block connected to S2. It forces the selection of the *Parker* block in case of strong wind. The last is the manual *Selector* block at port S3 which can freely chose one of the input sources as necessary. See Section 5.8.3 for the use of the *Selector* block during a pass.

### Tracking Accuracy

The *Rotator* block periodically reads the current pointing direction of the rotator at 5 Hz. This information is used to calculate the desired speed of the motors. Furthermore, these coordinates are logged by the *Logger* block into a logfile whenever the rotator moves or periodically during a pass.

The current pointing direction of the rotator is also compared inside the *Difference* block to yield the pointing errors  $\Delta\varphi$  and  $\Delta\vartheta$  of the rotator. The *Difference* block stores the input coordinates together with their timestamps and compares them with the current coordinates. Figure 5.46 shows azimuth  $\varphi$  and elevation  $\vartheta$  of an

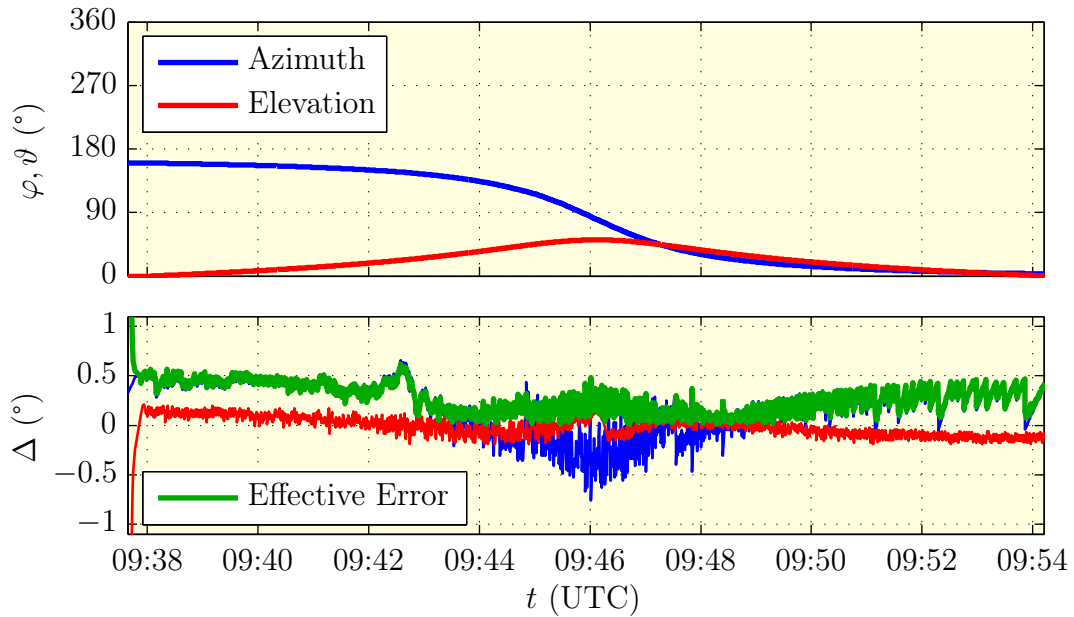


Figure 5.46: Tracking accuracy of an exemplary 2012-04-10 CoRoT pass.

exemplary CoRoT pass. The bottom subfigure shows the differences  $\Delta\varphi$  and  $\Delta\vartheta$  along with the effective error  $\delta$ . The latter is the arc length of an orthodrome on the azimuth/elevation hemisphere between the desired/set point  $(\varphi, \vartheta)$  and the actual current point  $(\varphi_{\text{curr}}, \vartheta_{\text{curr}}) = (\varphi + \Delta\varphi, \vartheta + \Delta\vartheta)$  [49]. The effective error is given by

$$\delta = \left| \arccos \left[ \sin(\vartheta) \sin(\vartheta - \Delta\vartheta) + \cos(\vartheta) \cos(\vartheta - \Delta\vartheta) \cos(\Delta\varphi) \right] \right|. \quad (5.18)$$

For each pass, the mean effective error  $\bar{\delta}$  is calculated and included in the report after the pass. Figure 5.47 shows the errors for 2760 passes. 91.3% of the passes have a mean tracking error smaller than  $1^\circ$ . In October 2011 the control algorithm inside the *Rotator* block has been optimized to reduce the tracking error below  $0.5^\circ$  and to minimize twitching in start/stop operation mode. Beside the mean tracking error for each pass, a weekly average of these passes has been plotted in Figure 5.47. It is as low as  $0.4^\circ$ . This figure is monitored regularly to ensure the performance of the ground station.

### Parking Position, Strong Wind and Shutdown

The parabolic dish is parked in between passes. The parking position is with the antenna pointing to zenith at  $\vartheta = 90^\circ$ . A special *Parker* block periodically emits this coordinate. The rotator also goes into parking position when there is strong

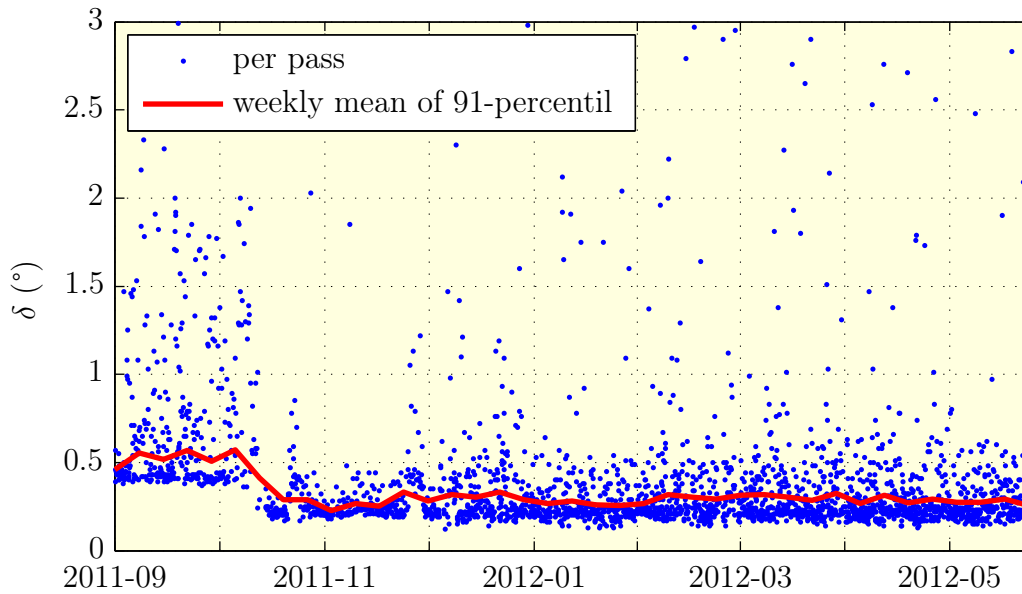


Figure 5.47: Tracking accuracy for each pass plotted over time together with a weekly mean value.

wind – i.e. initiated by the *Wind Sensor* block when wind mode is asserted. When the parking position is reached, the FSM in the *Rotator* block shuts down the motors and disables tracking.

There is also a *Shutdown* block which is used to get the rotator into parking position because of external events. In case of a power blackout, an uninterruptible power supply (UPS) supplies the ground station for a few minutes to allow a coordinated shutdown. In this case, the UPS triggers the *Shutdown* block. Another reason for coordinated shutdown of the ground station is because of over-temperature.

### 5.9.2 SGP4 Satellite Tracker

The TU Wien Ground Station uses TLEs from external sources to track the satellites. TLEs contain the orbital parameters of the satellites tracked in a simple format. They are especially suited for the SGP4 algorithms used for LEO satellites [85].

The *SGP4 Tracker* block in the ground station control software uses an SGP4 algorithm from an complementary library [85] and the provided TLEs to calculate

the selected satellite position. It periodically calculates the  $x$ ,  $y$  and  $z$  coordinates of the satellite and its speed  $\vec{r}$  in the GEI coordinate system. Then it takes the observer position (i.e. the longitude and latitude of the ground station) and calculates the azimuth  $\varphi$  and elevation  $\vartheta$  of the satellite in a topocentric-horizon system along with the satellite's range rate. With an update/calculation rate of 10 Hz, it notifies its connected peers of the updates.

The satellite is selected with a simple `setstr` write action to the block. The block is connected to the *Switch* block and is enabled before a pass.

The very same SGP4 codebase is shared with the *Pass Scheduler* block (see Section 5.8.1) to predict future AOS and LOS times of the satellites tracked.

The SGP4 codebase is also used in a complementary program to calculate the ground path of selected satellites for display in the *Web GUI* (see Section 5.7.4). Here, the GEI coordinates are converted to geographic longitude and latitude.

# Chapter 6

## Performance Measurements

This chapter reports a few performance measurements which have been accomplished with the TU Wien Ground Station to prove its operation and to fine tune some of its parameters. Some of these measurements are repeated on a regular basis to check the quality of the ground station.

### 6.1 Rotator Tracking Accuracy

After each pass, the mean effective tracking error  $\bar{\delta}$  is calculated (see equation (5.18) in Section 5.9.1). This figure is stored and the mean over one week's passes is calculated. Figure 5.47 shows this weekly mean in red. Nominally, the mean pass tracking error should be below  $1.0^\circ$ . It can be seen from the figure that this requirement is fulfilled, the weekly mean is around  $0.4^\circ$ . Higher values are typically caused by disruptions due to wind gusts during a pass.

### 6.2 CoRoT Radio Horizon

Each pass is recorded in a separate logfile by the control software. In these logfiles there are all of the modem parameters during the passes (see Section 5.2.10). These include the receiver lock status and the received signal power.

To assess the radio horizon of the ground station, measurements with CoRoT have been used. In Figure 6.1, the data of 1467 CoRoT passes between March 2011 and February 2012 is plotted. Due to its orbit, CoRoT takes a different path across the sky every pass. Therefore, the whole sky is covered gradually. Points with lower elevation show higher coverage. This coverage depends on the characteristics of the CoRoT orbit.

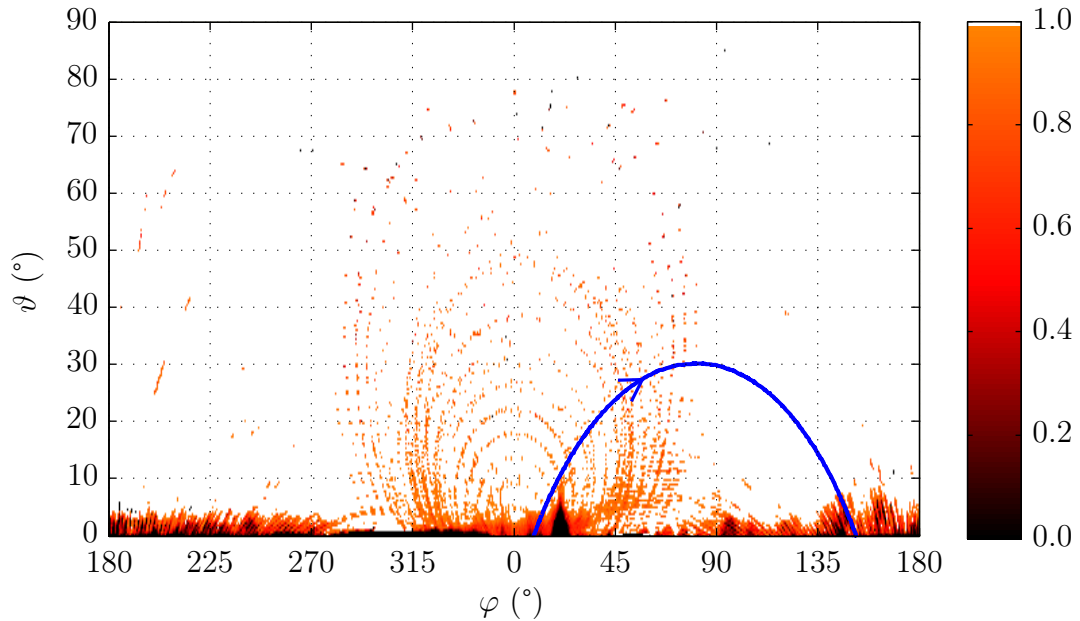


Figure 6.1: Receiver lock probability of CoRoT over 1467 passes. A probability of 99% is shown in orange, a probability of 100% is shown in white. Exemplarily, one pass of 2011-06-13 is highlighted in blue.

Figure 6.1 gives the probability for each point of the sky, if a receiver lock can be obtained with CoRoT or not. The color map used goes from black at 0% to orange at 99%. For clarity, the probability from 99% to 100% is shown in white, which emphasizes areas with lower probability. One exemplary pass from north over east to south is shown in blue. This example demonstrates how the sky is illuminated by the downlink signal during a CoRoT pass.

One can see, that above  $5^\circ$  elevation there is almost 100% of communication probability with CoRoT – with one exception: The circular rings around the north direction are discussed in the next section. At low elevations, the faint rings are due to the characteristics of the CoRoT orbit. The areas with low elevation where no contact with CoRoT is possible is the radio horizon of the ground station.

In Figure 6.2, the data from Figure 6.1 with an elevation from  $0^\circ$  to  $15^\circ$  is repeated. The color map in the pseudo color plot has been changed to allow for a better representation of the radio horizon. It goes from black at 0% over orange to yellow at 100% lock probability. Because not all areas of the sky are equally covered due to CoRoT's orbit, areas with no or low coverage have been desaturated in colors towards white. Below the pseudo color plot a  $360^\circ$  panorama photo is shown. The

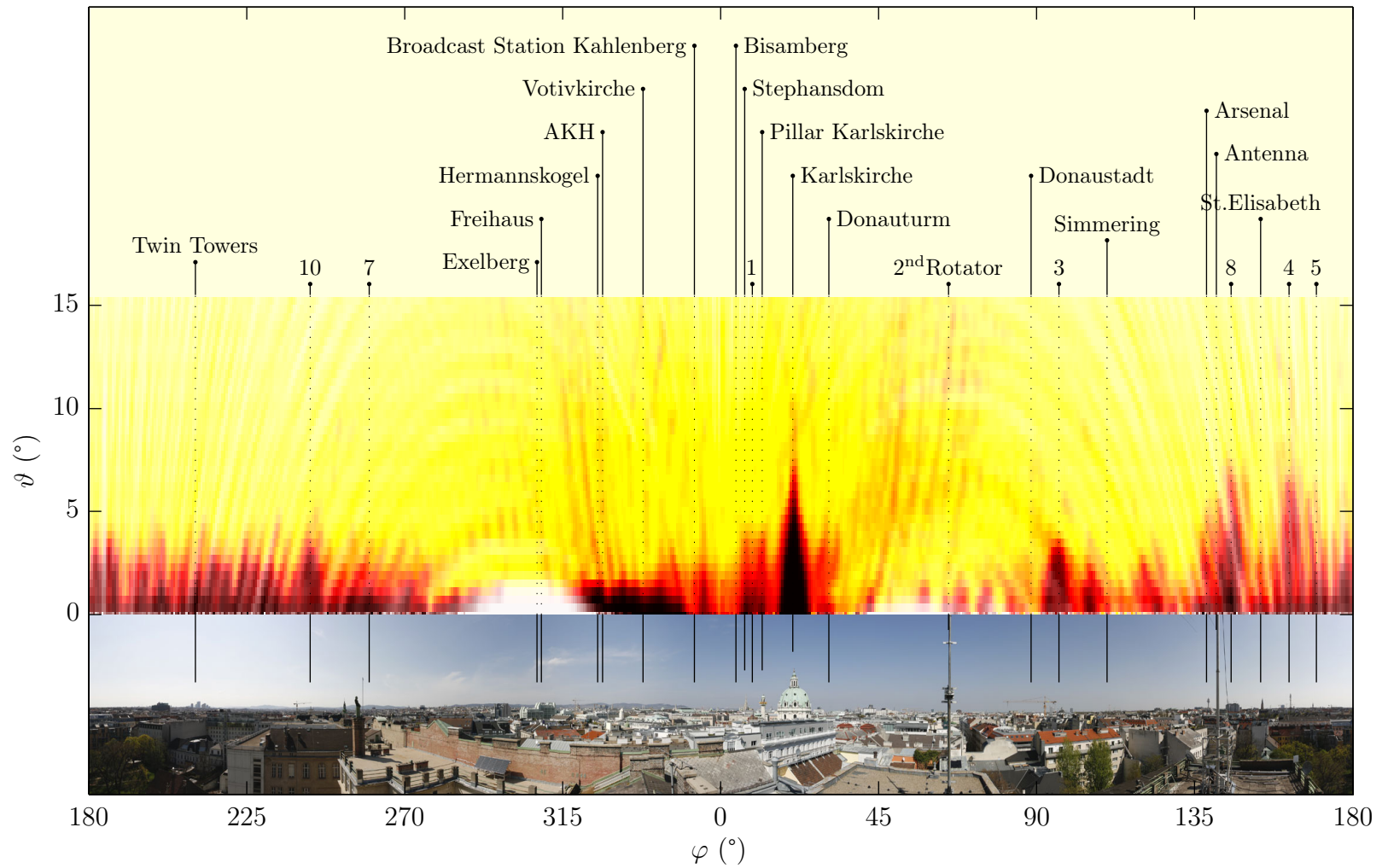


Figure 6.2: The radio horizon with the data from Figure 6.1 plotted on top of a panorama photo of the City of Vienna surrounding the ground station.

photo has been taken around the rotator’s azimuth axis on top of the antenna system’s maintenance platform. While the pseudo color plot covers elevations  $\vartheta$  from  $0^\circ$  to  $15^\circ$ , the photo covers approximately the area from  $-20^\circ$  to  $20^\circ$ . The legend at the top of the figure lists various landmarks in the nearby vicinity or hills around Vienna. The numbers correspond to the mobile communications base stations shown in Figure 3.5. Most of the distinguished landmarks can be seen in both panoramas – at 13 cm wavelength and in the optical regime.

## 6.3 CoRoT Satellite Antenna Pattern

In Figure 6.1, rings with a receiver lock probability below 100% are visible in the northern direction, even at moderate and high elevations. Figure 6.3 shows the azimuth and elevation as a function of time of the exemplary pass originally plotted in blue in Figure 6.1. At the bottom of the figure, the received signal strength is plotted. Unexpectedly, strong fading dips of the signal can be observed – even for elevations above  $25^\circ$  elevation (the maximum elevation of the pass is  $30^\circ$ ).

These “outage” regions form a pattern, if several passes are combined in one plot. The pattern is due to CoRoT’s antenna system: CoRoT utilizes two antennas for

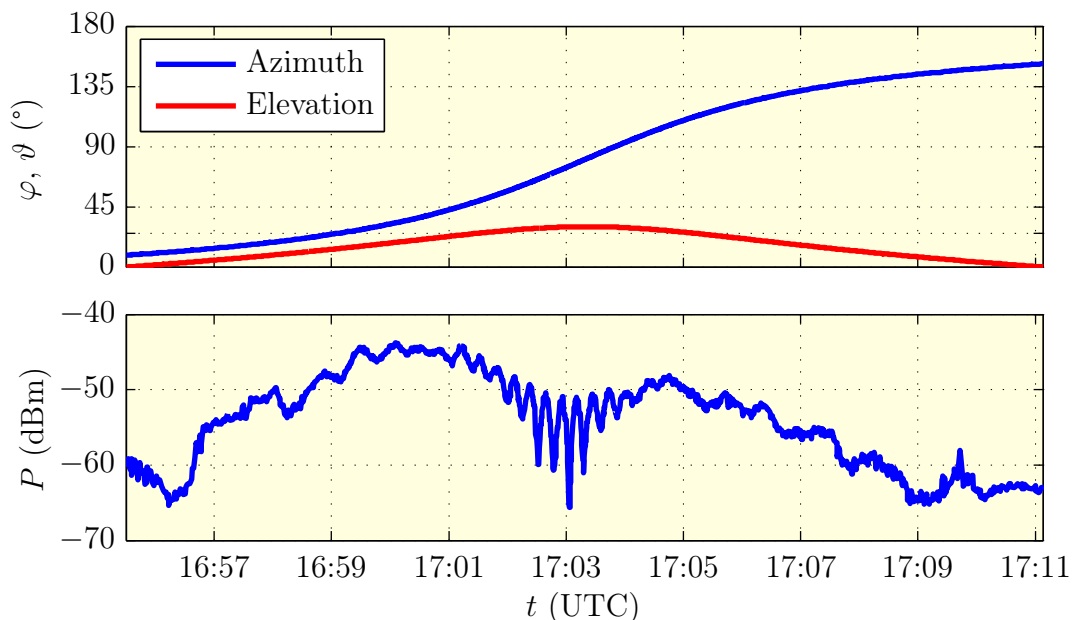


Figure 6.3: Azimuth, elevation and received signal power over time of a 2011-06-13 pass of CoRoT.



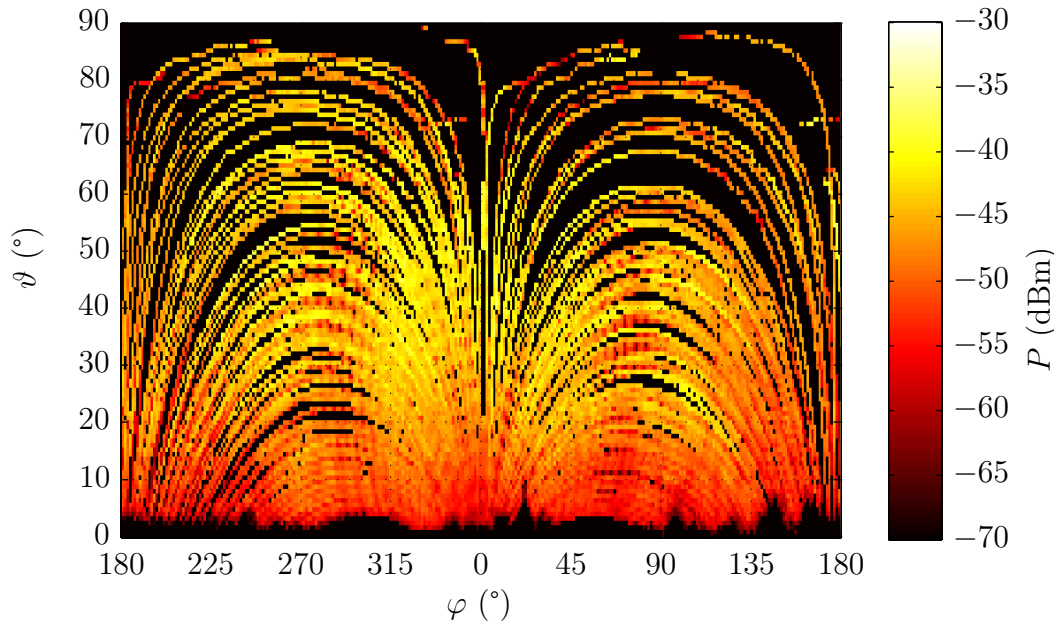


Figure 6.4: Mean received signal level over 245 passes of the CoRoT long run observation period LR07 from 2011-04-05 to 2011-06-30.

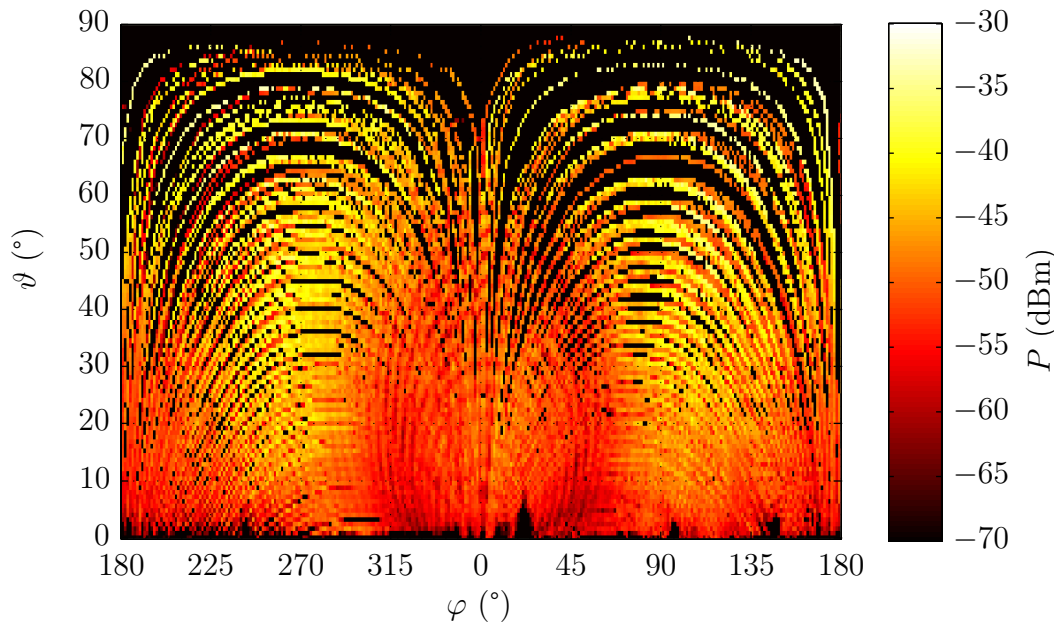


Figure 6.5: Mean received signal level over 377 passes of the CoRoT long run observation period LR08 from 2011-07-05 to 2011-09-30.

almost spherical coverage (see Figure 2.1 and [15]). However, the superposition of the two antennas does not give an isotropic radiator, but the resulting directional pattern shows strong dips in certain regions. This is the pattern visible on ground.

To emphasize this behavior, Figures 6.4 and 6.5 show the mean received signal levels during two observation periods of three months each. During each observation period, the satellite points to a different direction into space, observing different stars – resulting in different outage patterns over Vienna. The two different patterns can be easily seen and distinguished from each other. Areas without coverage from CoRoT during these periods are left black.

## 6.4 MOST Up- and Downlink

Similar to CoRoT, MOST has two transmit antennas as well. However, each of the antennas is assigned a different frequency (see Section 2.2). Therefore, MOST shows a different behavior than CoRoT.

In Figure 6.6, a spectrogram of a 2012-04-11 morning pass is shown. The pass begins at 6:59:33 in the morning (UTC). 117 s before the pass at 6:57:36 the LNA is switched on and the noise level increases. While the rotator goes from parking position with  $\vartheta = 90^\circ$  down to the horizon with  $\vartheta = 0^\circ$ , the noise level further increases when reaching the horizon. The ground station starts transmitting and wakes up the satellite. The first receiver lock on the downlink signal is obtained at 6:59:49 at  $\vartheta = 2.8^\circ$  on “Channel B”. Communication is lost and reobtained a few seconds later as the signal is still very weak. At 7:02:19 the signal is again lost because it gets too low in amplitude. The mission control center in Canada decides to switch to the satellite’s other antenna on “Channel A”. 10 s later, lock is obtained at this frequency. During the rest of the pass, we observe considerably stronger signals, because the “Channel A” antenna of the satellite points closer to the ground station in Vienna. We also observe a peak RSSI level of  $-64.8$  dBm detected with the modem in IF at  $\vartheta = 17.6^\circ$  which is not equal to the maximum elevation  $\vartheta_{\max}$  of  $19.4^\circ$ . At 7:12:51 the pass ends. We lose the signal and 29 s later the LNA is switched off again and the antenna goes back into parking position.

Figure 6.7 shows the uplink part of the communication with MOST, exemplary for three passes of 2012-06-03. The passes have a maximum elevation  $\vartheta_{\max}$  of  $18.8^\circ$ ,  $81.8^\circ$  and  $12.6^\circ$ , respectively. The satellite records the signal level received from ground. The uplink signal from the TU Wien Ground Station can be clearly distinguished from the noise level received when no communication with a ground station is established. During the 16:45 pass, the received signal power at the

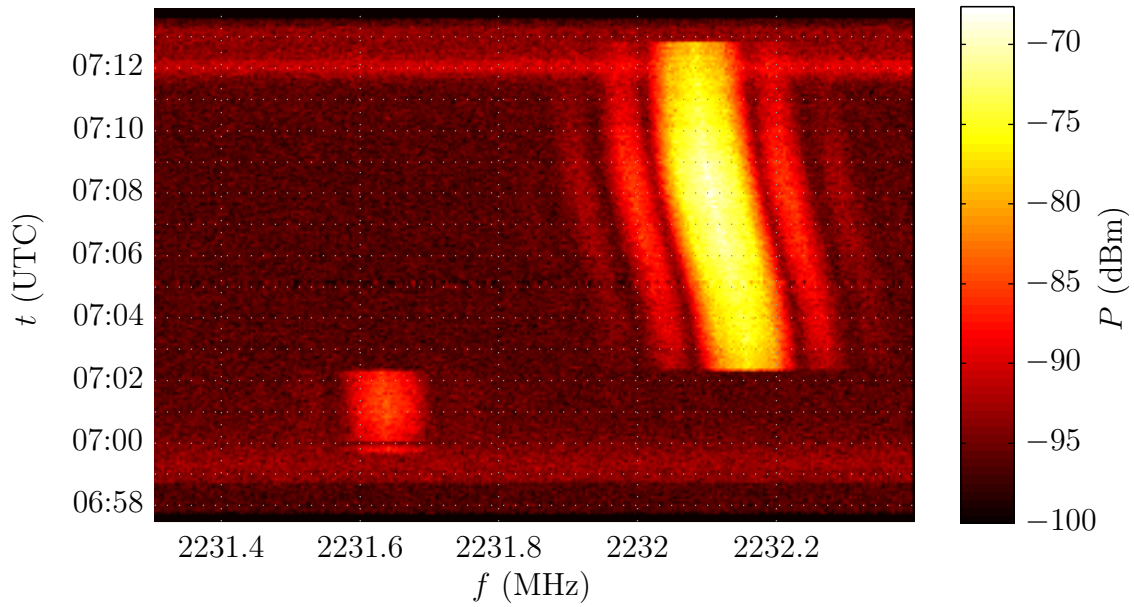


Figure 6.6: Spectrogram of a MOST pass of 2012-04-11.

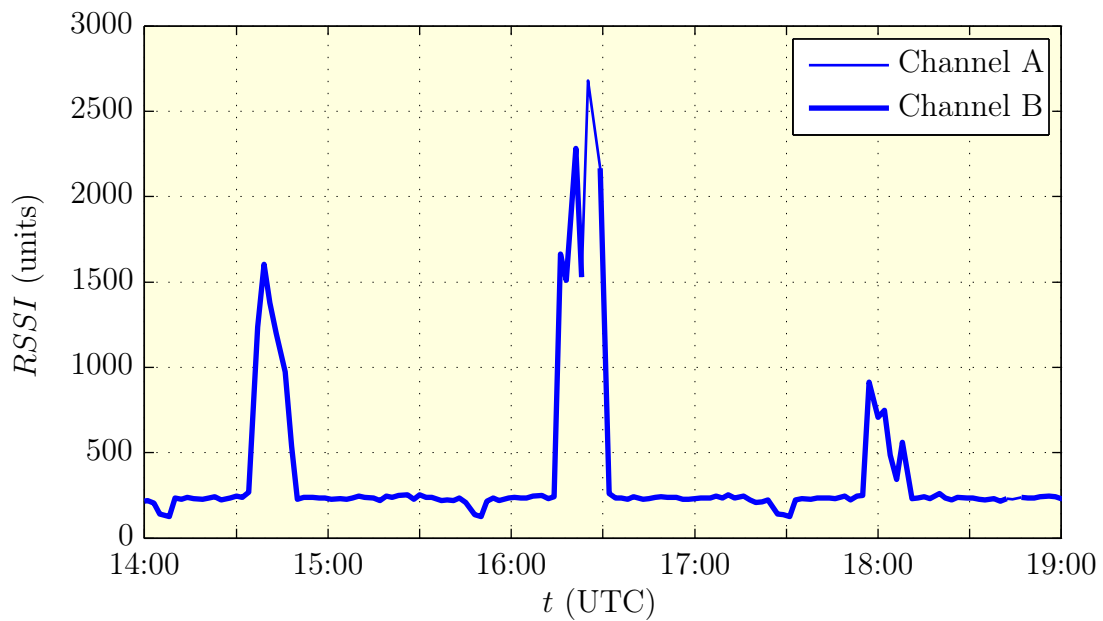


Figure 6.7: RSSI level of the MOST uplink for three 2012-06-03 passes.

satellite gets too low and therefore, the ground station switches to “Channel A” due to a command from Canada.

## 6.5 Automatic Noise Figure Assessment

The “figure of merit”  $G/T_s$  is a measure of quality of a receiver (see Section 5.2). It has been calculated to be 14.5 dB/K and is measured regularly. The measurement uses the Y-Factor Method [8, 86, 87] which consists of two power measurements of a hot and a cold source.  $Y$  is defined as

$$Y = \frac{P_{\text{hot}}}{P_{\text{cold}}}. \quad (6.1)$$

The Sun is used as the hot source. The cold source is the cold sky. The measured power levels  $P_{\text{Sun}}$  and  $P_{\text{sky}}$  at the receiver’s output depend on the noise sources and the gain and the noise figure of the receive front end. Because the contribution of the cold sky is small compared to the noise contribution of the receiver we can approximate

$$Y = \frac{P_{\text{Sun}}}{P_{\text{sky}}} = \frac{N_{\text{Sun}} + N_{\text{sys}}}{N_{\text{sky}} + N_{\text{sys}}} \approx \frac{N_{\text{Sun}} + N_{\text{sys}}}{N_{\text{sys}}} = \frac{N_{\text{Sun}}}{N_{\text{sys}}} + 1 \quad (6.2)$$

where  $N_{\text{Sun}}$ ,  $N_{\text{sky}}$  and  $N_{\text{sys}}$  are the noise power contributions of the Sun, the cold sky and the receive front end, respectively. The Sun’s noise contribution  $N_{\text{Sun}}$  is

$$N_{\text{Sun}} = \frac{F_{\text{Sun}}}{2} A \eta L_B B G_{\text{sys}} \quad (6.3)$$

with the solar flux density in one polarization state  $F_{\text{Sun}}/2$ , the effective antenna area  $A\eta$ , a beamsize correction factor  $L_B$ , the bandwidth  $B$  and the system’s gain  $G_{\text{sys}}$ . Substituting from equation (5.1) with the antenna’s gain  $G$  we get

$$N_{\text{Sun}} = \frac{F_{\text{Sun}}}{2} \frac{\lambda^2 G}{4\pi} L_B B G_{\text{sys}}. \quad (6.4)$$

The noise contribution of the system  $N_{\text{sys}}$  according to equation (5.6) is

$$N_{\text{sys}} = k_B T_s B G_{\text{sys}}. \quad (6.5)$$

Substituting this into (6.2) gives

$$Y = \frac{F_{\text{Sun}} \lambda^2 G L_B}{8 \pi k_B T_s} + 1. \quad (6.6)$$

This allows us to calculate  $G/T_s$  from two power measurements

$$G/T_s = \frac{8 \pi k_B}{F_{\text{Sun}} \lambda^2 L_B} (Y - 1) = \frac{8 \pi k_B f^2}{F_{\text{Sun}} L_B c^2} \left( \frac{P_{\text{Sun}}}{P_{\text{sky}}} - 1 \right). \quad (6.7)$$

The other required parameters are the Sun flux density and the beamsize correction factor. The Sun flux density is measured daily by different institutions and can be obtained, for example from the observatory of San Vito, Italy [88]. The beamsize correction factor is [89]

$$L_B = 1 + 0.38 \left( \frac{\theta_{\text{Sun}}}{\theta_{\text{ant}}} \right)^2. \quad (6.8)$$

The angular size of the Sun  $\theta_{\text{Sun}}$  is  $0.53^\circ$  at 2.22 GHz, the antenna beamwidth  $\theta_{\text{ant}}$  is  $3.1^\circ$  (see Section 5.2.2) resulting in a  $L_B$  of 1.01.

Two times a day, around noon,  $G/T_s$  is measured with the S-band receive front end. The sequence given in Figure 6.8 describes the measurement procedure. First, the modem and the front end including the LNA are switched on and the antenna is pointed at the Sun. While moving the antenna from the parking position to the Sun, the power level of the cold sky  $P_{\text{sky}}$  is measured. After the Sun's direction is reached, the power level of the Sun  $P_{\text{Sun}}$  is measured. Then, the LNA is switched off and a third power level  $P_{\text{off}}$  is measured. This measurement allows for a sanity check:  $P_{\text{off}}$  has to be significantly lower than the other two power levels. During the measurement with the antenna and the modem, the Sun flux density is automatically retrieved over the Internet. After the measurements,  $G/T_s$  is calculated with (6.7).

The measurement results of a period of ten weeks are shown in Figure 6.9. The mean  $G/T_s$  is 13.8 dB/K. Because this measurement is strongly influenced by clouds and the weather along the measurement path, the lower warning limit has been set to 12.8 dB/K.

## 6.6 Environmental Monitoring

Besides the monitored parameters and quality assurance procedures described in the previous sections, the environment of the ground station is monitored as well. Some of these parameters are visible using the *Web GUI* (see Figure 5.43). Figure 6.10 shows an exemplary, yet typical, measurement of wind speed, outdoor and indoor temperatures and power consumption of the ground station over a day. Similar graphs are available in the *Web GUI*.

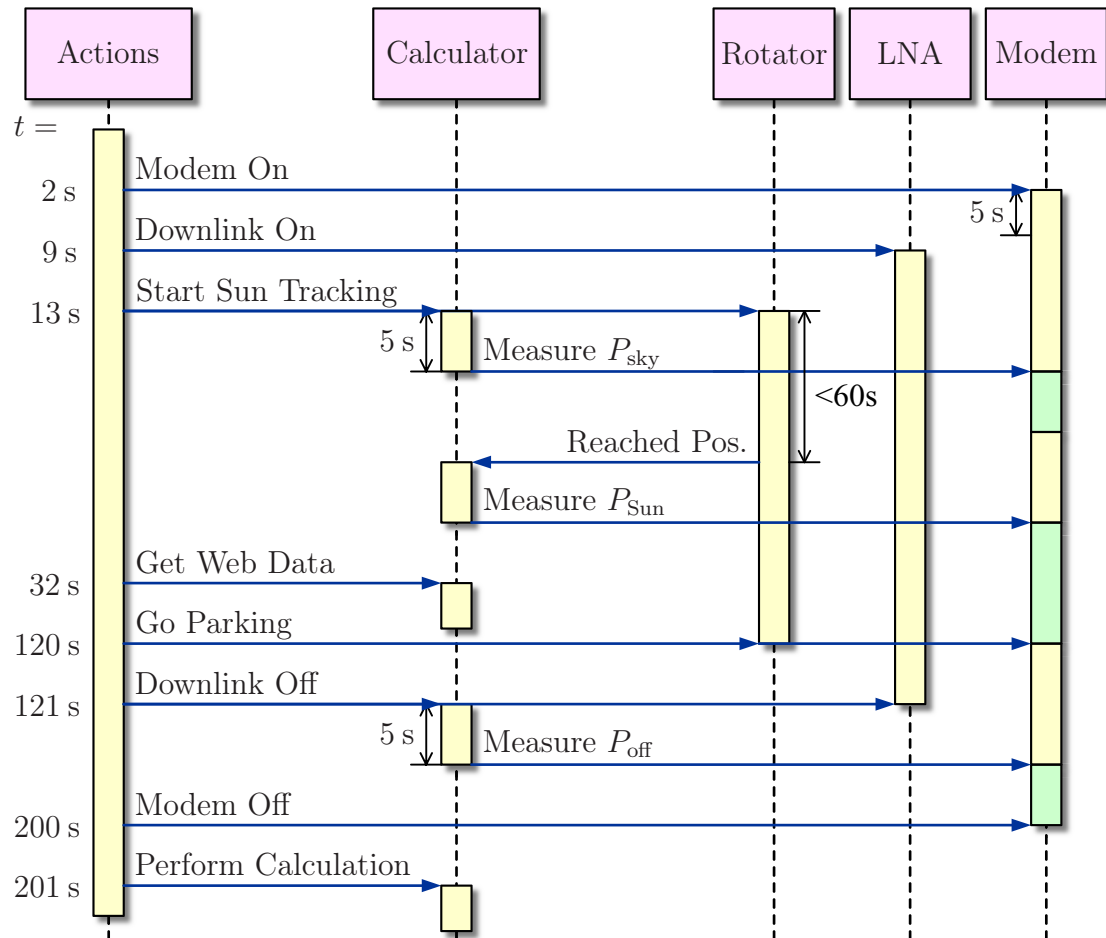


Figure 6.8: Sequence diagram for the daily measurement of the figure of merit  $G/T_s$  by means of the Sun.

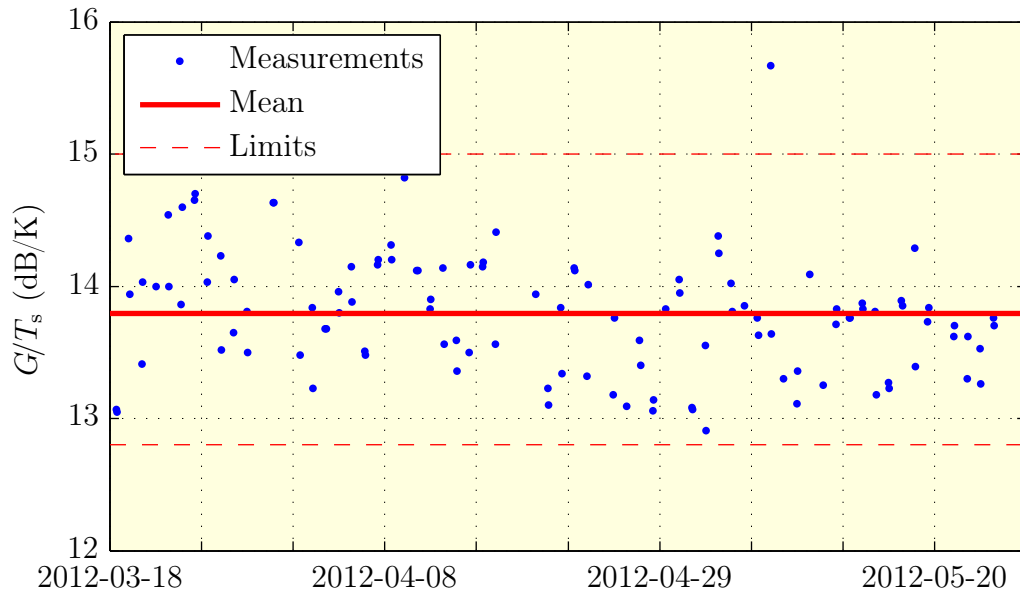


Figure 6.9: The figure of merit of the ground station observed over time. The mean value of  $G/T_s$  is 13.8 dB/K.

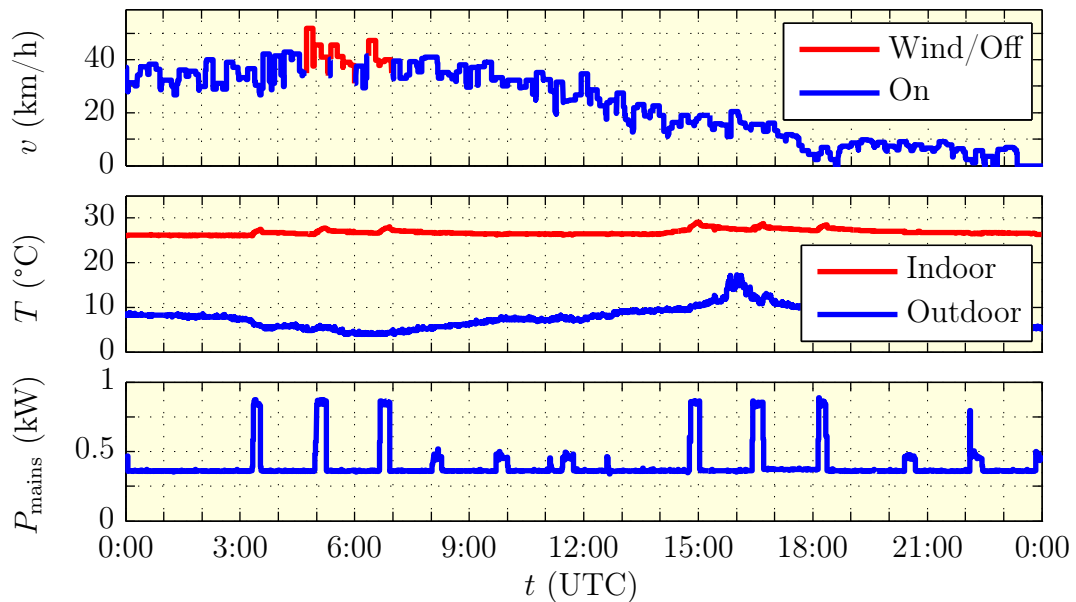


Figure 6.10: Wind speed, indoor temperature, outdoor temperature and power consumption recorded by the ground station on 2012-04-12.

The evolution of the wind speed shows periods, where the ground station is switched off because of wind speeds exceeding 45 km/h. At these times, the curve is shown in red. Wind mode is engaged for at least 10 minutes and is disabled when the wind speed falls below 40 km/h (see Section 5.7.2).

The middle area of the diagram shows the indoor and outdoor temperatures of the ground station. The bottom area gives the power consumption of the ground station. When there is an active satellite pass, the ground station activates the rotator and the RF front ends, thus consuming more power. In case of MOST the S-band uplink with its PA is also needed. This results in a significant rise of the indoor temperature during a MOST pass. The 5:00 morning pass was skipped on that day because of strong wind. As visible from the figure, the PA was still enabled to allow for a possible partial pass should the wind have decreased significantly during the pass. The two small power consumption peaks near 11:00 and 12:30 are due to the measurements on  $G/T_s$  of the ground station explained in Section 6.5.



# Chapter 7

## Summary and Conclusions

Beginning in 2008, I have built a ground station for satellite communication at the Vienna University of Technology – the TU Wien Ground Station. The ground station supports multiple satellite missions and has been designed to support research and education. First, I collected the requirements:

In Chapter 2, I highlighted three scientific satellite missions from the research field of astronomy which the ground station should be able to work with. CoRoT, MOST and BRITE Constellation are space telescopes of different sizes which measure light variations in stars by means of differential photometry. While all three missions use circular LEOs, they strongly differ in their communication parameters: CoRoT adheres to the CCSDS standard. MOST and BRITE Constellation use simpler protocols which are typical for smaller satellites.

Small satellites are ideal for universities. They give cheaper access to space technology and space research than big ones. When splitting the satellite project into smaller subprojects, small satellites are further ideally suited for the education of students. Students can learn teamwork, international communication with others and they can deepen their interdisciplinary skills. CubeSats are an example of small satellites often used in education. They are picosatellites which fulfill a few basic requirements, especially regarding their size and mass. These common rules allow for the development of standard components, which in turn reduces the development effort. Typically, the ground station necessary to communication with a specific CubeSat is understated and there is only one ground station per CubeSat. The TU Wien Ground Station should also be able to support such small satellite missions which typically use LEOs. Because of the missing standards and the multitude of parameters involved, this requires high flexibility. The ground station has been designed modular to fulfill this requirement.

Similar to small satellite missions, ground stations offer great learning opportunities for students of telecommunications. This led to the decision of choosing the roof of our institute, right in the center of Vienna, as the location of the ground station.

However, an urban city is an adverse environment for a receiver with high sensitivity. So in Chapter 3, I looked at the surroundings of the ground station and documented the possible interferers. A carefully designed overall downlink budget and a carefully designed feed assembly led to good results in the city.

The possible use of the ground station in student labs set further requirements on the ground station design. The before mentioned flexibility and the wish to be able to join educational ground station networks like GENSO further drove the design of the ground station.

Because of these requirements, I choose a segmented, modular setup of the ground station, dividing it in RF front ends, a frequency independent signal processing segment, a mission specific segment and a control and supervisory block spanning all three segments. This is documented in Chapter 4. In between the components and especially between the segments, I placed power dividers or switches to allow the easy setup of pipelines for the different satellite missions. Power dividers further allow building parallel pipelines by students who then can compare their results with the original pipeline. Clear and open interfaces between the segments and to the Internet allow an easy expansion and collaboration with multiple inhomogeneous missions. Regarding the education and training of students at our university, I showed which possibility the ground station design offers for the use in student laboratories.

Chapter 5 details the construction of the ground station. It gives its design and the selection of the components and it presents the characterization of the components. While the ground station is designed in a modular way to support a multitude of different space missions, it currently focuses on CoRoT, MOST and the S-band front ends. By the end of 2012 or the beginning of 2013 the first satellites of BRITE Constellation will be launched. Upon completion of the installation of the UHF antenna system and front end, the TU Wien Ground Station can – together with the other ground stations for BRITE in Graz, Warsaw and Toronto – also support these satellites.

For the ground station, I developed a special control software. It performs the scheduling of the different satellite passes and other tasks, and it switches between the missions. It further offers autonomous operation of the ground station and realizes the flexible interfaces used for remote operation and control over the Internet.

Last but not least, in Chapter 6, I presented measurement results of the ground station which document the successful operation of the ground station for more than six months. Some of the measurements are used to automatically and continuously monitor the performance of the ground station and assure its quality.

Because of its modular design, the ground station can be easily expanded. Future extensions can be the support of further missions, its inclusion in GENSO or the addition of front ends for other frequency bands, like the L-band around 1.2 GHz or the C-band around 5.7 GHz.

Closing, Figures 7.1 and 7.2 show two photographs of the inside components and the S-band antenna system of the TU Wien Ground Station.



Figure 7.1: Photo of the TU Wien Ground Station's indoor components.



Figure 7.2: Photo of the TU Wien Ground Station's S-band antenna system.

# Appendix A

## Topocentric-Horizon Coordinate System

The center of a topocentric-horizon coordinate system is the observer's position on Earth, i.e. the location of the ground station. The horizon is the plane tangential to the Earth's surface on that point. The elevation  $\vartheta$  is  $0^\circ$  in that plane. Above the observer, perpendicular to the horizon plane we find the zenith with  $\vartheta = 90^\circ$ . For each point on a hemisphere above the horizon, also an azimuth angle  $\varphi$  is defined. Azimuth is counted from north ( $0^\circ$ ) over east ( $90^\circ$ ), south ( $180^\circ$ ) and west ( $270^\circ$ ) back to north. Figure A.1 illustrates this hemisphere. The Earth is not shown but would touch below the center in the figure. The elevation can also be extended into the negative range below the horizon. The radius of the hemisphere is  $d$ , e.g. the distance to the satellite.

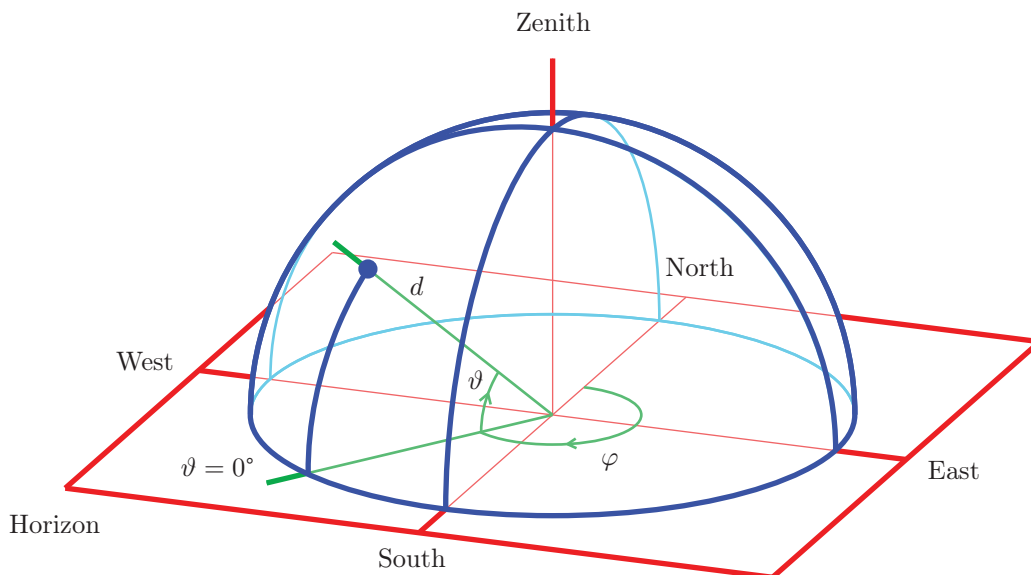


Figure A.1: Illustrating azimuth and elevation in a topocentric-horizon coordinate system.

# Appendix B

## Propagation Effects and Losses

Between the satellite and the ground station, the transmitted signals are attenuated for various reasons. Table B.1 lists such possible reasons. Most of these are negligible below 3 GHz or can be somehow mitigated [1, 8, 74, 79, 90, 91].

The equivalent isotropically radiated power  $EIRP$  is the product of the antenna gain  $G_{tx}$  of the transmit antenna and the transmit power  $P_{tx}$ ,

$$EIRP = G_{tx} P_{tx}. \quad (B.1)$$

The isotropically received power  $P_{rx}$  is the  $EIRP$  divided by the total losses on the path  $L_{total}$

$$P_{rx} = \frac{EIRP}{L_{total}} = \frac{EIRP}{L_{FSL} L_{atm} L_{pol} L_{point}}. \quad (B.2)$$

The biggest path loss is the free space loss (FSL)  $L_{FSL}$ . It is due to the fact, that the power transmitted is spherically spread with increasing distance  $d$ . It also depends on the frequency  $f$  used:

$$L_{FSL} = \left( \frac{4 \pi d}{\lambda} \right)^2 = \left( \frac{4 \pi d f}{c} \right)^2. \quad (B.3)$$

Gaseous molecules in the atmosphere, such as water vapor and oxygen, absorb energy from waves that pass through them, leading to some further attenuation. At frequencies below 3 GHz and for elevations above some  $10^\circ$  this loss is not very significant. In the link budgets in Appendix D,  $L_{atm}$  is included rounded up to 1 dB [74, 92, 93].

Faraday rotation and scintillation as well as depolarization effects due to rain can lead to severe polarization losses  $L_{pol}$  which can however be limited to 3 dB. This is discussed in the Appendix C.

Group	Name (Symbol)
Free space	Free space loss ( $L_{\text{FSL}}$ )
Ionosphere	Faraday rotation
Ionosphere	Effects dependent on total electron content
Ionosphere	Scintillation
Ionosphere	Absorption
Troposphere – clear air	Refraction and multipath fading
Troposphere – clear air	Scintillation
Troposphere – clear air	Defocusing
Troposphere – clear air	Gaseous attenuation ( $L_{\text{atm}}$ )
Troposphere – clear air	Bandwidth limitations
Troposphere – clear air	Fading due to elevation angle
Troposphere – precipitation	Rain attenuation
Troposphere – precipitation	Depolarization
Local	Interaction with features in vicinity
Local	Clouds and fog
Local	Dust and sand
Local	Snow
Local	Pointing loss ( $L_{\text{point}}$ )

Table B.1: Propagation effects for satellite links [1, 8, 74, 79, 90, 91].

Additionally, equation (B.2) accounts for pointing losses  $L_{\text{point}}$ . They arise if the antenna systems of the satellite and the ground station are not aligned properly toward each other. In the link budgets in Appendix D,  $L_{\text{point}}$  is included with 1 dB.

To be able to decode the transmitted signal, a minimum signal to noise ratio  $SNR$  is required. The noise power  $N$  is the total noise, either generated by the transmitter, acquired on the signal path or generated in the receiver. In the latter case, it is referred to the input of the receiving system. The noise power can be expressed using the bandwidth  $B$  occupied by the signal and the noise power density  $N_0$ . The noise power density can be expressed with the system’s equivalent noise temperature  $T_s$ , the Boltzmann constant  $k_B$  and considering the gain  $G$  of the system up to its reference point (see also equations (5.7) and (5.6)):

$$SNR = \frac{P_{\text{rx}}}{N} = \frac{P_{\text{rx}}}{N_0 B} = \frac{P_{\text{rx}} G}{k_B T_s B}. \quad (\text{B.4})$$

The factor  $G/T_s$  – the “figure of merit” of a receiving system – is detailed in Sec-

tion 5.2.1. For the downlink, a required  $G/T_s$  of the ground station for a specific satellite setup can be calculated from a required  $SNR$ .

Inserting (B.2) in (B.4) leads to

$$SNR = \frac{EIRP G}{L_{\text{total}} k_B T_s B} \quad (\text{B.5})$$

For the uplink, (B.5) can be used to calculate a required  $EIRP$  for the ground station from a required  $SNR$ , if the satellite's parameters like the satellite's  $G/T_s$  are known.



# Appendix C

## Polarization Selection for Satellites

The polarization state of every electromagnetic wave can be described by its Stokes parameters [76]. In case of fully polarized waves the Stokes parameters can be written as

$$\begin{aligned} S_0 &= I, \\ S_1 &= I \cos 2\psi \cos 2\chi, \\ S_2 &= I \sin 2\psi \cos 2\chi \quad \text{and} \\ S_3 &= I \sin 2\chi \end{aligned} \tag{C.1}$$

with the wave's intensity  $I$ , the tilt angle  $\psi$  of the polarization ellipse and its ellipticity angle  $\chi = \arctan(1/\varepsilon)$ . An ellipticity of  $\varepsilon = 0$  corresponds to LP, while an ellipticity of  $\varepsilon = \pm 1$  corresponds to LHCP and RHCP respectively.

The Stokes parameters can also be expressed in terms of the electric field as

$$\begin{aligned} S_0 &= E_{0x}^2 + E_{0y}^2, \\ S_1 &= E_{0x}^2 - E_{0y}^2, \\ S_2 &= 2 E_{0x} E_{0y} \cos \delta \quad \text{and} \\ S_3 &= 2 E_{0x} E_{0y} \sin \delta, \end{aligned} \tag{C.2}$$

if  $E_{0x}$  and  $E_{0y}$  are the magnitudes of two orthogonal LP waves with a relative phase shift of  $\delta$  [94]. The two orthogonal waves, with angular frequency  $\omega = 2\pi f$ , wavenumber  $k$  and propagation direction  $z$ , are

$$\begin{aligned} E_x &= E_{0x} \cos \{ kz - \omega t \} \quad \text{and} \\ E_y &= E_{0y} \cos \{ (kz - \omega t) + \delta \}. \end{aligned} \tag{C.3}$$

Figure C.1 shows the resulting losses  $L_{\text{pol}}$  for any polarization of the impinging wave, when received by antennas with different polarizations. For the LP receive antennas, either  $E_x$  and  $E_y$  is used in the simulation (see Figure C.1 a) and b)) while the other signal is omitted. For the simulation of the CP receive antennas  $E_y$  is shifted by  $\pm 90^\circ$  respectively, before being combined with  $E_x$  in a lossless Wilkinson power combiner (see Figure C.1 c) and d)).

For communications with satellites which do not have a fixed orientation with respect to the observer, typically CP is chosen, because – as visible from Figure C.1 c) and d) – the polarization losses  $L_{\text{pol}}$  are independent on the tilt angle  $\psi$  between the transmit antenna polarization and the receive antenna polarization. One has only to be prepared for a maximum of 3 dB of losses, if at the ground station, one of both orthogonal CPs can be selected as antenna polarization (i.e. LHCP or RHCP).

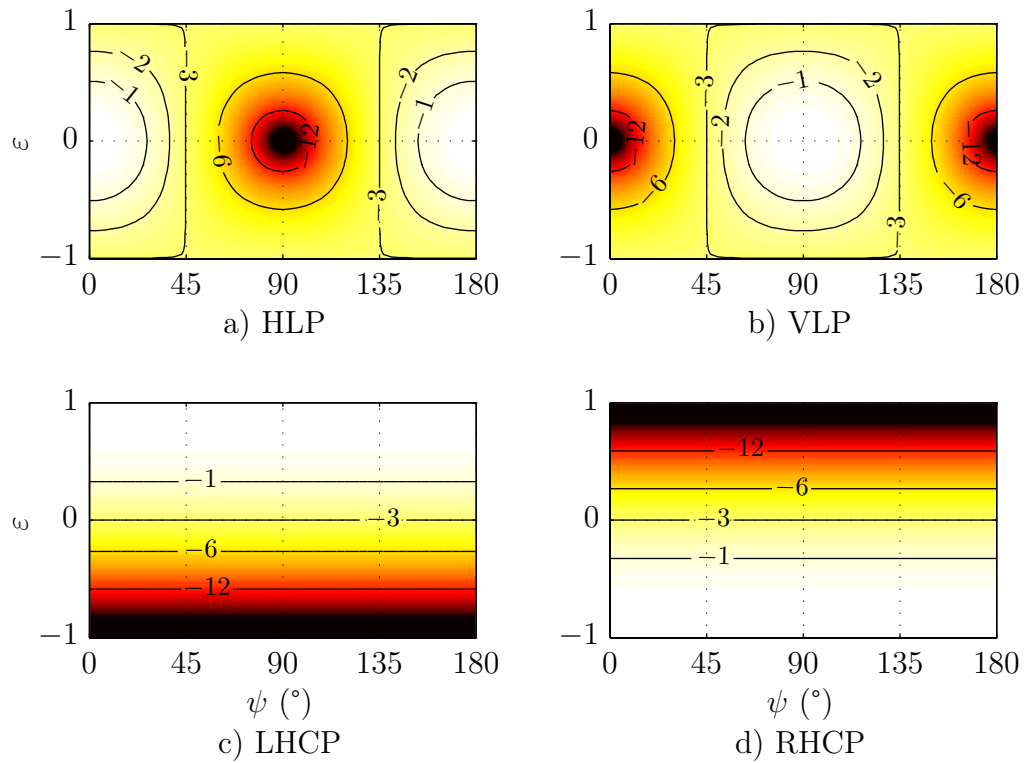


Figure C.1: Contour plots of the polarization loss  $L_{\text{pol}}$  in dB as a function of the received wave's polarization angle  $\psi$  and ellipticity  $\epsilon$  for differently polarized receive antennas.

# Appendix D

## Satellite Link Budgets

This appendix evaluates the RF power levels of the CoRoT, MOST and the BRITE satellites described in Chapter 2. The resulting figures are

- the necessary  $G/T_s$  of the ground station for the downlink from the satellites and
- the necessary  $EIRP$  of the ground station for the uplink to the satellites.

The figures calculated here have been used as requirements for the design of the ground station in Chapter 5.

### D.1 Link Budget for CoRoT

Table D.1 gives the link budget for the CoRoT downlink. The table lists the satellite's downlink frequency, its altitude and its transmit power expressed as  $EIRP$ . For the calculation I assume the elevation angles  $\vartheta$  not to be less than  $5^\circ$ . This gives a maximum distance  $d$  of about 3000 km (see Section 3.1) which I use to calculate the maximum  $L_{FSL}$ .

As discussed before, for polarization loss, atmospheric loss and pointing loss, in sum 5.0 dB have been assumed (see Appendix B and C). This results in a total loss  $L_{total}$  of 174.1 dB or an isotropically received power  $P_{rx}$  of  $-136.4$  dBm available to the ground station.

The demodulator (see Section 5.2.10) requires an  $SNR$  of 5.1 dB for QPSK demodulation together with the FEC used with CoRoT. An extra margin  $L_{margin}$  of 6.0 dB is assumed to provide a margin for varying signal levels caused by rain or other phenomena. Together with the receiver bandwidth  $B$  of some 800 kHz, we get a required minimum signal quality  $P_{rx}/N_0$  of 70.4 dBHz which gives us a minimum required  $G/T_s$  of 8.2 dB/K for the CoRoT S-band downlink of the ground station.

Frequency	$f =$	2280 MHz	
Altitude	$h =$	897 km	
minimum Elevation	$\vartheta \geq$	5 °	
maximum Distance	$d \leq$	2986 km	
EIRP of satellite	$EIRP =$	5.9 W	37.7 dBm
Free space loss	$L_{FSL} \leq$		169.1 dB
Polarization loss	$L_{pol} =$		3.0 dB
Atmospheric losses	$L_{atm} =$		1.0 dB
Pointing loss	$L_{point} =$		1.0 dB
Total propagation loss	$L_{total} \leq$		174.1 dB
Isotropic power received	$P_{rx} \geq$		-136.4 dBm
SNR required	$SNR \geq$		5.1 dB
Margin recommended	$L_{margin} \geq$		6.0 dB
Receiver bandwidth	$B =$	0.8 MHz	59.2 dBHz
$P_{rx}/N_0$ required	$P_{rx}/N_0 \geq$		70.4 dBHz
$G/T_s$ required	$G/T_s \geq$		8.2 dB/K

Table D.1: Link budget for the CoRoT downlink.

## D.2 Link Budget for MOST

The MOST satellite transmits less power  $P_{tx}$  than the CoRoT satellite resulting in a lower  $EIRP$  for its downlink. It has a lower altitude and uses a different modulation scheme and different data rates. Overall, the isotropically received power  $P_{rx}$  is some 12 dB lower than that of CoRoT. This is mitigated by the lower data rate, resulting in a minimum required  $G/T_s$  for the ground station of 9.9 dB/K. The figures are given in Table D.2.

MOST requires also an S-band uplink for operation. This time, the satellite's receiver parameters are given and the minimum required  $EIRP$  of the ground station is calculated. Together with its low gain, omnidirectional antennas, MOST only offers a  $G/T_s$  of -33.8 dB/K. This has to be compensated with a big  $EIRP$  of 69.4 dBm on the ground station side as indicated in Table D.3.

## D.3 Link Budget for BRITE Constellation

The BRITE downlink uses similar frequencies as MOST and CoRoT. BRITE has a lower orbit and a slightly lower bit rate than MOST while using the same

Frequency	$f =$	2232 MHz	
Altitude	$h =$	826 km	
minimum Elevation	$\vartheta \geq$	5 °	
maximum Distance	$d \leq$	2838 km	
EIRP of satellite	$EIRP =$	0.3 W	25.0 dBm
Free space loss	$L_{\text{FSL}} \leq$		168.5 dB
Polarization loss	$L_{\text{pol}} =$		3.0 dB
Atmospheric losses	$L_{\text{atm}} =$		1.0 dB
Pointing loss	$L_{\text{point}} =$		1.0 dB
Total propagation loss	$L_{\text{total}} \leq$		173.5 dB
Isotropic power received	$P_{\text{rx}} \geq$		-148.5 dBm
SNR required	$SNR \geq$		5.1 dB
Margin recommended	$L_{\text{margin}} \geq$		6.0 dB
Receiver bandwidth	$B =$	76.8 kHz	48.9 dBHz
$P_{\text{rx}}/N_0$ required	$P_{\text{rx}}/N_0 \geq$		60.0 dBHz
$G/T_s$ required	$G/T_s \geq$		9.9 dB/K

Table D.2: Link budget for the MOST downlink.

Frequency	$f =$	2055 MHz	
Altitude	$h =$	826 km	
minimum Elevation	$\vartheta \geq$	5 °	
maximum Distance	$d \leq$	2838 km	
Free space loss	$L_{\text{FSL}} \leq$		167.8 dB
Polarization loss	$L_{\text{pol}} =$		3.0 dB
Atmospheric losses	$L_{\text{atm}} =$		1.0 dB
Pointing loss	$L_{\text{point}} =$		1.0 dB
Total propagation loss	$L_{\text{total}} \leq$		172.8 dB
SNR required	$SNR \geq$		5.0 dB
Margin recommended	$L_{\text{margin}} \geq$		6.0 dB
Receiver bandwidth	$B =$	110 kHz	50.4 dBHz
$P_{\text{rx}}/N_0$ required	$P_{\text{rx}}/N_0 \geq$		61.4 dBHz
$G/T_s$ of satellite	$G/T_s =$		-33.8 dB/K
Isotropic power received required	$P_{\text{rx}} \geq$		-103.4 dBm
EIRP required	$EIRP \geq$	8657 W	69.4 dBm

Table D.3: Link budget for the MOST uplink.

modulation scheme and FEC. This relaxes the requirements on the ground station's  $G/T_s$  to 7.9 dB/K. Therefore, no detailed figures are given here. In the case that good  $SNR$  values are available during a pass on the ground, the satellite however can be commanded to utilize higher data rates.

The uplink of BRITE uses UHF signals near 437 MHz. Table D.4 gives the figures for the calculation of the minimum required  $EIRP$  for BRITE. To be on the safe side, a higher margin of 10.0 dB is assumed here. This leads to an  $EIRP$  of about 2 kW, which is used for the design of the ground station in Section 5.5.1.

Frequency	$f =$	437 MHz
Altitude	$h =$	800 km
minimum Elevation	$\vartheta \geq$	5 °
maximum Distance	$d \leq$	2783 km
Free space loss	$L_{\text{FSL}} \leq$	154.1 dB
Polarization loss	$L_{\text{pol}} =$	3.0 dB
Atmospheric losses	$L_{\text{atm}} =$	1.0 dB
Pointing loss	$L_{\text{point}} =$	1.0 dB
Total propagation loss	$L_{\text{total}} \leq$	159.1 dB
SNR required	$SNR \geq$	5.0 dB
Margin recommended	$L_{\text{margin}} \geq$	10.0 dB
Receiver bandwidth	$B =$	110 kHz
$P_{\text{rx}}/N_0$ required	$P_{\text{rx}}/N_0 \geq$	65.4 dBHz
$G/T_s$ of satellite	$G/T_s =$	-37.0 dB/K
Isotropic power received required	$P_{\text{rx}} \geq$	-96.2 dBm
EIRP required	$EIRP \geq$	1975 W
		63.0 dBm

Table D.4: Link budget for the BRITE uplink.

# Acknowledgments

This work has been supported by the Fund for Student Laboratories of the Vienna University of Technology and by the Hochschuljubiläumsstiftung of the City of Vienna.

I would like to thank my supervisor Arpad L. Scholtz for his guidance and support throughout my PhD studies at the Vienna University of Technology.

Furthermore, I am very grateful to Miroslav Kasal for agreeing to review the thesis and to serve as external examiner in the defense.

Also, I would like to thank my friends and my colleagues from the university for their encouragement and help during my studies. Particularly, I wish to thank Robert Dallinger, Jasmin Grosinger, Werner Keim, Robert Langwieser and Gregor Lasser for fruitful discussions and a careful reading of the manuscript. Moreover, I wish to thank my diploma students for their support in setting up the ground station and my colleagues from the teams of CoRoT, MOST and BRITE Constellation for the good collaboration.

But above all, I would like to thank my wife Rita and my family. This work would not have been achievable without their continual support.

# List of Abbreviations

AF	audio frequency
AMSAT	The Radio Amateur Satellite Corporation
AOS	acquisition of signal
ASCII	American standard code for information interchange
BER	bit error rate
BPF	band pass filter
BPSK	binary phase shift keying
BRITE	bright target explorer
CanX	Canadian Advanced Nanospace eXperiment
CCD	charge-coupled device
CCSDS	Consultative Committee for Space Data Systems
CNES	Centre National d'Études Spatiales (French space agency)
CoRoT	convection, rotation and planetary transits
CP	circularly polarized, circular polarization
CPU	central processing unit
CSA	Canadian Space Agency
ELaNa	Educational Launch of Nanosatellites
ESA	European Space Agency
FEC	forward error correction
FM	frequency modulation
FSL	free space loss
FSM	finite state machine
FTP	file transfer protocol
FWHM	full width at half maximum
GEI	geocentric equatorial inertial coordinate system
GENSO	Global Educational Network for Satellite Operations
GEO	geostationary Earth orbit
GMSK	Gaussian minimum shift keying



GNB	generic nanosatellite bus (microsatellite bus by UTIAS-SFL)
GSM	global system for mobile communications (a mobile communications standard)
GUI	graphical user interface
HDLC	high-level data link control
HLP	horizontally linearly polarized, horizontal linear polarization
HTML	hypertext markup language
HTTP	hypertext transfer protocol
HTTPS	hypertext transfer protocol over secure socket layer
IF	intermediate frequency
IP	internet protocol
ISRO	Indian Space Research Organization
LAN	local area network
LEO	low Earth orbit
LHCP	left hand circularly polarized, left hand circular polarization
LOS	line of sight
LNA	low noise amplifier
LNB	low noise block
LO	local oscillator
LOS	loss of signal
LP	linearly polarized, linear polarization
LTE	long term evolution (a mobile communications standard)
MATLAB	matrix laboratory (a numerical computing environment by MathWorks, Inc.)
MEO	medium Earth orbit
MOST	microvariability and oscillations of stars
NASA	National Aeronautics and Space Administration
NORAD	North American Aerospace Defense Command
NSP	nanosatellite protocol
NTS	nanosatellite tracking ships
OSCAR	orbiting satellite carrying amateur radio
PA	power amplifier
PC	personal computer
P-POD	poly picosatellite orbital deployer

PROTEUS	Plate-forme Reconfigurable pour l'Observation, les Télécommunications et les Usages scientifiques (Reconfigurable Platform for Observation, Telecommunications and Scientific Uses)
PWM	pulse width modulation
QAM	quadrature amplitude modulation
QPSK	quadrature phase shift keying
RF	radio frequency
RHCP	right hand circularly polarized, right hand circular polarization
RSSI	received signal strength indicator
Rx	receive, receiver
SDR	software defined radio
SFL	Space Flight Laboratory (UTIAS-SFL)
SFTP	secure file transfer protocol
SGP4	simplified perturbations model 4
SMA	sub-miniature version A (connector)
SNR	signal to noise ratio
SSB	single side band modulation
SSETI	Student Space Exploration and Technology Initiative
TLE	two line element (set of orbital parameters by NORAD)
TNC	terminal node controller
Tx	transmit, transmitter
UHF	ultra high frequency (300 MHz to 3000 MHz)
UMTS	universal mobile telecommunications system (a mobile communications standard)
URL	uniform resource locator
UPS	uninterruptible power supply
UTC	coordinated universal time
UTIAS	University of Toronto, Institute for Aerospace Studies
VHF	very high frequency (30 MHz to 300 MHz)
VLP	vertically linearly polarized, vertical linear polarization
VPN	virtual private network
WLAN	wireless local area network

# List of Symbols

$A$	area (in $\text{m}^2$ )
$\alpha$	tilt angle of orbit (in $^\circ$ )
$B$	spectral bandwidth (in Hz)
$c$	speed of light (299 792 458 m/s)
$\chi$	ellipticity angle of polarization ellipse (in $^\circ$ )
$D$	diameter (in m)
$d$	distance (in m)
$\delta, \bar{\delta}$	effective pointing error, mean effective pointing error (in $^\circ$ )
$\delta$	phase shift (of waves, in $^\circ$ )
$e$	end time (LOS)
$E$	electrical field strength (in V/m)
$EIRP$	equivalent isotropically radiated power (in W)
$\varepsilon$	ellipticity of polarization ellipse (1)
$\eta, \eta_{\text{ohm}}$	efficiency, ohmic efficiency (1)
$F$	noise figure (when in dB) or noise factor (when in linear scale)
$f$	frequency (in Hz)
$f_d$	focal distance of parabolic dish (in m)
$\Delta f_{\text{Doppler}}$	Doppler shift (in Hz)
$F_{\text{Sun}}$	sun flux density (in $\text{W}/\text{m}^2/\text{Hz}$ )
$f(\vartheta, \varphi)$	normalized radiation pattern (of antenna, 1)
$G$	gain (1)
$G$	gravitational constant ( $6.674 \cdot 10^{-11} \text{ m}^3/\text{kg}/\text{s}^2$ )
$G/T_s$	figure of merit of a receiver (in 1/K or dB/K)
$h$	altitude (of satellite, in m)
$I$	current (in A)
$I$	wave's intensity (proportional to power, normalized)
$IIP_3$	input 3 <sup>rd</sup> order intercept point (in W)
$i, j$	indices

$k$	wavenumber ( $= 2\pi/\lambda$ )
$k_B$	Boltzmann's constant ( $1.3806488 \cdot 10^{-23}$ J/K)
$L$	loss, attenuation (1)
$\lambda$	wavelength ( $= c/f$ )
$L_B$	beamsize correction factor (1)
$M$	mass of Earth ( $5.97 \cdot 10^{24}$ kg)
$\mu$	standard gravitational parameter ( $\mu = G M = 398\,600$ km <sup>3</sup> /s <sup>2</sup> )
$N$	noise power (in W)
$N_0$	noise power density (in W/Hz)
$\omega$	angular frequency ( $= 2\pi f$ )
$P$	power (in W)
$P_{1dB}$	1 dB compression point (in W)
$\varphi$	azimuth ( $0^\circ =$ north, $90^\circ =$ east, . . .)
$\psi$	tilt angle of polarization ellipse (in $^\circ$ )
$r$	radius (in m)
$RBW$	resolution bandwidth (of spectrum analyzer, in Hz)
$r_E$	radius of Earth (6371 km)
$RSSI$	received signal strength indicator (in units or in W)
$\vec{r}$	vector from ground station to satellite (in m)
$s$	start time (AOS)
$S_{0\dots 3}$	Stokes parameters (proportional to power, normalized)
$S_{ii}$	reflection coefficient, scattering parameters (1)
$S_{ij}$	transmission coefficient, scattering parameters ( $i \neq j, 1$ )
$SNR$	signal to noise ratio (1)
$t$	time (in s)
$T$	equivalent noise temperature (in K)
$T_0$	standard temperature (290 K)
$\vartheta$	elevation ( $0^\circ =$ horizon, $90^\circ =$ zenith)
$\vartheta_{\max}$	maximum elevation of a satellite pass (in $^\circ$ )
$\theta, \theta_\alpha$	pass angle, pass angle of tilted orbit (in $^\circ$ )
$\dot{\theta}$	angular velocity (of satellite, in $^\circ$ /s)
$\theta_{\text{ant}}$	antenna beamwidth (FWHM, 3 dB, in $^\circ$ )
$\theta_{\text{Sun}}$	angular size of the Sun (in $^\circ$ )
$t_o$	orbital period (in s)
$t_p, \bar{t}_p$	pass duration, mean pass duration (in s)

$T_s$	overall system's equivalent noise temperature (in K)
$U$	voltage (in V)
$v$	speed (of wind, in m/s or km/h)
$\vec{v}$	vectorial speed (of satellite, in m/s)
$v_\varphi, v_\vartheta$	rotational speed (in °/s)
$v_{rr}$	range rate (relative satellite speed, in m/s)
$v_t$	tangential speed (of satellite, in m/s)
$x, y, z$	x, y and z coordinates of a Cartesian coordinate system (in m)
$Y$	Y-Factor (for noise measurement, 1)

# Bibliography

- [1] L. J. Ippolito, *Satellite communications systems engineering*. John Wiley & Sons, 2008, Atmospheric effects, satellite link design and system performance.  
<http://dx.doi.org/10.1002/9780470754443>
- [2] G. M. Maral and M. Bousquet, *Satellite Communications Systems*, 2nd ed. John Wiley & Sons, 1993.
- [3] K. Schilling, “Design of Pico-Satellites for Education in Systems Engineering,” *IEEE Aerospace and Electronic Systems Magazin*, vol. 21, pp. 9–14, 2006.  
<http://dx.doi.org/10.1109/MAES.2006.1684269>
- [4] M. Schmidt and K. Schilling, “Small Satellites for Educational Purposes,” in *Proc. of 60th International Astronautical Congress (IAC2009)*, Daejon, Korea, October 12–16, 2009.
- [5] J. A. Larsen and J. D. Nielsen, “Development of CubeSats in an Educational Context,” in *Proc. of 5th International Conference on Recent Advances in Space Technologies (RAST)*, pp. 777–782, Istanbul, Turkey, June 9–11, 2011.  
<http://dx.doi.org/10.1109/RAST.2011.5966948>
- [6] T. S. Tuli, N. G. Orr, and R. E. Zee, “Low Cost Ground Station Design for Nanosatellite Missions,” in *Proc. of 24th AMSAT North American Space Symposium*, San Francisco, CA, USA, October 5–11, 2006.
- [7] M. Kasal, “Experimental Satellite Laboratory BUT Education and Research,” in *Proc. of 17th International Conference on Microwaves, Radar and Wireless Communications (MIKON 2008)*, pp. 367–374, Warsaw, Poland, May 19–21, 2008.
- [8] W. Keim, “Scientific Satellite Ground Station at 2 GHz in Urban Environment,” Ph.D. dissertation, TU Wien, Institut für Nachrichtentechnik und Hochfrequenztechnik, 2004.
- [9] K. Farzaneh, L. Mohamady, and A. Eidi, “Building and Controlling Customizable Satellite GS Networks,” in *Proc. of International Symposium on Communications and Information Technologies (ISCIT 2007)*, pp. 774–779, 2007.
- [10] J. Cutler, “Ground Station Virtualization,” in *Proc. of The Fifth International Symposium on Reducing the Cost of Spacecraft Ground Systems and Operations (RCSGSO 2003)*, Pasadena, CA, USA, July 2003.
- [11] G. Biraud, M. Eduardo, H. Page, and N. Kurahara, “Global Educational Network for Satellite Operations (GENSO),” in *Proc. of 60th International Astronautical Congress 2009 (IAC 2009)*, p. 3577, Daejeon, Republic of Korea, October 12–16, 2009.

- [12] “Convection Rotation and Planetary Transits (CoRoT),” accessed 2012-05-30.  
<http://smsc.cnes.fr/COROT/>
- [13] M. Auvergne, P. Bodin, L. Boissard, J.-T. Buey, *et al.*, “The CoRoT Satellite in Flight: Description and Performance,” *Astronomy & Astrophysics*, vol. 509, no. 1, pp. 411–424, October 2009. <http://dx.doi.org/10.1051/0004-6361/200810860>
- [14] A. Baglin, M. Auvergne, P. Barge, M. Deleuil, E. Michel, *et al.*, “CoRoT: Description of the Mission and Early Results,” *Proceedings of the International Astronomical Union Symposium*, vol. 4, no. 253, pp. 71–81, 2008. <http://dx.doi.org/10.1017/S1743921308026252>
- [15] P. Landiech and F. Douillet, “Proteus Platform and Application Satellites,” in *Proceedings of The 4S Symposium: Small Satellites, Systems and Services (ESA SP-571)*, B. Warmbein, Ed., p. 13, September 2004.
- [16] CNES, ALCATEL SPACE, *Proteus User’s Manual*, 2004, ed. 06.03.
- [17] R. E. Zee, S. C. O. Grocott, and J. Matthews, “The MOST Microsatellite Mission: All Systems Go for Launch,” in *12th CASI Conference on Astronautics*, November 2002.
- [18] “Microvariability and Oscillations of Stars,” accessed 2012-05-30.  
<http://www.astro.ubc.ca/MOST/>
- [19] G. Walker, J. Matthews, R. Kuschnig, R. Johnson, S. Rucinski, J. Pazder, G. Burley, A. Walker, K. Skaret, R. Zee, S. Grocott, K. Carroll, P. Sinclair, D. Sturgeon, and J. Harron, “The MOST Asteroseismology Mission: Ultraprecise Photometry from Space,” *Publications of the Astronomical Society of the Pacific*, vol. 115, no. 811, pp. 1023–1035, July 2003. <http://dx.doi.org/10.1086/377358>
- [20] R. E. Zee and P. Stibrany, “Canada’s First Microsatellite - An Enabling Low-Cost Technology for Future Space Science and Technology Missions,” *Canadian Aeronautics and Space Journal*, vol. 48, no. 1, March 2002. <http://dx.doi.org/10.5589/q02-008>
- [21] K. Zwintz, T. Kallinger, D. B. Guenther, M. Gruberbauer, R. Kuschnig, W. W. Weiss, M. Auvergne, L. Jorda, F. Favata, J. Matthews, and M. Fischer, “Pulsational Analysis of V 588 Mon and V 589 Mon Observed with the MOST and CoRoT Satellites,” *Astrophysical Journal*, vol. 729, no. 1, p. 14, March 2011. <http://dx.doi.org/10.1088/0004-637X/729/1/20>
- [22] M. Gruberbauer, D. Huber, R. Kuschnig, W. W. Weiss, D. B. Guenther, J. Matthews, A. F. J. Moffat, J. F. Rowe, S. Rucinski, D. Sasselov, and M. Fischer, “MOST Observations of the roAp Stars HD 9289, HD 99563, and HD 134214,” *Astronomy & Astrophysics*, vol. 530, p. 11, June 2011. <http://dx.doi.org/10.1051/0004-6361/201116736>
- [23] O. Koudelka, G. Egger, B. Josseck, N. Deschamp, C. Grant, D. Foisy, R. Zee, W. W. Weiss, R. Kuschnig, A. L. Scholtz, and W. Keim, “TUGSAT-1/BRITE-Austria - The First Austrian Nanosatellite,” *Acta Astronautica*, vol. 64, no. 11-12, pp. 1144–1149, June–July 2009. <http://dx.doi.org/10.1016/j.actaastro.2009.01.016>
- [24] A. Schwarzenberg-Czerny, W. Weiss, A. F. J. Moffat, R. E. Zee, S. Rucinski, S. Mochnacki, J. Matthews, M. Breger, R. Kuschnig, O. Koudelka, P. Orleanski, A. Pamyatnykh, A. Pigulski, and C. Grant, “The BRITE Nanosatellite Constellation Mission,” in *38th COSPAR Scientific Assembly*, Bremen, Germany, July 15–18, 2010.

- 
- [25] “BRITE Constellation,” accessed 2012-05-30. <http://www.brite-constellation.at/>
- [26] R. Kuschnig and W. W. Weiss, “BRITE-Constellation: Nano-Satellites for Asteroseismology,” *Communications in Asteroseismology*, pp. 351–353, 2009.
- [27] A. F. J. Moffat, W. W. Weiss, S. M. Rucinski, R. E. Zee, M. H. van Kerkwijk, S. W. Mochnecki, J. M. Matthews, J. R. Percy, P. Ceravolo, and C. C. Grant, “The Canadian BRITE Nanosatellite Mission,” in *13th Canadian Astronautics Conference (ASTRO)*. Montreal, Canada: Canadian Aeronautics and Space Institute (CASI), 2006.
- [28] “TUGSAT-1/BRITE-Austria, Austria’s first satellite,” accessed 2012-06-09. <http://www.tugsat.at/>
- [29] F. M. Pranajaya and R. E. Zee, “Generic Nanosatellite Bus for Responsive Mission,” in *5th Responsive Space Conference*, Los Angeles, CA, USA, April 23–26, 2007.
- [30] A. Shah, K. Sarda, C. Grant, S. Eagleson, D. Kekez, and R. E. Zee, “Canadian Advanced Nanospace eXperiment 2 Orbit Operations: One Year of Pushing the Nanosatellite Performance Envelope,” in *Proc. of 60th International Astronautical Congress (IAC2009)*, Daejeon, Korea, October 12–16, 2009.
- [31] F. Pranajaya, J. Cain, R. Zee, and R. Kolacz, “Nanosatellite Tracking Ships: From Concept to Launch in Seven Months,” in *Proc. of the 23rd Annual AIAA/USU Conference on Small Satellites*, Logan, Utah, USA, August 2009.
- [32] R. Munakata *et al.*, *CubeSat Design Specification*, California Polytechnic State University, August 2009, Rev 12. [http://www.cubesat.org/images/developers/cds\\_rev12.pdf](http://www.cubesat.org/images/developers/cds_rev12.pdf)
- [33] J. Puig-Suari, C. Turner, and W. Ahlgren, “Development of the Standard CubeSat Deployer and a CubeSat Class PicoSatellite,” in *Proc. of IEEE Aerospace Conference*, pp. 1/347–1/353, Big Sky, Montana, USA, March 10–17, 2001. <http://dx.doi.org/10.1109/AERO.2001.931726>
- [34] I. Nason, J. Puig-Suari, and R. Twiggs, “Development of a Family of PicoSatellite Deployers Based on the CubeSat Standard,” in *Proc. of IEEE Aerospace Conference*, pp. 1/457–1/464, Big Sky, Montana, USA, March 9–16, 2002. <http://dx.doi.org/10.1109/AERO.2002.1036865>
- [35] “CubeSat.org,” accessed 2012-06-08. <http://www.cubesat.org/>
- [36] A. Toorian, K. Diaz, and S. Lee, “The CubeSat Approach to Space Access,” in *Proc. of IEEE Aerospace Conference*, Big Sky, Montana, USA, March 1–8, 2008. <http://dx.doi.org/10.1109/AERO.2008.4526293>
- [37] M. Schmidt, “Ground Station Networks for Efficient Operation of Distributed Small Satellite Systems,” Ph.D. dissertation, Universität Würzburg, Würzburg, 2011, Schriftenreihe Würzburger Forschungsberichte in Robotik und Telematik, Vol. 6.
- [38] B. Klofas, “A Survey of CubeSat Communication Systems,” in *5th CubeSat Developers Conference*, Cal Poly, San Luis Obispo, CA, USA, April 9–11, 2008.



- 
- [39] R. Nugent, R. Munakata, A. Chin, R. Coelho, and J. Puig-Suari, “The CubeSat: The Picosatellite Standard for Research and Education,” in *AIAA SPACE Conference*, San Diego, California, USA, September 9–11, 2008.
- [40] J. Bouwmeester, G. T. Aalbers, and W. J. Ubbels, “Preliminary Mission Results and Project Evaluation of the Delfi-C3 Nano-Satellite,” in *Proc. of Small Satellite Systems and Services*, Rhodes, Greece, May 26–30, 2008.
- [41] J. F. D. Nielsen, J. A. Larsen, J. D. Grunnet, M. N. Kragelund, A. Michelsen, K. K. Sørensen, J. D. Grunnet, M. Kragelund, and A. Michelsen, “AAUSAT-II, A Danish Student Satellite,” *I S A S Nyusu*, 2009, accessed 2012-06-09.  
[http://www.aprsaf.org/interviews\\_features/features\\_2008/feature\\_71.php](http://www.aprsaf.org/interviews_features/features_2008/feature_71.php)
- [42] W. A. Beech, D. E. Nielsen, and J. Taylor, *AX.25 Link Access Protocol for Amateur Packet Radio*, 2nd ed., L. Knoper and G. Jones, Eds. Tucson Amateur Packet Radio Corporation TAPR, July 1998. [http://www.tapr.org/pub\\_ax25.html](http://www.tapr.org/pub_ax25.html)
- [43] “NASA’s Educational Launch of Nanosatellites (ELaNa),” accessed 2012-06-10.  
[http://www.nasa.gov/offices/education/centers/kennedy/technology/elana\\_feature.html](http://www.nasa.gov/offices/education/centers/kennedy/technology/elana_feature.html)
- [44] ESA, “ESA’s New Vega Launcher Scores Success on Maiden Flight,” February 13, 2012, accessed 2012-06-28. [http://www.esa.int/SPECIALS/Vega/SEMJ8LYXHYG\\_0.html](http://www.esa.int/SPECIALS/Vega/SEMJ8LYXHYG_0.html)
- [45] J. Muylaert, “Call for CubeSat Proposals for QB50,” February 15, 2012, A network of 50 double and triple CubeSats for the exploration of the lower thermosphere, re-entry research and in-orbit. <https://www.qb50.eu/>
- [46] M. Davidoff, *The Radio Amateur’s Satellite Handbook*. The American Radio Relay League, Inc. (ARRL), 2003.
- [47] International Telecommunication Union (ITU), *Radio Regulations*,  
<http://www.itu.int/pub/R-REG-RR-2008> and <http://life.itu.int/radioclub/rr/fr/rr.htm>, 2008.
- [48] A. Bohrmann, *Bahnen künstlicher Satelliten*, 2nd ed. Mannheim: Bibliographisches Institut, April 1966.
- [49] I. N. Bronstein, K. A. Semendjajew, G. Musiol, and H. Mühlig, *Taschenbuch der Mathematik*, 7th ed. Harri Deutsch Verlag, 2008.
- [50] D. Roddy, *Satellite Communications*, 3rd ed. McGraw-Hill, 2001.  
<http://dx.doi.org/10.1036/0071371761>
- [51] S. Cakaj, M. Fischer, and A. L. Scholtz, “Sun Synchronization of Low Earth Orbits (LEO) Through Inclination Angle,” in *Proceedings of the 28th IASTED International Conference on Modelling, Identification and Control*, pp. 156–161, Innsbruck, Austria, February 16–18, 2009.
- [52] R. L. Freeman, *Radio system design for telecommunications*, 3rd ed. John Wiley & Sons, 2006. <http://dx.doi.org/10.1002/0470050446>

- 
- [53] W. Keim, V. Kudielka, and A. L. Scholtz, "A Scientific Satellite Ground Station for an Urban Environment," in *Proceedings of the IASTED International Conference on Communication Systems and Networks*, pp. 280–284, 2004.
- [54] Wikipedia, "GSM Frequency Bands – Wikipedia, The Free Encyclopedia," accessed 2012-03-15. [http://en.wikipedia.org/wiki/GSM\\_frequency\\_bands](http://en.wikipedia.org/wiki/GSM_frequency_bands)
- [55] Wikipedia, "UMTS Frequency Bands – Wikipedia, The Free Encyclopedia," accessed 2012-03-15. [http://en.wikipedia.org/wiki/UMTS\\_frequency\\_bands](http://en.wikipedia.org/wiki/UMTS_frequency_bands)
- [56] "Senderkataster Austria," accessed 2012-03-16. <http://www.senderkataster.at/>
- [57] J. W. Cutler and C. A. Kitts, "Mercury: A Satellite Ground Station Control System," in *Proceedings of the IEEE Aerospace Conference 1999*, pp. 51–58, Snowmass at Aspen, Colorado, USA, March 6–13, 1999. <http://dx.doi.org/10.1109/AERO.1999.793142>
- [58] Y. Peng, "Ground Station Design for UWE-1 (University of Würzburg's Experimental-Satellite 1)," Master's thesis, Luleå University of Technology, Department of Space Science, Luleå/Kiruna, Sweden, 2007.
- [59] J. Cutler and A. Fox, "A Framework for Robust and Flexible Ground Station Networks," *Journal of Aerospace Computing, Information, and Communication*, vol. 3, March 2006.
- [60] M. Stolarski, "Distributed Ground Station System Experimental Theory Confirmation," in *Proc. of the European Ground System Architecture Workshop (ESAW)*, Darmstadt, Germany, May 5–6, 2011.
- [61] "The GENSO Network," Global Educational Network for Satellite Operations (GENSO), accessed 2012-01-05. <http://www.genso.org/>
- [62] H. Page, B. Preindl, and V. Nikolaidis, "GENSO: The Global Educational Network for Satellite Operations," in *Proc. of 59th International Astronautical Congress (IAC2008)*, Glasgow, Scotland, September 29–October 3, 2008.
- [63] M. Fischer, W. Keim, and A. L. Scholtz, "Low-cost Erdefunkstelle Wien: 5 Jahre Betriebserfahrung," in *Radar, Communication and Measurement RADCOM 2009*, Hamburg, Germany, March 31–April 1, 2009, English title: 5 Years of Operation Experience with the low-cost Vienna Ground Station.
- [64] M. Fischer and A. L. Scholtz, "Design of a Multi-Mission Satellite Ground Station for Education and Research," in *Proceedings of the Second International Conference on Advances in Satellite and Space Communications (SPACOMM) 2010*, pp. 58–63, June 2010. <http://dx.doi.org/10.1109/SPACOMM.2010.13>
- [65] J. Cutler, "Ground Station Markup Language," in *Proc. of IEEE Aerospace Conference 2004*, pp. 3337–3343, March 6–13, 2004.
- [66] M. Fischer and A. L. Scholtz, "Matlab-Based Interface for Operation of a LEO Satellite Ground Station by Students," in *Proceedings of the First International Conference on Small Satellite Systems (CSSS) 2011*, 2011.

- 
- [67] D. Schor, W. Kinsner, and A. Thoren, "Satellite Ground Station Emulator: An Architecture and Implementation Proposal," in *Proc. of Canadian Conference on Electrical and Computer Engineering (CCECE 2009)*, pp. 868–873, St. John's, Canada, May 3–6, 2009. <http://dx.doi.org/10.1109/CCECE.2009.5090253>
- [68] R. M. Rodríguez-Osorio, S. R. Díaz-Miguel Coca, and F. R. Vedal, "Educational Ground Station Based on Software Defined Radio," in *Proc. of 59th International Astronautical Congress 2008 (IAC08)*, Glasgow, Scotland, September 29–October 3, 2008.
- [69] T. Reymund, "Software Defined Radio with Graphical User Interface," Master's thesis, supervised by M. Fischer, W. Keim and A. L. Scholtz, TU Wien, Institut für Nachrichtentechnik und Hochfrequenztechnik, 2007.
- [70] A. Martinez Torio, "Software Defined S-Band Ground Station Transceiver for Satellite Communications," Master's thesis, supervised by M. Fischer and A. L. Scholtz, TU Wien, Institute of Telecommunications, 2011.
- [71] A. Martin Recuenco, "SSETI Groundstation," Master's thesis, supervised by M. Fischer and A. L. Scholtz, TU Wien, Institut für Nachrichtentechnik und Hochfrequenztechnik, 2008.
- [72] B. F. Lassacher, "Erdefunkstelle für Satellitenkommunikation," Master's thesis, supervised by M. Fischer and A. L. Scholtz, TU Wien, Institut für Nachrichtentechnik und Hochfrequenztechnik, 2008.
- [73] P. Witschel, "Errichtung einer Satellitenfunkanlage mit automatischer Antennennachführung," Master's thesis, supervised by M. Fischer and P. Goldmann, TU Wien and FH Technikum Wien, 2010.
- [74] A. A. Solana Esteban, "Front-End Design for a Multi-Mission, Multi-Standard Satellite Ground Station," Master's thesis, supervised by M. Fischer and A. L. Scholtz, TU Wien, Institut für Nachrichtentechnik und Hochfrequenztechnik, 2010.
- [75] B. Sklar, *Digital Communications: Fundamentals and Applications*, 2nd ed. Prentice Hall, 2001.
- [76] J. Detlefsen and U. Siart, *Grundlagen der Hochfrequenztechnik*, 3rd ed. Oldenbourg, 2009. <http://dx.doi.org/10.1524/9783486598575>
- [77] T. Y. Otoshi, *Noise Temperature Theory and Applications for Deep Space Communications Antenna Systems*. Norwood, Massachusetts, USA: Artech House, May 2008.
- [78] ITU-R, *Recommendation ITU-R P.372-10 – Radio Noise*, October 2009, accessed 2012-05-09. <http://www.itu.int/rec/R-REC-P.372-10-200910-I/en>
- [79] S. R. Saunders, *Antennas and Propagation for Wireless Communication Systems*. John Wiley & Sons, 1999.
- [80] I. Glover and P. M. Grant, *Digital Communications*, 2nd ed. Essex, England: Pearson Education, Prentice Hall, 2004.

- 
- [81] S. Cakaj, W. Keim, and K. Malaric, "Composite Noise Temperature at Low Earth Orbiting Satellite Ground Station," in *Proceedings of IEEE International Conference on Software, Telecommunications, and Computer Networks (Soft-COM) 2006*, pp. 214–217, Split, Croatia, September 2006.
- [82] L. D. Halliday, "Communications Infrastructure for the MOST Microsatellite Project," Master's thesis, University of Toronto, Department of Aerospace Science and Engineering, 2000.
- [83] NASA - National Aeronautics and Space Administration, "Blue Marble: Land Surface, Shallow Water, and Shaded Topography," February 11, 2002, Visible Earth, A catalog of NASA images and animations of our home planet. <http://visibleearth.nasa.gov/>
- [84] The Open Group, "crontab - Schedule Periodic Background Work," *Base Specifications Issue 7 IEEE Std 1003.1-2008*, December 2008, accessed 2012-02-10. <http://pubs.opengroup.org/onlinepubs/9699919799/utilities/crontab.html>
- [85] D. A. Vallado, P. Crawford, R. Hujsak, and T. S. Kelso, "Revisiting SpacetrackReport #3," in *AIAA/AAS Astrodynamics Specialist Conference*, p. 88, Keystone, CO, August 21–24, 2006. <http://celestrak.com/publications/AIAA/2006-6753/>
- [86] Agilent Technologies, *Noise Figure Measurement Accuracy - The Y-Factor Method*, May 2010, Application Note 57-2. <http://cp.literature.agilent.com/litweb/pdf/5952-3706E.pdf>
- [87] S. Cakaj, W. Keim, and K. Malaric, "Sun Noise Measurement at Low Earth Orbiting Satellite Ground Station," in *Proceedings ELMAR-2005*, pp. 345–348, 2005. <http://dx.doi.org/10.1109/ELMAR.2005.193714>
- [88] O. Duffy, "Quite Sun Radio Flux Interpolations," accessed 2012-06-09. <http://vk1od.net/calc/qsrf/>
- [89] R. Flagg, "Determination of G/T," *SETI League Publications*, July 2006, accessed 2012-05-29. <http://www.setileague.org/articles/g-t.htm>
- [90] W. L. Flock, *Propagation Effects on Satellite Systems at Frequencies below 10 GHz: A Handbook for Satellite Systems Design*, ser. NASA Reference Publication. National Aeronautics and Space Administration (NASA), December 1983, vol. 1108.
- [91] S. Cakaj, "Analysis of Parameter Influence on Performance of LEO Scientific Satellite Ground Stations in Urban Areas," Ph.D. dissertation, University of Zagreb, Faculty of Electrical Engineering and Computing, January 2008.
- [92] ITU-R, *Recommendation ITU-R P.676-9 - Attenuation by Atmospheric Gases*, February 2012, accessed 2012-06-26. <http://www.itu.int/rec/R-REC-P.676-9-201202-I/en>
- [93] ITU-R, *Recommendation ITU-R P.1510 - Annual Mean Surface Temperature*, February 2001, accessed 2012-06-26. <http://www.itu.int/rec/R-REC-P.1510-0-200102-I/en>
- [94] E. W. Weisstein, "Jones Vector," *Eric Weisstein's World of Physics*, 2007, accessed 2012-03-26. <http://scienceworld.wolfram.com/physics/JonesVector.html>